

See discussions, stats, and author profiles for this publication at: <https://www.researchgate.net/publication/353606394>

# Wave Propagation Control Using Active Acoustic Metamaterials

Thesis · April 2017

DOI: 10.13140/RG.2.2.10935.85924

---

CITATIONS

0

1 author:



**Ahmed Allam**

Georgia Institute of Technology

12 PUBLICATIONS 45 CITATIONS

SEE PROFILE



AIN SHAMS UNIVERSITY

FACULTY OF ENGINEERING

Mechatronics Engineering

# **Wave Propagation Control Using Active Acoustic Metamaterials**

A Thesis submitted in partial fulfillment of the requirements of the degree of

Master of Science in Mechanical Engineering

(Mechatronics Engineering)

by

Ahmed Abdelshakour Abdelfattah Elhousseiny Allam

Bachelor of Science in Mechanical Engineering

(Mechatronics Engineering)

Faculty of Engineering, Ain Shams University, 2012

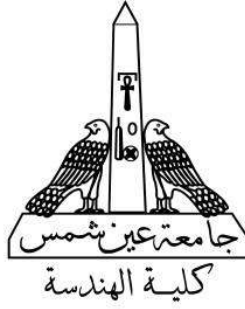
Supervised By

**Prof. Wael Nabil Akl**

**Assoc. Prof. Adel Moneeb Elsabbagh**

Cairo - (2017)





AIN SHAMS UNIVERSITY  
FACULTY OF ENGINEERING

*Wave propagation control using active acoustic  
metamaterials*

By

*Ahmed Abdelshakour Abdelfattah Elhousseiny Allam*

B.Sc., Mechanical Engineering, Mechatronics Section  
Ain Shams University, 2012

**EXAMINERS COMMITTEE**

Name

Signature

**Prof. Amr Mohamed Baz**

Mechanical Engineering, University of Maryland

.....

**Prof. Amr Mohamed Ezzat Safwat**

Electronics & Electrical Communication  
Engineering, Ain Shams University

.....

**Prof. Wael Nabil Akl**

Design and Production Engineering, Ain Shams  
University

.....

Date: 5/4/2017



# Statement

This thesis is submitted as a partial fulfillment of Master of Science in Mechanical Engineering, Faculty of Engineering, Ain shams University. The author carried out the work included in this thesis, and no part of it has been submitted for a degree or a qualification at any other scientific entity.

**Ahmed Abdelshakour Abdelfattah Elhousseiny Allam**

Signature

.....

**Date:** 05 04 2017



# Researcher Data

**Name:** Ahmed Abdelshakour Abdelfattah Elhousseiny Allam

**Date of Birth:** 02/08/1990

**Place of Birth:** Giza, Egypt

**Last academic degree:** BSc. in mechanical Engineering

**Field of specialization:** Mechatronics Engineering

**University issued the degree:** Ain Shams University

**Date of issued degree:** 2012

**Current job:** Demonstrator at Mechatronics Department, Faculty of Engineering,  
Ain Shams University



# Summary

Acoustic metamaterials (AMM) are artificial materials with engineered sub-wavelength structures that possess acoustic material properties which are not readily available in nature. The material properties of AMMs can be manipulated by embedding active elements inside their structure (active AMMs). This manipulation of properties is done by an external voltage signal and is hardly available in any natural material.

In this work, existing designs for passive and active AMMs are reviewed and summarized. Existing homogenization techniques for the material properties of passive metamaterials are investigated and extended to be applied for active AMMs. Three new designs for active plate-type AMM with tunable density are proposed and verified analytically, numerically and experimentally.

The first design is a one dimensional (1D) AMM consisting of clamped piezoelectric disks in air. The effective density of the material is controlled by an external static electric voltage. An analytic model based on the acoustic two-port theory, the theory of piezoelectricity and the pre-stressed thin plate theory is developed to predict the behavior of the material. The results are verified using the finite element method. Excellent agreement is found between both models for the studied frequency and voltage ranges. The results show that the density is tunable within orders of magnitude relative to the uncontrolled case. This is done with a limited effect on the bulk modulus of the material. The results also suggest that simple controllers could be used to program the material density.

The first design was modified and extended to construct a two-dimensional AMM with controllable anisotropic density. The modified design consists of composite lead-lead zirconate titanate (PZT) plates clamped to an aluminum structure with air as the background fluid. The effective anisotropic density of the material is controlled, independently for two orthogonal directions, by means of an external static electric voltage signal. An analytic model based on the acoustic two-port theory, the theory of piezoelectricity, the laminated pre-stressed plate theory is developed to predict the behavior of the material. The results are verified also using the finite element method. Excellent agreement is found between both models for the studied frequency and voltage ranges. The results show that, below 1600 Hz, the density is controllable within orders of magnitude relative to the uncontrolled case. A reconfigurable wave guide was constructed using the developed material and its performance was evaluated numerically and analytically. The waveguide can control the direction of the acoustic waves propagating through it.

The results obtained from the previous models were used to construct and experimentally verify a third design with a fully real-time controllable effective density. The effective density of the AMM can be programmed and set to any value ranging from  $-100 \text{ kg/m}^3$  to  $100 \text{ kg/m}^3$  passing by near zero density conditions. This is done through an interactive graphical user interface and is achievable for any frequency between 500 and 1500 Hz. The modified design consists of clamped composite piezoelectric diaphragms suspended in air. The dynamics of the diaphragms are controlled by connecting a closed feedback control loop between the piezoelectric layers of the diaphragm. The density of the material is adjustable through an outer adaptive feedback loop that is implemented by the real-time estimation of the density of the material using the 4-microphone technique. Applications for the new material include programmable active acoustic filters, non-symmetric acoustic transmission and programmable acoustic superlens.

**Keywords:** Acoustic metamaterials, Piezoelectric materials, Feedback control, Adaptive control



# Acknowledgment

I would like to thank my supervisors Prof. Dr. Wael Akl and Dr. Adel Elasabbagh for their devoted support throughout all the stages of this work and for providing me with the tools and the working environment required for finishing it. I would like to specially thank Prof. Dr. Wael for introducing the topic of the thesis to me and sharing with me all his profound knowledge of it. I would like to thank Dr. Adel Elasabbagh for interfering in the right moments whenever he felt that I have lost my thrust or went off track.

I would like to thank Prof. Dr. Tamer Elnady for his support with the experimental details especially those related to signal analysis and duct acoustics.

I would like to thank all my colleagues in the ASU group for advanced research in dynamic systems (ASU-GARDS) and also my colleagues in mechatronics department, I would specify Eng. Weam Elsayhar and Eng. Mohamed Talaat Harb for their valuable help with the theoretical and experimental details of my work. I would like also to thank Eng. Mohamed Ibrahim for providing me with the necessary background on electromagnetic metamaterials, Eng. Ahmed Barakat for our fruitful discussions about control systems, Eng. Ahmed Abosrea for helping me with the manufacturing of the cell and Dr. Maaz Farouqi for our long discussions about metamaterials . I would like to thank my friends and colleagues Eng. Yehia Zakaria, Eng. Ahmed Elrakaybi, Eng. Ali Zein and Eng. Ahmed Hesham, you have always been there for me whenever I needed any kind of support.

I also cannot forget the role of Mrs. Fatma. I appreciate her valuable support whenever it came to any administrative tasks.

I would not have reached this point without the keen support of my family. I would like to thank my mother and father for being there for me and for their continuous encouragement to finish my work in the best way possible. I would also like to thank my brother Mohamed and my sister Samaa for their support and for helping me with the preparation of the data and thesis material.

# Contents

<b>Contents</b>	<b>xii</b>
<b>List of Figures</b>	<b>xv</b>
<b>List of Tables</b>	<b>xix</b>
<b>Abbreviations</b>	<b>xxi</b>
<b>1 Literature Review</b>	<b>1</b>
1.1 Introduction to Acoustic metamaterials (AMM)	1
1.2 Sign Interpretation	3
1.2.1 Single Negative Metamaterials (SNG)	5
1.2.2 Double Negative Metamaterials (DNG)	5
1.3 Classification of AMM	6
1.3.1 Resonant AMM	6
1.3.1.1 Mass-in-mass AMM	8
1.3.1.2 Acoustic resonator based AMM	9
1.3.1.3 Membrane/Plate-type AMM	9
1.3.1.4 DNG resonant AMM	11
1.3.2 Non-resonant AMM	13
1.3.2.1 Phononic crystal based AMM	13
1.3.2.2 Space coiling AMM	14
1.4 Applications of AMM	15
1.4.1 Spatial Manipulation	15
1.4.1.1 Acoustic Cloaking	16
1.4.1.2 Other spatial Devices	16
1.4.2 Subwavelength acoustic imaging	17
1.4.3 Perfect Absorption	17
1.4.4 Extraordinary Transmission	17
1.5 Active AMM	17
1.6 Problem Statement	20
1.7 Work Objective	20
1.8 Scope of Work	20
1.9 Thesis Summary	22
<b>2 Theoretical Background</b>	<b>23</b>
2.1 Analytic modelling of AMM	23
2.1.1 Volume Averaging	24

2.1.2	The multiple scattering theory . . . . .	25
2.1.3	Acoustic two-port theory . . . . .	26
2.1.4	Retrieval of the effective material properties . . . . .	28
2.2	Piezoelectricity . . . . .	29
<b>3</b>	<b>Open loop 1D active AMM</b>	<b>33</b>
3.1	Theoretical formulation . . . . .	34
3.1.1	Characterizing the open loop AMM cell . . . . .	35
3.2	The finite element model . . . . .	39
3.3	Results and discussion . . . . .	42
3.3.1	Characterization of a single cell . . . . .	42
3.3.2	Characterization of multiple cells . . . . .	46
3.4	Conclusion . . . . .	47
<b>4</b>	<b>Open loop 2D AMM</b>	<b>49</b>
4.1	Theoretical Formulation . . . . .	50
4.1.1	Characterizing the 2D active MAM cell . . . . .	51
4.1.2	Characterizing the 1D building block of the 2D active AMM . . . . .	52
4.2	Numerical Model . . . . .	56
4.3	Results and Discussion . . . . .	57
4.4	Applications . . . . .	63
4.5	Conclusion . . . . .	64
<b>5</b>	<b>Closed loop 1D AMM</b>	<b>67</b>
5.1	Material Construction . . . . .	68
5.2	Theoretical Formulation . . . . .	68
5.2.1	Acoustic impedance of the piezoelectric diaphragm . . . . .	68
5.3	Stability of the Cell . . . . .	76
5.4	Characterization of the AMM cell . . . . .	77
5.5	Controller transfer function . . . . .	80
5.6	Adaptive control of the cell density . . . . .	81
5.7	Conclusion . . . . .	84
<b>6</b>	<b>Conclusion and Future Work</b>	<b>87</b>
6.1	Conclusion . . . . .	87
6.2	Future Work . . . . .	89
	<b>Bibliography</b>	<b>91</b>

# List of Figures

1.1	Construction of the first proposed metamaterials. (a) Thin wire structure exhibiting negative $\epsilon$ /positive $\mu$ , (b)split ring resonators exhibiting negative $\mu$ / positive $\epsilon$ and (c) double split ring resonator exhibiting double negativity. Taken from (Ref.[7]). . . . .	2
1.2	Construction of the (a) unit cell and (b) structure of the first proposed AMM consisting of silicon rubber coated lead balls in an epoxy matrix. Taken from (Ref.[5]). . . . .	3
1.3	A simple mass spring damper system. . . . .	6
1.4	Bode plot of the effective mass of the system shown in Figure 1.3 with $M = 1, k = 1, b = 0.01$ . . . . .	7
1.5	Comparison between resonators with (a) dipolar resonance and (b) monopolar resonance . The neutral position is shown with the dotted line while the resonator is represented by a block. The arrows represents the direction motion of the block in case of the monopolar resonator and the direction of deformation of the block in case of the dipolar resonator. . . .	8
1.6	Construction of the (a) unit cell and (b) structure of the first proposed AMM to include Helmholtz resonators in its design. Taken from (Ref.[15]).	10
1.7	Construction of the (a) unit cell and (b)resonant modes of the decorated membrane AMM introduced by Ma <i>et al.</i> Taken from (Ref.[32]). . . . .	11
1.8	Construction of the composite structure to form first DNG AMM with (a) negative density structure, (b)negative modulus structure, (c) composite structure. Taken from (Ref.[37]). . . . .	12
1.9	Fok and Zhang design for a DNG metamaterial showing (a) the spring rod resonator, (b) the helmholtz resonator and (c) the construction of the unit cell. Taken from (Ref.[39]). . . . .	13
1.10	AMM with anisotropic density suggested by Torrent and Sanchez-Dehesa. Taken from (Ref.[54]). . . . .	14
1.11	The first space coiling AMM as (a) designed by Liang and Li[57] and (b) fabricated and tested by Xie <i>et al.</i> [59] . . . . .	15
1.12	The first 2D acoustic cloak suggested by Cummer and Schurig[62]. . . . .	16
1.13	The first proposed active metamaterial with (a) controllable density and (b) and controllable bulk modulus. Taken from (Ref.[75] and Ref.[77]) . . .	18
1.14	(a) Construction and (b) feedback circuit of the first realized active AMM. Taken from ( Ref.[78]) . . . . .	19
1.15	(a) Construction and (b) feedback circuit of the AMM cell capable of non-reciprocal transmission as designed by Popa and Cumer. Taken from ( Ref.[87]) . . . . .	20

2.1	Different relations between the wavelength and the feature size of the medium it is propagating in. . . . .	24
2.2	Homogenization of AMM. . . . .	24
2.3	Representation of two port networks using (a) the transfer matrix and (b) the scattering matrix. . . . .	26
2.4	Schematic of a layered AMM structure. . . . .	27
2.5	The crystal structure of a piezoelectric material (a) before the poling process and (b) after the poling process . . . . .	30
2.6	Piezoelectric bimorph for the amplification of the displacement of piezoelectric material. . . . .	31
3.1	Construction of the suggested active open loop AMM cell. . . . .	34
3.2	Material model of the suggested 1D active plate-type AMM. . . . .	34
3.3	Four microphone setup for estimating the reflection and transmission coefficients of an acoustic sample. . . . .	41
3.4	Finite element mesh including the impedance tube and the open loop AMM cell. The positions of the virtual microphones are indicated and the open loop AMM cell is highlighted. . . . .	41
3.5	Amplitude and phase of the complex pressure reflection coefficient with no voltage applied to the piezoelectric disk (Black lines with circular markers) and subjected to a static voltage of 75V (Red lines with triangular markers) and 150V (Blue lines with diamond markers). . . . .	42
3.6	Amplitude and phase of the complex pressure transmission coefficient with different voltages applied to the piezoelectric disk $V = 0, 75, 100V$ . . . . .	42
3.7	Transmission loss calculated analytically (Solid) and using the FEM (Dashed) with different voltages applied to the piezoelectric disk $V = 0, 75, 100V$ . . . . .	44
3.8	Real and imaginary components of the (a,b)effective density , (c,d) effective Bulk's modulus and (e,f) effective speed of sound . With no voltage applied to the piezoelectric disk (Black lines with circular markers) and subjected to a static voltage of 75V (Red lines with triangular markers) and 150V (Blue lines with diamond markers). . . . .	45
3.9	The effect of the applied voltage on the real component of (a) the effective density and (b) Bulk's modulus calculated analytically (Solid) and using the FEM (Dashed) at a constant frequency of 600Hz (Black lines with circular markers), 1000Hz (Red lines with triangular markers) and 1400Hz (Blue lines with diamond markers). . . . .	46
3.10	The effect of the variation of the number of samples on the effective density of the material calculated analytically with no applied voltage to all cells. In (a) a constant branch number $m = 0$ is used for all frequencies, while in (b) it is chosen correctly using Kramers-Kronig relationship. . . . .	47
3.11	The effective density calculated from a sample consisting of seven cells ( $N = 7$ ) analytically (Solid) and using the FEM (Dashed) with different voltages applied to the piezoelectric disk $V = 0, 75, 100V$ . . . . .	48
4.1	A new concept for a 2D active membrane-type metamaterial. (a) A visualization for the construction of the suggested 2D AMM. (b) Schematic representation for the 2D building block of the material. (c) Acoustic 2-Port representation for the building block. (d) Schematic representation of the construction of the 1D building block (1D AMM cell). . . . .	52

4.2	A cross section in the finite element mesh of the (a) 1D building block sample with quarter symmetry placed in a square impedance tube, and (b) 2D AMM sample with half symmetry placed in a rectangular impedance tube. . . . .	58
4.3	The effect of applying different voltages on the amplitude of (a) $R$ and (b) $T$ . The analytic two-port values are compared to those obtained from the FEM using one 1D cell in the incident wave propagation direction (x-direction), as well as, one 2D cell with the voltage being varied on the plates normal to the y-direction. . . . .	59
4.4	The analytic and numerical results for the real components of (a) the effective density, (b) effective bulk modulus and (c) the effective speed of sound estimated from (1, 4 and 7) 1D cells placed in the wave propagation direction (x-direction), as well as, one 2D cell while varying the voltage applied to the plates normal to the y-direction. . . . .	60
4.5	The TL estimated from a sample consisting of (a) only one 1D cell and (b) four 1D cells in the propagation direction. The TL is calculated analytically (Lines) and using the FEM (Markers) with different voltages applied to the piezoelectric annulus $V=0,150,300$ V. . . . .	61
4.6	The effect of the applied voltage on the real component of the effective density, which is calculated analytically (Lines) and using the FEM (Markers) for one 1D cell at three different frequencies namely 600,720 and 800 Hz. . . . .	62
4.7	The developed 2-port network model for the reconfigurable waveguide. The “Air” blocks indicate quarter cell sections terminated by the rigid walls of the guide. Incident pressure is applied to the node donated $P_{in}$ . . . . .	63
4.8	The normalized pressure inside the suggested waveguide for an incident acoustic wave of frequency 727 Hz. The pressure is estimated using the FEM (a) and (c) and the analytic network model (b) and (d). The incident excitation and the propagation direction are marked with white arrows. The incident wave is controlled to (a),(b) split between the two ducts and (c),(d) exit from the upper duct only . . . . .	65
5.1	Schematic for the construction of the suggested 1D AMM unit cell. . . . .	69
5.2	An electrical circuit model for piezoelectric layer $k$ connected to an arbitrary circuit represented by its Thevenin’s equivalent . . . . .	74
5.3	A block diagram representing the dynamics of the closed loop cell with adaptive control . . . . .	76
5.4	(a) Schematic for the test setup connections and the construction of the AMM cell (b) Photo of the actual test setup. . . . .	78
5.5	The dispersion effective density of the developed AMM characterized analytically and experimentally. The results obtained without any control applied to the cell are compared to those obtained (a) using controller 1 (Equation (5.47)) with $K_c=-1000$ and $K_c=2500$ and (b) using controller 2 (Equation (5.48)) with $f_c=700$ Hz and $K_c = 4 \times 10^6$ and controller 3 (Equation (5.49)) with $f_c=1300$ Hz and $K_c=-120$ . . . . .	79
5.6	Flowchart for the procedure of the adaption of the cell density based on the incident excitation. . . . .	83

- 
- 5.7 Dispersion plot of the (a) effective density and (b) Bulk modulus of the closed loop AMM cell with the adaptive control algorithm. Three different set points for the controller are compared  $\rho_{desired}=-100 \text{ kg/m}^3$ ,  $\rho_{desired}=0 \text{ kg/m}^3$  and  $\rho_{desired}=100 \text{ kg/m}^3$ . The measured open loop effective density is also plotted as a reference. . . . . 85
- 5.8 Step response of the closed loop AMM cell with the adaptive control algorithm. The density set-point is initially set for zero density and later stepped to  $100 \text{ kg/m}^3$ . This is done for different excitation frequencies. . . . . 85

# List of Tables

3.1	Properties of PZT-5A. . . . .	43
4.1	Summary of the dimensions of the 2D open loop active MAM cell. . . . .	50
4.2	Properties of the materials used in the construction of the 2D open loop active MAM cell. . . . .	50
5.1	Properties of the materials used in the construction of the AMM cell. . . . .	68

# Abbreviations

<b>AMM</b>	<b>A</b> coustic <b>M</b> etamaterial.
<b>SNG</b>	<b>S</b> ingle <b>N</b> egative metamaterial.
<b>DNG</b>	<b>D</b> ouble <b>N</b> egative metamaterial.
<b>TL</b>	<b>T</b> ransmission <b>L</b> oss
<b>dB</b>	<b>D</b> ecibel
<b>FCC</b>	<b>F</b> ace <b>C</b> entered <b>C</b> ube.
<b>1D</b>	<b>O</b> ne <b>D</b> imensional.
<b>2D</b>	<b>T</b> wo <b>D</b> imensional.
<b>3D</b>	<b>T</b> hree <b>D</b> imensional.
<b>FEM</b>	The <b>F</b> inite <b>E</b> lement <b>M</b> ethod.
<b>DNZ</b>	<b>D</b> ensity <b>N</b> ear <b>Z</b> ero.
<b>PZT</b>	<b>L</b> ead <b>Z</b> irconate <b>T</b> itanate.
<b>MAM</b>	<b>M</b> embrane-type <b>A</b> coustic <b>M</b> etamaterial.

# Chapter 1

## Literature Review

### 1.1 Introduction to Acoustic metamaterials (AMM)

Metamaterials are the current focus of a lot of theoretical and experimental work in the fields of electromagnetic, acoustic and elastic wave propagation. They are defined as materials which possess material properties not readily available in nature. To be more specific, the material properties here are those that directly affect the propagation of energy waves inside the material. For electromagnetic waves, they are the permittivity ( $\epsilon$ ) and the permeability ( $\mu$ ), for acoustic waves they are the mass density  $\rho$  and the bulk modulus  $B$ , and for elastic waves they are mass density and the elastic modulus ( $E$ ). For traditional materials, these properties are always positive and are usually isotropic; however, in metamaterials and specifically from the point of view of wave propagation they can have any sign combination. The origin of the concept of metamaterials dates back to 1968 when Veselago[1] imagined the consequences of an electromagnetic material having simultaneous negative permittivity and permeability. He discussed the unusual phenomena such as reverse Doppler effect and reverse Snell's law. At the time of his publication Veselago admitted that there weren't any experimental observations that suggest that such material could exist; however, he discussed several approaches for achieving this. 30 years later, Pendry and his colleagues succeeded in manufacturing materials with negative  $\epsilon$  /positive  $\mu$  [2] and positive  $\epsilon$ / negative  $\mu$  [3]. Later on, Smith *et al.* succeeded in manufacturing the first double negative metamaterial (DNG)[4]. Pendry and Smith did not discover a physical material as Veselago had predicted, they rather engineered structures with feature length much smaller than the wavelength of the

waves propagating through them. These structures could be thought of as effectively homogeneous materials with extraordinary material properties (metamaterials). The structures of the first proposed materials are shown in Figure 1.1. Roughly the same year, Liu *et al.* succeeded in manufacturing the first acoustic metamaterial (AMM)[5]. They used a sub-wavelength structure consisting of hard lead balls coated with soft rubber (Figure 1.2). They claimed that their material could achieve a negative elastic modulus due to the vibration of the lead balls in the rubber. They also demonstrated that their material could break the mass law which states that the sound insulation of ordinary materials, sound transmission loss (TL), increases by 6 decibels (dB) for each doubling of the mass of the material or frequency[6].

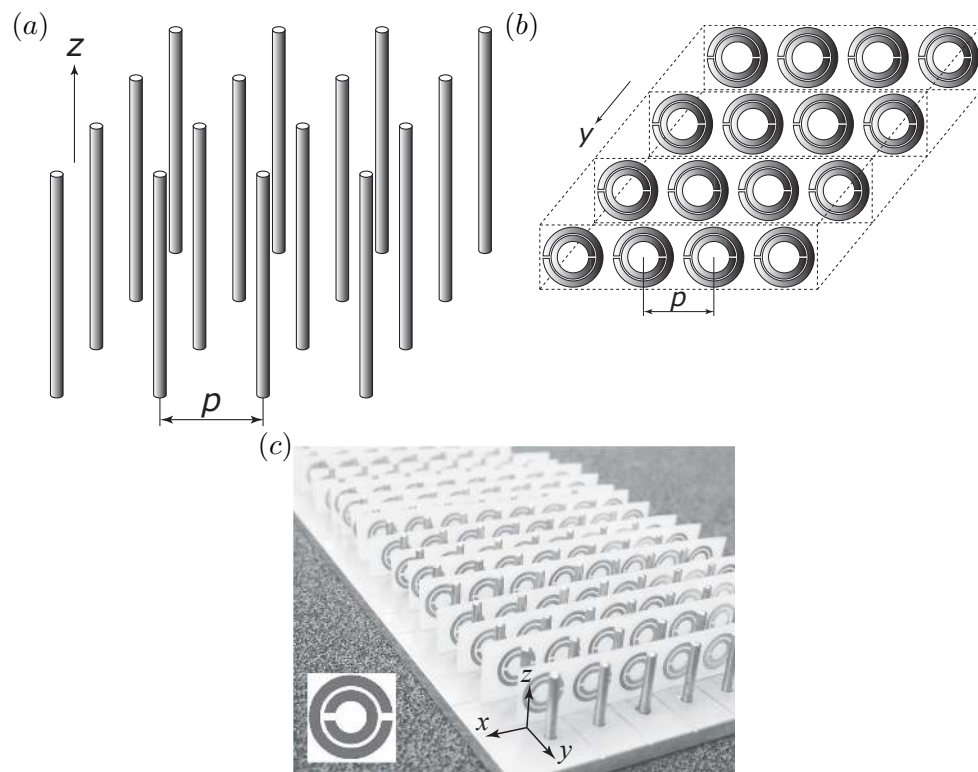


FIGURE 1.1: Construction of the first proposed metamaterials. (a) Thin wire structure exhibiting negative  $\epsilon$  / positive  $\mu$ , (b) split ring resonators exhibiting negative  $\mu$  / positive  $\epsilon$  and (c) double split ring resonator exhibiting double negativity. Taken from (Ref.[7]).

Since then different structure designs for AMM have been suggested, studied and experimentally validated. These designs can be classified into *resonant AMM* which depends on the presence of subwavelength local resonators embedded in the structure of the material, *phononic crystal AMM* which depends on the multiple scattering effects of

subwavelength scatterers and *space coiling AMM* which depends on the effect of constructing a subwavelength maze-like structure to delay the acoustic waves propagating through it.

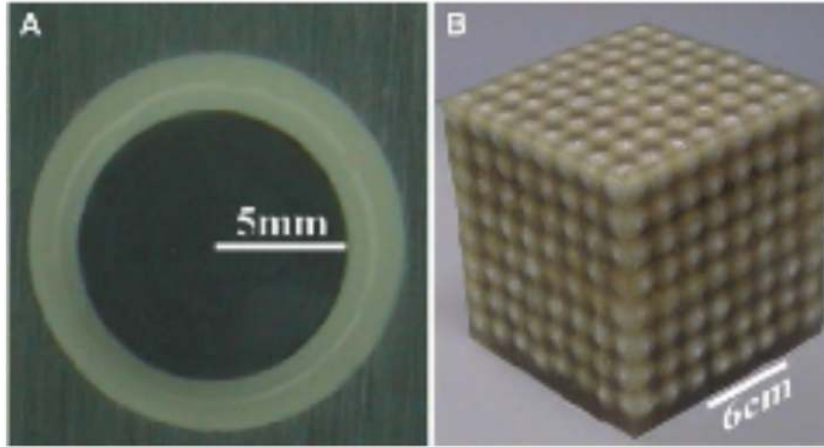


FIGURE 1.2: Construction of the (a) unit cell and (b) structure of the first proposed AMM consisting of silicon rubber coated lead balls in an epoxy matrix. Taken from (Ref.[5]).

## 1.2 Sign Interpretation

Considering an acoustic pressure wave traveling through a homogeneous loss-less stationary fluid, the behavior of the wave could be described by the linearized equations of conservation of mass and conservation of momentum which are given by:

$$\rho \frac{\partial \bar{u}}{\partial t} + \nabla p = 0 \quad (1.1a)$$

$$\frac{1}{B} \frac{\partial p}{\partial t} + \nabla \cdot \bar{u} = 0 \quad (1.1b)$$

where  $p$  is the acoustic pressure,  $\bar{u}$  is the acoustic particle velocity vector,  $\rho, B$  are the density and compressibility of the fluid,  $\nabla$  is the gradient operator and  $(\nabla \cdot)$  is the divergence operator. If we are to consider harmonic fields with time dependence,  $e^{j\omega t}$  then we could write:

$$\bar{u}(\bar{r}, t) = \bar{u}(\bar{r})e^{j\omega t} \quad (1.2a)$$

$$p(\bar{r}, t) = p(\bar{r})e^{j\omega t} \quad (1.2b)$$

Substituting in Equation 1.1 and rearranging we arrive to:

$$\bar{u}(\bar{r}) = \frac{j}{\omega\rho} \nabla p(\bar{r}) \quad (1.3a)$$

$$p(\bar{r}) = \frac{jB}{\omega} \nabla \cdot \bar{u}(\bar{r}) \quad (1.3b)$$

For simplicity without loss of generality we will consider the previous equations in one dimension ( $z$ ) hence:

$$u = j \frac{1}{\omega\rho} \frac{dp}{dz} \quad (1.4a)$$

$$p = j \frac{B}{\omega} \frac{du}{dz} \quad (1.4b)$$

These equations show the mechanism behind acoustic wave propagation in fluids. For traditional materials ( $\rho, B$ ) are both positive. Hence Spatial pressure gradients in Equation 1.4a induce velocity fields whose spatial gradients in turn produces pressure fields in Equation 1.4b. The mechanism repeats as long as the wave propagates in the medium. If we take the divergence of Equation 1.3a and substitute into Equation 1.3b we arrive to the famous Helmholtz wave equation:

$$\nabla^2 p + \frac{\omega^2}{c^2} p = 0 \quad (1.5)$$

where  $c$  is the speed of sound propagation in the fluid medium and is given by:

$$c^2 = \frac{B}{\rho}, c = \pm \sqrt{\frac{B}{\rho}} \quad (1.6)$$

For a plane wave traveling in  $z$  direction, the solution of Equation 1.5 is well known and is given by:

$$p(z) = Ae^{-jkz} + Be^{jkz} \quad (1.7)$$

which represents two waves traveling in the positive and negative directions of  $z$  with a wave number  $k$  given by:

$$k = \frac{\omega}{c} \quad (1.8)$$

For a traditional medium ( $\rho, B$ ) are both positive and frequency independent hence  $c$  is positive and constant and  $k$  is always positive. Metamaterials on the other hand

can be synthesized to have effective density  $\rho_{eff}$  and bulk's modulus  $B_{eff}$  with different sign combinations at specific frequency bands. The possible sign combinations for  $(\rho, B)$  is Traditional Materials (TM)(+, +), Single Negative Metamaterials (SNG) (+, -) or (-, +) and Double Negative Metamaterials (DNG) (-, -). The behavior of traditional materials is well known so we will examine the other sign combinations.

### 1.2.1 Single Negative Metamaterials (SNG)

The behavior of SNG is almost the same for whether  $(\rho, B)$  are  $(-, +)$  or  $(+, -)$ . In either case, the speed of sound in the medium, Equation 1.6, is imaginary and hence the wave number ( $k$ ). The presence of an imaginary wave number in Equation 1.7 produces real exponentials and hence evanescent wave propagation. This leads to the presence of band gaps in the SNG in which the acoustic waves cannot propagate. The mechanism behind this phenomenon is clear in Equation 1.4. Pressure gradients induces particle velocities whose direction depends on the magnitude and sign of  $(\rho, B)$  if we assume  $(\rho < 0, B > 0)$  then the induced particle velocities will induce pressure fields such that they oppose the fields producing them and hence the wave propagation decays.

### 1.2.2 Double Negative Metamaterials (DNG)

In case of DNG the situation is different. Since  $(\rho, B)$  are both negative then the speed of sound  $c$  is real but negative. The negative sign here is with respect to the direction of energy propagation. For traditional non-dispersive materials,  $c$  represents the phase speed of acoustic waves as well as their group velocity (i.e. speed of propagation in the medium). The group velocity for DNG is given by:

$$v_g = \left(\frac{dk}{d\omega}\right)^{-1} = \frac{d}{d\omega}\left(\frac{\omega}{c(\omega)}\right) \quad (1.9)$$

Since  $c$  is function of  $\omega$ , then  $v_g$  is no longer equal to  $c$  and  $c$  is no longer representing the speed of propagation of the acoustic wave in the medium. The fact that  $c$  is negative doesn't mean that the waves are propagating towards the source rather than the direction of the phase propagation is opposite to that of energy propagation.

## 1.3 Classification of AMM

### 1.3.1 Resonant AMM

Resonant AMMs were the first type of AMMs to be realized [5]. They are also the most common type of AMM. Resonant AMM are constructed by creating a metamaterial cell with one or more resonators. These resonators could be mechanical resonators in the form of vibrating elastic objects or acoustic resonators like Helmholtz resonators or quarter wavelength resonators. The material is formed by repeating this unit cell in one or more dimensions. Its properties are studied as if it was a single homogeneous material. The presence of such resonators could produce materials whose acoustic properties are very different from the properties of its individual components. To demonstrate this, we will study a material consisting of a mass ( $M$ )- spring ( $k$ )- damper ( $b$ ) resonator. Assuming an incident acoustic pressure wave on the one dimensional (1D) mechanical resonator shown in Figure 1.3, the acoustic pressure waves will induce a harmonic force  $f(t)$  acting on the system. The vibration of this resonator is of the form:

$$M\ddot{x} + b\dot{x} + kx = f(t) \quad (1.10)$$

Assuming that the dimensions of the resonator is so small that it is considered as a

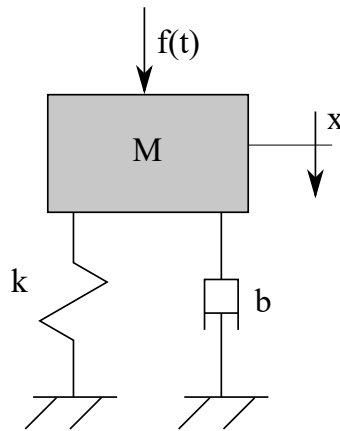


FIGURE 1.3: A simple mass spring damper system.

material with only an effective mass  $M_{eff}$ . This effective mass can be calculated from the relation  $m = \frac{f}{a}$ . This can be done by converting Equation (1.10) to the frequency

domain using Laplace transform:

$$\frac{F(s)}{A(s)} = \frac{Ms^2 + bs + k}{s^2} = M_{eff}(s) \quad (1.11)$$

Equation (1.11) shows that the effective mass of the material formed from this resonator is not constant, but depends on the frequency of the incident acoustic excitation. Figure 1.4 shows a Bode plot of a material formed from such resonator. Below the resonance frequency of the resonator, the phase of  $M_{eff}$  is  $-180$  deg which indicates that the effective mass is, in fact, negative. This is observed, even though all the system properties of the resonator are positive and can be achieved with any ordinary material organized to behave as the resonator in Figure 1.4. Resonant AMM can be further classified depend-

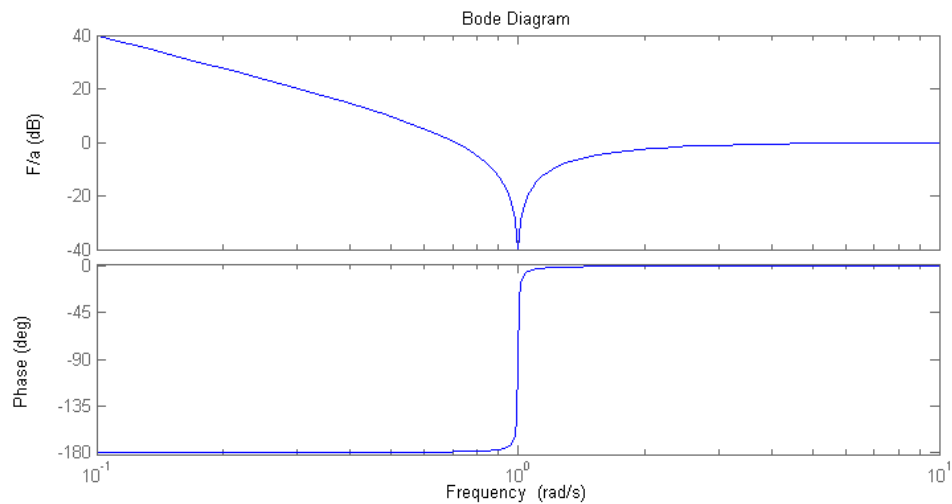


FIGURE 1.4: Bode plot of the effective mass of the system shown in Figure 1.3 with  $M = 1, k = 1, b = 0.01$ .

ing on the resonator type used to create the material. Resonators can be classified to monopolar and dipolar resonators depending on their interaction with the propagating acoustic waves. The classification of dipolar and monopolar resonators depends on the interaction of the resonator with the background fluid as shown in Figure 1.5. It is observed that the presence of a dipolar resonator in the structure of the material affects mainly its effective density, while monopolar resonators affect its bulk modulus. So usually, if it is desired to fabricate DNG metamaterial, both types of resonators are used in the construction of the material at the same time.

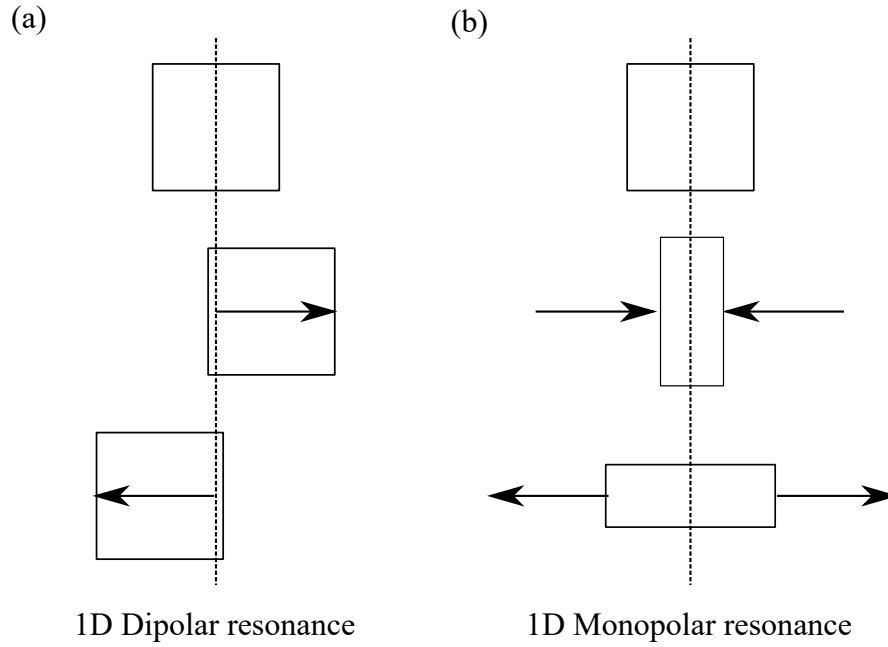


FIGURE 1.5: Comparison between resonators with (a) dipolar resonance and (b) monopolar resonance . The neutral position is shown with the dotted line while the resonator is represented by a block. The arrows represents the direction motion of the block in case of the monopolar resonator and the direction of deformation of the block in case of the dipolar resonator.

### 1.3.1.1 Mass-in-mass AMM

The term mass-in-mass AMM normally refers to the type of AMMs formed by constructing an array of cells consisting of a combination of light material with high elasticity and dense materials with low elasticity. This was first demonstrated by Liu *et al.*[5], when they fabricated the first AMM. They constructed their material from dense lead balls coated with a silicon rubber shell, and used epoxy as a hard background material to join the balls. The experimental estimation of the TL of such material was found to be exceptionally large at frequencies near the resonance of the lead/rubber balls. They attributed this behavior to the assumption that their material achieved a negative effective bulk modulus; however, they didn't provide any theoretical details or quantitative estimation of the effective acoustic properties of their material. It wasn't until later, that they showed analytically that a material with such construction could only achieve negative effective density but not negative effective bulk modulus as they originally speculated[8, 9]. Ding *et al.*[10] proposed a design for a DNG metamaterial. The design consisted of an epoxy background matrix that contains a face centered cube (FCC) array of spheres made of water and another FCC array made from gold rubber coated spheres. The gold rubber coated spheres, being a dipolar resonator, would

achieve negative effective density, while the water spheres, being a monopolar resonator, would cause the bulk modulus to be negative at certain frequency regions. The concept of mass-in-mass in AMM was later extended to elastic wave propagation[11–13]. This includes experimentally evaluating physical mass-spring systems to further analyze the mechanism of wave propagation in materials with negative and zero mass densities[14].

### 1.3.1.2 Acoustic resonator based AMM

An acoustic resonator is usually incorporated in the design of this type of material. Fang *et al.*[15] succeeded in fabricating the first AMM with negative bulk modulus using arrays of Helmholtz resonators placed in a 1D waveguide. As shown in Figure 1.6, Helmholtz resonators are acoustic cavities with a small neck opening. The air in the neck acts as an oscillating mass, while the air in the cavity acts as a spring. Helmholtz resonators are usually connected parallel to a waveguide; thus, they normally act as monopolar resonators which affects mainly the effective bulk modulus of the material. The AMM developed by Fang could achieve a negative bulk modulus in the ultrasonic frequency range around 30 kHz. Different configurations and sizes with similar structures have been later studied. Cheng *et al.*[16] studied the effect of the number of Helmholtz resonators on the bandgap caused by the material. Hu *et al.*[17] extended the theoretical analysis to 2D and 3D arrays of Helmholtz resonators. Lee *et al.*[18] suggested and experimentally verified the first AMM to achieve negative bulk modulus in the audible frequency range below 500 Hz. The structure of their AMM consisted of a 1D waveguide with side slits instead of Helmholtz resonators. Zhang *et al.*[19] used 2D arrays of Helmholtz resonators to construct a flat ultrasonic acoustic lens. Fey *et al.*[20] used an array of 1D detuned Helmholtz resonators to achieve a series of acoustic band gaps. Lemoult *et al.*[21] used a 2D array of Helmholtz resonators made from soda cans to focus audible acoustic waves in air. They showed later that such material could be organized arbitrarily to control the propagation of sound in air, including the construction of subwavelength waveguides[22].

### 1.3.1.3 Membrane/Plate-type AMM

Elastic membranes and plates have been used extensively in the manufacturing resonant AMM with various configurations[23]. The dipolar resonance associated with the vibration of membranes facilitated the fabrication of AMM with negative dynamic mass

densities below the resonance of the membranes. AMM with membranes as resonators are characterized by their simple construction and by being compact and lightweight. Yang *et al.*[24] fabricated the first membrane-type AMM from clamping a thin circular rubber membrane with a center mass disk in a 1D duct. They showed experimentally that their developed material broke the mass law significantly and achieved negative mass density at the frequency region from 100-1000 Hz. Lee *et al.*[25] fabricated a similar structure consisting of 1D periodic membranes, this time without the center mass. The developed material demonstrated negative mass density at the frequency range below the first resonance of the membrane (735 Hz). Naify *et al.* studied the extraordinary transmission loss of membranes with center mass experimentally and using the finite element method (FEM) [26]. They studied the effect of adding center mass rings on increasing the bandwidth of the TL of AMM[27]. They also evaluated the practical limitations of manufacturing a multi-celled panel of membrane-type AMM on the TL, taking into consideration the effect of including a rigid frame to support the membranes[28], and stacking these frames in series[29]. A similar study was done by Yang *et al.*[30] with a variation of the panel dimensions and frame material. Dec-

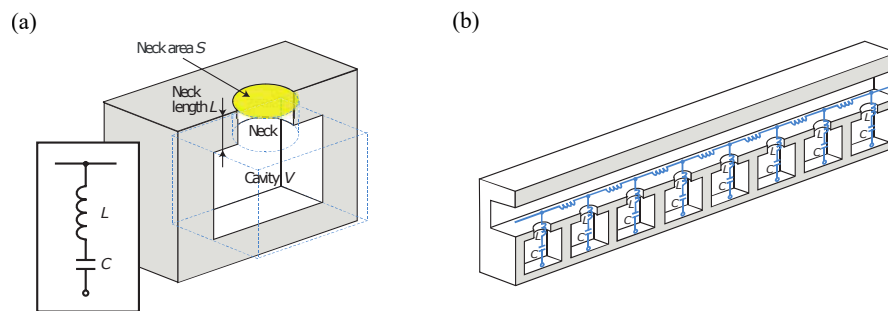


FIGURE 1.6: Construction of the (a) unit cell and (b) structure of the first proposed AMM to include Helmholtz resonators in its design. Taken from (Ref.[15]).

orated membranes, i.e. membranes with attached masses, were used to design nearly perfect sound absorption at low frequencies (10-1000Hz)[31]. At certain frequencies, the impedance of the decorated membrane is matched with that of air, allowing it to absorb and dissipate almost all incident acoustic energy falling on it. Mei *et al.*[31] demonstrated that a single asymmetric decorated membrane panel can absorb up to 86% of the acoustic waves falling on it at 170 Hz, while two layers of the same material can absorb up to 99% of the incident waves. Ma *et al.*[32, 33] improved Mei's design by using center decorated membrane, but this time coupled to an air sealed chamber (Figure 1.7). A single layer of the proposed AMM succeeded in absorbing up to 99% of the acoustic

waves falling on it at a single tunable frequency. On the opposite side, membrane-type AMM can achieve density near zero (DNZ) conditions. DNZ is interpreted as the ability of the material to transport acoustic waves without any phase change. This phenomenon was first used theoretically and numerically by Fleury and Alu[34] to transmit acoustic waves through channels much smaller than their wavelength with nearly no reflection. It was also used by Park *et al.*[35] to create almost invisible walls. This was done by transmitting acoustic waves through a very narrow hole which is much smaller than the dimensions of the incident waves. Gu *et al.*[36] demonstrated that a 2D structure of the material could achieve nearly perfect transmission through sharp corners and efficient wave splitting.

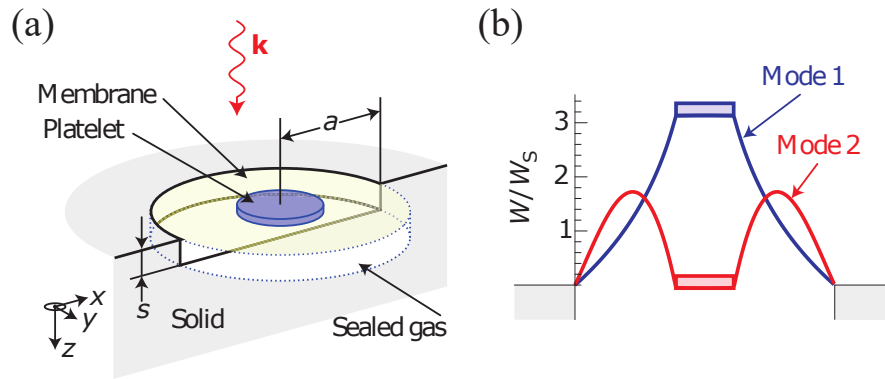


FIGURE 1.7: Construction of the (a) unit cell and (b) resonant modes of the decorated membrane AMM introduced by Ma *et al.* Taken from (Ref.[32]).

#### 1.3.1.4 DNG resonant AMM

As mentioned before, dipolar resonators can be used to create resonant AMM with negative density, and monopolar ones for AMM with negative bulk modulus. Combining the two approaches, one could manufacture a material with double negative properties (Veselago materials). This was first suggested by Lee *et al.*[37], when they manufactured a 1D AMM constructed by merging two of their previous AMM cell designs: a duct with transverse elastic membranes[25] and side holes[18] (Figure 1.8). They demonstrated that their material had double negative properties below 500 Hz by measuring a negative speed of sound at this band. At the same time, they also demonstrated for the first time the reverse Doppler effect long predicted by Veselago. In the region of double negativity, a sound source approaching an observer in their material would appear down-shifted, i.e. with a lower frequency than its actual frequency. This is the exact

opposite of what happens in air and all traditional materials when it appears with a higher frequency. At the same year Bongard *et al.*[38] manufactured a similar material with almost the same structure but with side slits instead of side holes. The double negativity in Bongard's design extended between 600 and 1000 Hz. Fok and Zhang[39] suggested a design of an AMM that could achieve double negativity. Their design, however, did not achieve DNG in their experimental verification, even though it achieved it numerically. This was attributed to the material losses that they didn't incorporate in the numerical simulations. They used, for the first time, two acoustic resonators in the design of AMM. A Helmholtz resonator for monopolar resonance and a spring rod resonator for dipolar resonance (Figure 1.9). The first material to achieve double negativity with membranes/Helmholtz resonator was developed by Seo *et al.*[40]. They could achieve a negative refractive index between -0.06 and -3.7 in the frequency region from 200 to 300 Hz. Yang *et al.*[41] suggested a design for a DNG that didn't involve any acoustic resonator, instead they suggested, and verified numerically, that a design of a AMM cell with two coupled decorated membranes could achieve double negativity. They demonstrated that their structure could achieve monopolar and dipolar resonance at the same time. This was demonstrated for the frequency range between 820-830 Hz. They didn't verify their design experimentally; however, they patented it in 2014[42].

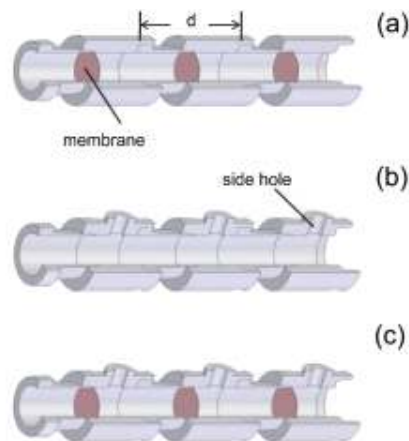


FIGURE 1.8: Construction of the composite structure to form first DNG AMM with (a) negative density structure, (b) negative modulus structure, (c) composite structure. Taken from (Ref.[37]).

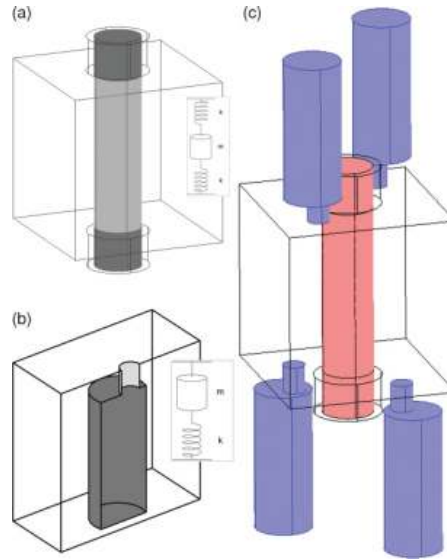


FIGURE 1.9: Fok and Zhang design for a DNG metamaterial showing (a) the spring rod resonator, (b) the helmholtz resonator and (c) the construction of the unit cell. Taken from (Ref.[39]).

### 1.3.2 Non-resonant AMM

#### 1.3.2.1 Phononic crystal based AMM

Phononic crystals are constructed by the periodic placement of scatterers in a background fluid. The periodicity of the scatterers is comparable to the incident acoustic waves; hence, acoustic band gaps due to Bragg scattering are observed. Sonic Crystals have been the focus of a lot of research efforts in the past few decades[43–50]. Phononic crystal based AMM, on the other hand, are constructed using sub-wavelength scatterers. The anomalous effective material properties in this case arise due to the multiple scattering effects in the material. Cervera *et al.* [51] studied an array of subwavelength cylindrical scatterers in air. They used the designed material to fabricate a convex acoustic lens and estimated the speed of sound inside the developed material to be less than that of air. They didn't however attempt to calculate the effective material properties of their developed material. Torrent and Sanchez-Dehesa[52, 53] proposed and experimentally verified an approach to calculate the effective parameters of cylindrical scatterers in air based on the multiple scattering theory. Although the developed material properties were not exceptional, they were different from the volume averaged properties of the cylinders and the background air. Later, they analyzed[54] and realized[55] an AMM with an effective radially anisotropic density. The suggested material consists of a cavity with circular shaped grooves in one of its sides (Figure1.10). They later suggested a

design for a phononic crystal based AMM that can achieve DNZ conditions[56]. They demonstrated acoustic tunneling as one of the potential applications for the developed cell.

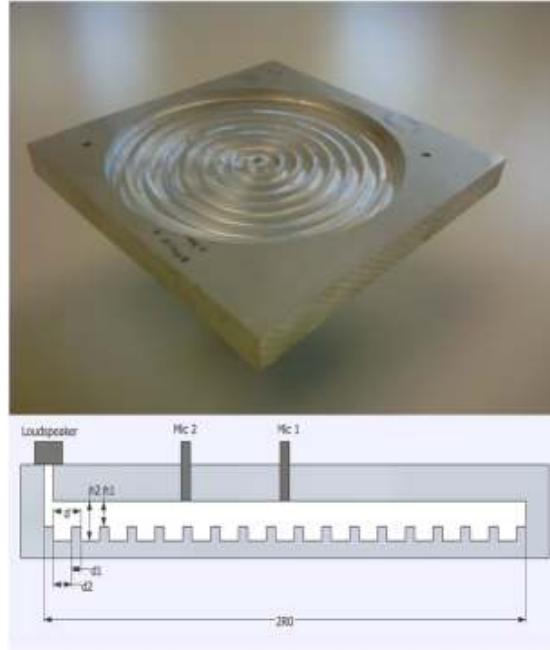


FIGURE 1.10: AMM with anisotropic density suggested by Torrent and Sanchez-Dehesa. Taken from (Ref.[54]).

### 1.3.2.2 Space coiling AMM

The effective material properties of AMMs are observed to depend on how much they can delay the acoustic propagation through them. Based on this observation a relatively new type of AMMs is constructed. Space coiling AMMs are mainly constructed from subwavelength waveguides made from a relatively rigid material. The waveguides are shaped in the form of a maze-like structure, so that the incident acoustic waves propagate through the material in arbitrary paths. By manipulating the length of these paths, the material properties of space coiling AMMs can be tuned to extreme values. Liang and Li[57] introduced space coiling AMMs in 2012. They showed that their introduced material shown in Figure 1.11a was able to achieve double negativity in a very compact structure. Using the developed material, they could achieve a negative refractive index ( $n = -1$ ) and to demonstrate DNZ effects including wave tunneling. Later they used the same approach to numerically demonstrate an acoustic length with a large refractive index and low losses[58]. Xie *et al.*[59] could experimentally verify the results obtained

by Liang and Li by measuring the effective 1D material properties (Figure 1.11b). They also confirmed the negative refraction obtained by the material. Frenzel *et al.*[60] could fabricate 3D space coiling AMM from aluminum waveguides. They demonstrated that the effective speed of sound in their material was much smaller than air in a broadband extending from 1 to 4 kHz. This would allow the fabrication of broadband efficient absorbers. Later Xie *et al.*[61] suggested modified designs for space coiling metamaterials that offered better impedance matching with air than the previous designs.

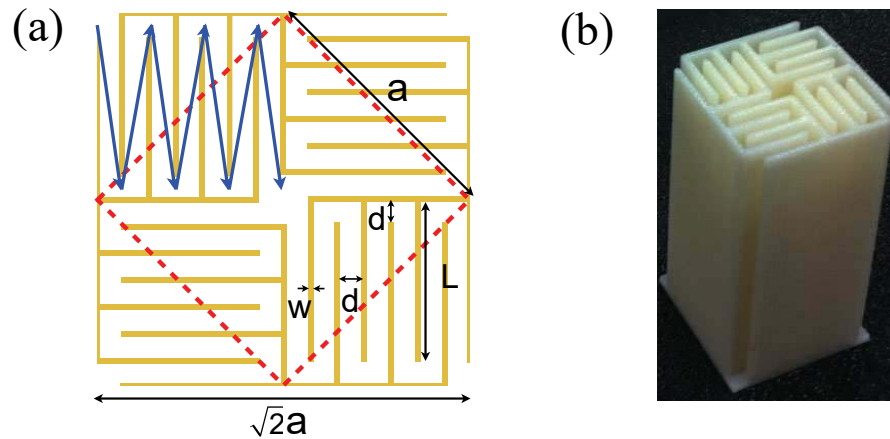


FIGURE 1.11: The first space coiling AMM as (a) designed by Liang and Li[57] and (b) fabricated and tested by Xie *et al.*[59]

## 1.4 Applications of AMM

The ability to create materials with extraordinary material properties paves the way to many interesting applications that were once thought impossible. Some of these applications have already been implemented, others are still discussed in literature and others are yet to come as the topic matures with time.

### 1.4.1 Spatial Manipulation

Coordinate transformation design is an approach to wave propagation control where we want to design a device which causes the acoustic waves propagating through it to take a certain trajectory. The procedure of such approach is by considering a coordinate system that fulfills this functionality and then transforming this coordinate system and

mapping it to the existing coordinates. This mapping step yields the necessary distribution for the material properties required to construct such device. Being a purely mathematical approach, it usually yields distributions that involves negative or even anisotropic material properties. A requirement that is achievable using AMMs.

#### 1.4.1.1 Acoustic Cloaking

One of the most discussed devices that can be designed using this approach are acoustic cloaks. Acoustic cloaks are devices that are manufactured to acoustically hide any objects inside them. This is done by guiding the acoustic waves in a path around the object without causing any reflection, diffraction or absorption of the incident wave (Figure 1.12). Several approaches for the theoretical design of acoustic cloaks have been proposed. Cummer and Schurig[62] showed that the principle of coordinate transformation could be applied to the acoustic domain. They demonstrated this by designing a 2D acoustic cloak that was capable of partially hiding a cylindrical object. Chen and Chan[63] and later Cummer *et al.*[64] extended this concept to 3D object and considered hiding a spherical object using two different approaches. Torrent and Sanchez-Dehesa[65] suggested a structure made from two isotropic radially distributed material to implement the approach suggested by Cummer.

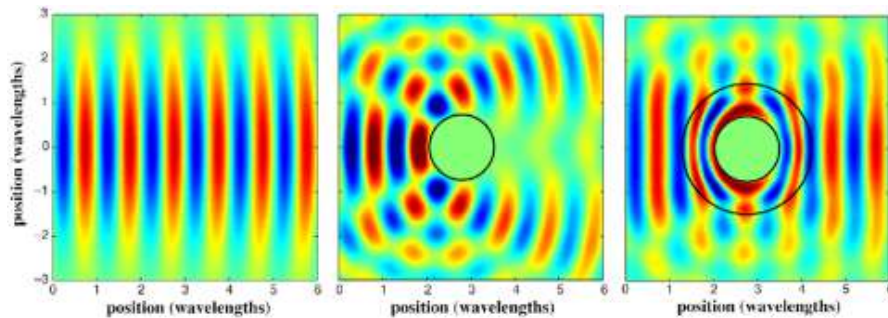


FIGURE 1.12: The first 2D acoustic cloak suggested by Cummer and Schurig[62].

#### 1.4.1.2 Other spatial Devices

With the aid of transformation acoustics techniques, these anomalous properties could be spatially distributed to construct devices which were otherwise difficult to fabricate. An example for such devices are the acoustic beam shifter suggested by Akl and Baz[66] and the field rotator suggested by Chen and Chan[67]

### 1.4.2 Subwavelength acoustic imaging

The diffraction limit states that acoustic waves cannot be focused to less than third the wavelength of the wave. A superlens is a device that overcomes the diffraction limit and has a lot of applications in high resolution acoustic imaging. Subwavelength imaging could be realized using DNG materials[68] by taking advantage of their negative refractive index. It could be also realized using SNG materials with negative density[69–71] using surface waves at an interface with a limited thickness of the material.

### 1.4.3 Perfect Absorption

AMM can achieve impedance matching as well as slow sound propagation. These two phenomena allow for the design of extraordinary sound absorbing devices. Examples of such devices include the already discussed nearly perfect absorbers developed by Ma *et al.*[32, 33] and the use of slow sound in resonator based AMMs as proposed by Groby *et al.*[72].

### 1.4.4 Extraordinary Transmission

DNZ materials can transform acoustic waves with almost zero phase change, this enables the manufacturing of acoustic devices capable of transmitting sound through very narrow channels and steep bends with virtually no losses[34, 35, 73, 74].

## 1.5 Active AMM

The dispersive nature of passive AMM restricts their anomalous characteristics to limited frequency bands. Once the material is fabricated, its properties cannot be tuned or adjusted. This poses many restrictions on the manufacturing process of AMM and requires that they are fabricated by special processes to ensure that they achieve their design targets; moreover, for resonant AMM, since they depend mainly on the local resonance within their structure, they are very sensitive to geometrical defects and their boundary conditions. To overcome these limitations, as well as provide a mean to control the effective properties of the material, active elements have recently been used in AMM

to construct active AMMs. These elements are used to control the material properties of AMMs, and to enhance the frequency range of the desired material properties.

The first active AMM was first suggested by Baz[75, 76] when he suggested a structure based for active acoustic metamaterials consisting of acoustic cavities with walls made of piezoelectric diaphragms connected to a passive electrical circuit (Figure 1.13a). He demonstrated analytically that the newly suggested material could achieve a tunable effective density. Akl and Baz[77] later applied the same approach to design and analyze an active AMM with tunable bulk modulus. The suggested structure consisted of an array of Helmholtz resonators with one of the walls of the resonator replaced by a piezoelectric diaphragm (Figure 1.13b). They were later able to experimentally verify their predicted results[78, 79], when they manufactured an AMM cell consisting of two piezoelectric diaphragms with water as the background fluid. One of the diaphragms was used as a sensor for the incident acoustic excitations and the other was used as an actuator, so that a closed loop is constructed between the diaphragms (Figure 1.14). Through positive and negative feedback, they could shift the resonance of the diaphragm and hence control the effective density of the cell.

Chen *et al.* [80] suggested the use of gradient magnetic fields to actively tune the

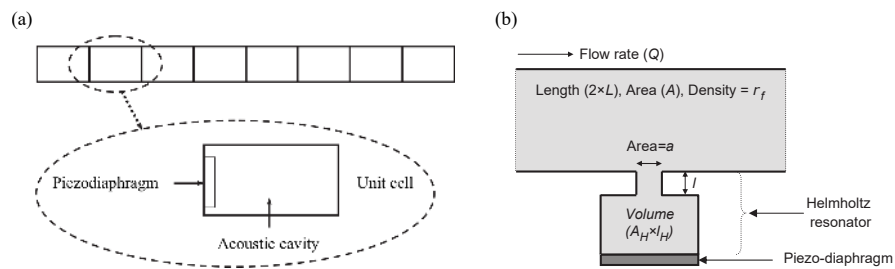


FIGURE 1.13: The first proposed active metamaterial with (a) controllable density and (b) and controllable bulk modulus. Taken from (Ref.[75] and Ref.[77])

material properties of membrane-type AMM. They suggested an active AMM cell made of an aluminum circular ring with a magnetorheological elastomer at the center. They used a magnetic field to control the stiffness of the elastomer and hence the effective density. Their approach however was limited to tuning the effective properties of the cell near the first mode of the membrane. Xiao *et al.* [81] suggested the use of an electric field formed between a fishnet electrode and a metal coated central platelet attached to a circular rubber membrane. Their design required the application of voltages exceeding 300 V to control the effective density within a limited frequency range. In the domain of phononic crystal based AMMs, several designs were suggested for a tunable AMM

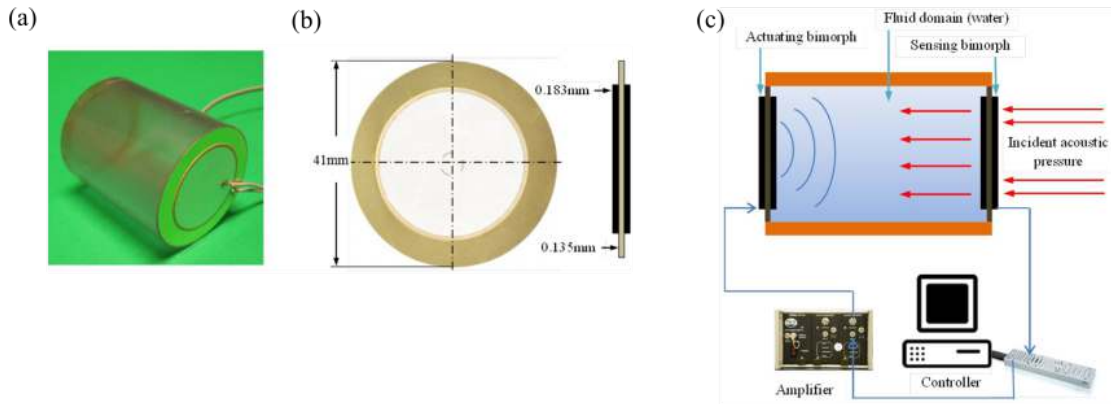


FIGURE 1.14: (a) Construction and (b) feedback circuit of the first realized active AMM. Taken from ( Ref.[78])

by introducing a 1D layered structures that included piezoelectric material layers. By changing the boundary conditions of the layers, the effective material properties could be tuned[82–84].

Chen *et al.*[85] experimentally demonstrated a DNG material whose effective density can be controlled using elastic membranes tensioned by direct current electromagnets. The material had a similar construction to the passive material suggested by Lee *et al.*[37] (Figure 1.8).

The introduction of active AMM has paved the way to a set of additional applications for AMMs. This was demonstrated by the construction of interesting acoustic reconfigurable and programmable devices. Casadei *et al.*[86] used a 2D array of piezoelectric patches shunted on a plate structure to construct a reconfigurable elastic waveguide. Popa and Cummer[87] suggested and experimentally evaluated an active AMM cell that transmits the incident waves in one direction while blocks them in the other direction. Their cell consisted of a piezoelectric diaphragm inserted between two Helmholtz resonators (Figure 1.15). Later Popa *et al.*[88] suggested a similar design for active AMM that could be reconfigured in real-time. They demonstrated their design by constructing a reconfigurable acoustic lens and beam shifter from the developed material. Most of the mentioned approaches however are limited to tuning the original properties of the AMM by shifting the dispersion plots; moreover, they are of open loop nature in the sense that their effective properties can be changed, but they cannot be guaranteed in a closed loop sense. Any change in the operating conditions of the material would require that they are readjusted.

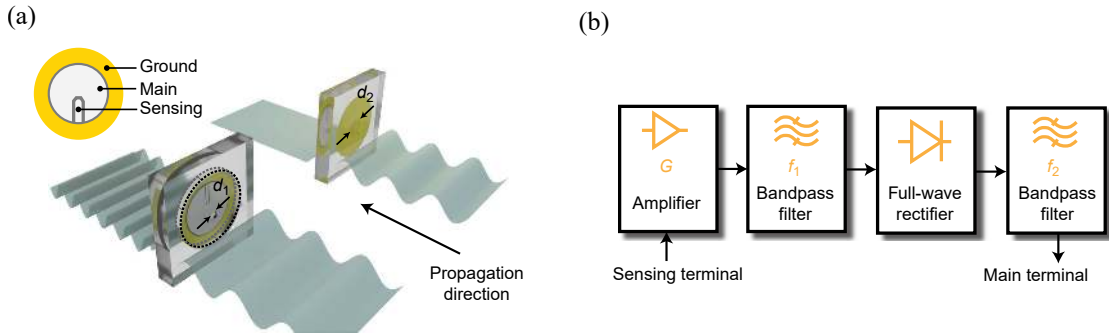


FIGURE 1.15: (a) Construction and (b) feedback circuit of the AMM cell capable of non-reciprocal transmission as designed by Popa and Cumer. Taken from ( Ref.[87])

## 1.6 Problem Statement

To completely manipulate the propagation of acoustic waves in a medium, it must be constructed from a material with acoustic properties  $(\rho, B)$  not readily available in nature (acoustic metamaterials).

The propagation of the wave inside acoustic metamaterials can be controlled by embedding active elements in the structure of the material. The accurate adjustment of the material properties of the metamaterial cell requires the incorporation of a closed loop feedback control system in the design of the material. An approach which has not yet been investigated.

## 1.7 Work Objective

The main objective of the current study is to design, model, simulate and experimentally test a new class of an active acoustic metamaterial with controllable material properties (mass density). The properties of the material should be configurable in real time through the implementation of a closed loop feedback control system. This control system ensures that the achieved material properties are identical to the desired set values.

## 1.8 Scope of Work

1. Review the existing literature covering:

- 
- (a) Passive and active acoustic metamaterials covering the basic concepts that govern their operation in addition to their applications in the control of acoustic wave propagation.
  - (b) Homogenization techniques for the estimation of the effective density and effective bulk modulus of passive AMMs.
2. Review the existing theory covering:
    - (a) Piezoelectric materials and how to model them analytically.
    - (b) Feedback control systems and their applications regarding to acoustic wave propagation control.
  3. Develop a homogenization technique for active acoustic metamaterials.
  4. Develop a 1D active acoustic metamaterial cell with tunable material properties in the low frequency range up to 2 kHz.
  5. Construct a theoretical model to predict the effective properties of the developed cell.
  6. Create a finite element model “FEA” of the cell to simulate its behavior and verify the theoretical model.
  7. Extend the analysis of the 1D AMM cell to 2D and investigate the limitations and potential applications of such system.
  8. Adjust the design of the suggested cell to be able to work in a closed loop manner.
  9. Design a control system for the effective material properties of the active acoustic metamaterial.
  10. Design and conduct the necessary experiments to validate the theoretical and numerical results.
  11. Implement and test the control system to estimate its performance.

## 1.9 Thesis Summary

In this chapter, we introduce the origins of active and passive AMM, discussing the mechanisms behind the extraordinary characteristics of such materials. The main approaches for the design of passive and active AMMs are discussed and the suggested designs present in literature are reviewed. The achieved and potential applications for AMMs are also discussed. In Chapter 2, the theory necessary to model active AMM is reviewed and summarized. This includes the acoustic two-port theory and the homogenization techniques for AMMs. For the active part of the material, the theory of piezoelectricity is reviewed.

In Chapter 3, a design for a 1D plate-type active AMM is introduced and analyzed analytically. A numerical model is also developed to predict the behavior of the material and verify the analytic calculations. The performance of the developed cell is evaluated and the analytic and numerical results are discussed.

In Chapter 4, the previous design is extended to 2D AMM and the analytic and numerical models are further developed to account for the complications of studying the material in two dimensions. The numerical and analytic predictions of the cell are analyzed and compared. An efficient controllable waveguide is constructed and analyzed both numerically and analytically to demonstrate one of the potential applications of the 2D active AMM.

In Chapter 5, a new design for 1D plate-type active AMM is introduced. The new design incorporates a closed loop feedback system for an enhanced control over the material properties of the AMM. An analytic model for the closed loop system is developed and used for the evaluation of the performance of potential controllers. The stability of the material is also discussed. An experimental setup is developed to verify the predicted analytic results and implement the necessary control algorithms. An adaptive control system is designed to manipulate the effective density of the cell in a closed loop manner by adjusting the controller transfer function of developed cell.

In Chapter 6, the main findings of the current work are summarized and discussed. Also, several paths for extending the current work are proposed and discussed.

## Chapter 2

# Theoretical Background

The construction of an active plate-type AMM requires a theoretical background that covers several disciplines, this includes but is not limited to physical acoustics, engineering acoustics, smart materials, mechanics of materials, control engineering, electronics, signal processing and software engineering. This chapter is concerned with the review of the basic theory required to model and analyze passive AMM, as well as, the basic theory behind piezoelectric materials that will be used to construct the active AMM. The necessary theory for the other disciplines will be briefly introduced when encountered in the following chapters.

### 2.1 Analytic modelling of AMM

The analytic approach used to model the acoustic wave propagation depends on the frequency of the waves and the relation between their wavelength and the feature size of the geometry of the medium in which they are propagating. Figure 2.1 shows the possible relations between the wavelength and the feature size of the medium. When the wavelength is much smaller than the dimensions of the medium, it is usually treated as a ray and ray acoustics is used in the analysis of the propagation of the wave. When the wavelength is comparable to the object dimension, especially in the presence of periodicity, Bragg scattering occurs and Bloch's theorem is used to analyze the propagation of the medium. When the dimensions of the object are much smaller than the wavelength, as in the case of metamaterials, homogenization approaches are usually incorporated.

The frequency of the traveling waves below which the medium can be homogenized is often called the low frequency limit or the long wavelength limit. Structures whose dimensions are much less than the wavelength are normally called subwavelength structures. Homogenization is the process in which a composite medium, consisting of two

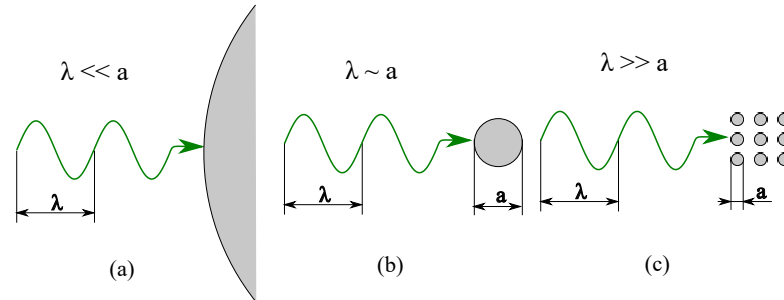


FIGURE 2.1: Different relations between the wavelength and the feature size of the medium it is propagating in.

or more materials organized in a subwavelength structure, is converted to a homogeneous medium with a single effective value for  $\rho$  and  $B$  (Figure 2.2). Several methods

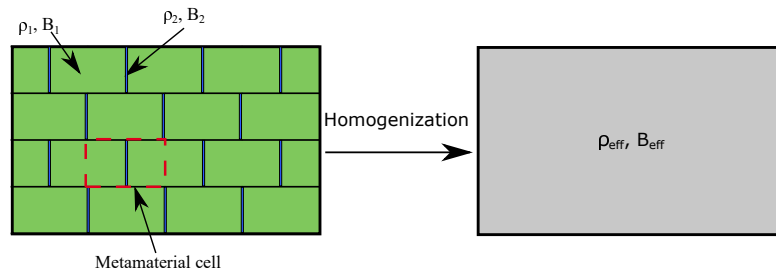


FIGURE 2.2: Homogenization of AMM.

for the homogenization of materials have been proposed in literature[53, 89, 90]. The applicability of a homogenization method depends mainly on the shape and nature of the material structure. In the following sections, some of the most common approaches for the homogenization of metamaterials are introduced and criticized.

### 2.1.1 Volume Averaging

Perhaps the most basic and straight forward method for the calculation of the effective parameters of a composite medium is to consider the volume average of the constitutive components forming the materials. For example, the effective density of a composite material consisting of  $n$  different materials can be given by:

$$\rho_{eff} = \frac{\sum_1^n \rho_i V_i}{\sum_1^n V_i} \quad (2.1)$$

where  $V_i$  is the volume occupied by each component  $i$  of the medium.

While this approach might be suitable for the evaluation of the static material properties of the composite material, it doesn't take into consideration the nature of the propagation of the waves inside the medium. It also doesn't take into consideration the geometry of the structure and the geometrical relations between the different components of the medium. Given the previous limitations, volume averaging cannot be used to homogenize AMM.

### 2.1.2 The multiple scattering theory

The multiple scattering theory describes the propagation of a wave in a medium consisting of a background homogeneous fluid with embedded scatterers made from a different material and placed in arbitrary positions. Considering an acoustic wave incident on the studied medium, the acoustic pressure at any given location in the material is the sum of the incident acoustic excitation in addition to the scattered waves from all scatterers[91]:

$$P(r, \theta) = P^{ext}(r, \theta) + \sum_{\alpha=1}^N P_{\alpha}^{scat}(r, \theta) \quad (2.2)$$

where  $r, \theta$  are the polar coordinates,  $P(r, \theta)$  is the total pressure field,  $P^{ext}(r, \theta)$  is the external incident pressure field,  $P_{\alpha}^{scat}(r, \theta)$  is the scattered pressure field from scatterer  $\alpha$  and  $N$  is the total number of scatterers in the material. Considering only cylindrical scatterers, the scattered waves from each cylinder can be described as the sum of Hankel functions of the first kind[91]:

$$P_{\alpha}^{scat}(r, \theta) = \sum_{q=-\infty}^{\infty} (A_{\alpha})_q H_q(kr_{\alpha}) e^{-jq\theta_{\alpha}} \quad (2.3)$$

where  $j$  is engineering complex number,  $(A_{\alpha})_q$  are coefficients to be determined,  $H_q$  is the  $q$ th order Hankel function and  $(r_{\alpha}, \theta_{\alpha})$  are the polar coordinates with the origin located at the center of cylinder. The determination of the coefficients  $(A_{\alpha})_q$  allows for the estimation of the pressure field inside the material. Torrent and Sanchez-Dehesa[53] suggested a procedure based on the multiple scattering theory to homogenize a material consisting of clusters of rigid cylinder in air. The main drawback of their approach is that it is practically applicable to only cylindrical or spherical scatterers in air. While this might be suitable for homogenizing a limited set of phononic crystal based AMM,

it is not applicable to resonant AMM or any other AMM whose structure is not in the form of a cylinder or sphere.

### 2.1.3 Acoustic two-port theory

The acoustic two-port theory, also known as ‘Acoustic transmission line theory’, is commonly used in acoustics to analyze acoustic duct networks at low frequencies[92]. Since one of the basic assumptions of AMM is the operation in the long wavelength limit, *i.e.* at low frequencies; the acoustic two-port theory has recently been used to characterize AMM for different configurations[38, 93, 94]. One of the main elements of the acoustic two port theory is the transfer matrix ( $\mathbf{T}$ ) which relates the acoustic pressure ( $p$ ) and velocity ( $v$ ) at point  $a$  to the pressure and velocity at point  $b$  (Figure 2.3a) through the relation:

$$\begin{bmatrix} p_a \\ v_a \end{bmatrix} = \mathbf{T} \begin{bmatrix} p_b \\ v_b \end{bmatrix}, \quad \mathbf{T} = \begin{bmatrix} T_{11} & T_{12} \\ T_{21} & T_{22} \end{bmatrix} \quad (2.4)$$

Equation (2.4) is useful when connecting two networks in series as the case in layered

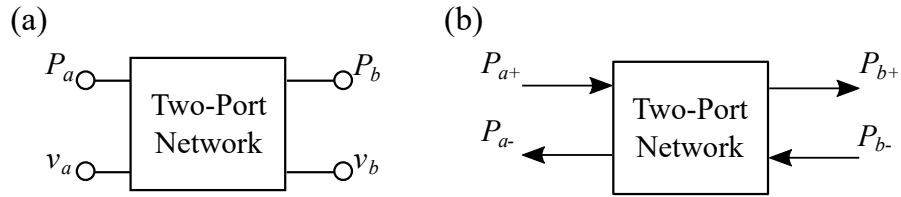


FIGURE 2.3: Representation of two port networks using (a) the transfer matrix and (b) the scattering matrix.

AMM (Figure 2.4). Given a 1D metamaterial cell consisting of  $n$  cascaded layers with different material properties, the transfer matrix of the whole cell can be written as:

$$\mathbf{T}_{cell} = \mathbf{T}_1 \quad \mathbf{T}_2 \quad \dots \quad \mathbf{T}_n \quad (2.5)$$

where  $\mathbf{T}_1, \mathbf{T}_2, \dots, \mathbf{T}_n$  are the transfer matrices of each layer. For an acoustic layer with acoustic impedance  $Z_n$  and thickness  $t_n$ , the transfer matrix can be calculated from the relation [92]:

$$\mathbf{T}_n = \begin{bmatrix} \cos(k_n t_n) & jZ_n \sin(k_n t_n) \\ j \sin(k_n t_n)/Z_n & \cos(k_n t_n) \end{bmatrix} \quad (2.6)$$

where  $k_n = \omega/c_n$  is the wave number of the acoustic wave in layer  $n$ ,  $\omega$  is the angular frequency of the incident acoustic wave,  $c_n$  is the speed of sound in the layer and  $j = \sqrt{-1}$  is the engineering complex number. Another important element of the acoustic two

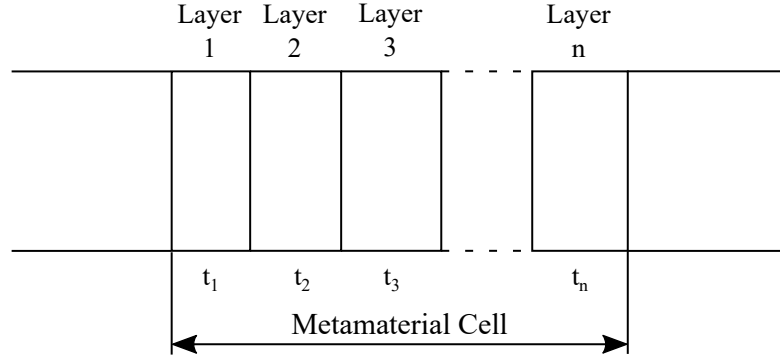


FIGURE 2.4: Schematic of a layered AMM structure.

port theory is the scattering matrix ( $\mathbf{S}$ ) which relates the incident and scattered wave pressures on an acoustic sample (Figure 2.3b). The scattering matrix formulation is given by:

$$\begin{bmatrix} p_a^- \\ p_b^+ \end{bmatrix} = \mathbf{S} \begin{bmatrix} p_a^+ \\ p_b^- \end{bmatrix}, \quad \mathbf{S} = \begin{bmatrix} S_{11} & S_{12} \\ S_{21} & S_{22} \end{bmatrix} \quad (2.7)$$

where  $p_a^\pm, p_b^\pm$  are the complex pressures traveling in the positive and negative directions at points  $a$  and  $b$  respectively. The scattering matrix can be calculated from the elements of the transfer matrix from[95]:

$$\mathbf{S} = \begin{bmatrix} 1 & -T_{11} - \frac{T_{12}}{Z_b} \\ -\frac{1}{Z_a} & -T_{21} - \frac{T_{22}}{Z_b} \end{bmatrix}^{-1} \begin{bmatrix} -1 & T_{11} - \frac{T_{12}}{Z_b} \\ -\frac{1}{Z_a} & T_{21} - \frac{T_{22}}{Z_b} \end{bmatrix} \quad (2.8)$$

where  $Z_a$  and  $Z_b$  are the acoustic impedance at points  $a$  and  $b$ . The elements of the scattering matrix represent the complex pressure reflection and transmission coefficients ( $R$ ,  $T$ ) for incident upstream and downstream acoustic waves. For geometrically symmetric AMM cells the scattering matrix can be written as:

$$\mathbf{S} = \begin{bmatrix} R & T \\ T & R \end{bmatrix} \quad (2.9)$$

### 2.1.4 Retrieval of the effective material properties

The effective material properties of AMM can be estimated by computing the elements of the transfer matrix or the scattering matrix of the material either analytically from the constitutive layers of the cell, experimentally or numerically. These elements are then compared to those of a homogeneous acoustic layer and the material properties are evaluated. Given that the elements of the transfer matrix for an AMM sample are determined, the effective material properties can be estimated using equation (2.6). For example, assuming that the effective parameters are  $Z_{eff}, n_{eff}, t_{eff}$ , they can be determined using:

$$n_{eff} = \frac{\pm \cos^{-1}(T_{11}) + 2\pi m}{k_o t_{eff}}, \quad Z_{eff} = \frac{-jT_{12}}{\sin(n_{eff} k_o t_{eff})} \quad (2.10)$$

where  $n_{eff} = \frac{c_o}{c_{eff}} = \frac{k_{eff}}{k_o}$  is the effective refractive index of the material,  $c_o, c_{eff}$  are the speed of sound in air and the effective speed of sound in the material respectively,  $k_o$  is the acoustic wave number of the incident wave in air,  $m = 0, 1, 2, \dots$ .

An equivalent approach employs the use of the Scattering matrix elements (S-parameters). This approach was first introduced in the electromagnetic domain [96–98] and later adapted to the acoustic domain [89]. It was used to calculate the effective constitutive material properties of an AMM from measuring the S-parameters from a sample consisting of a few number of cells down to a sample consisting of a single symmetric metamaterial cell [93, 99–101].

Using the S-parameters ( $R, T$ ) instead of the transfer matrix elements, the effective parameters  $Z_{eff}, n_{eff}$  can be calculated by [89]:

$$n_{eff} = \frac{-j \ln(\phi) + 2\pi m}{k_o d}, \quad Z_{eff} = \frac{\rho_o c_o q}{1 - 2R + R^2 - T^2} \quad (2.11)$$

where

$$q = \pm \sqrt{(R^2 - T^2 - 1)^2 - 4T^2}, \quad \phi = \frac{1 - R^2 + T^2 + q}{2T} \quad (2.12)$$

$Z_{eff}, n_{eff}$  are related to the effective density and the effective bulk modulus of the AMM ( $\rho_{eff}, B_{eff}$ ) by:

$$Z_{eff} = \rho_{eff} c_{eff}, \quad n_{eff}^2 = \frac{\rho_{eff} c_o^2}{B_{eff}} \quad (2.13)$$

Reordering the equations, the effective properties can thus be calculated from

$$\rho_{eff} = \frac{n_{eff}Z_{eff}}{c_o}, \quad B_{eff} = \frac{Z_{eff}c_o}{n_{eff}} \quad (2.14)$$

Two issues must be addressed before equations (2.10) to (2.14) can be used to uniquely determine the effective material properties of the AMM. The First is the estimation of the sign of  $n_{eff}$ . For passive AMM this issue is addressed by imposing the real part of the acoustic impedance to be positive  $Real(Z) \geq 0$ , or the imaginary component of the refractive index to be negative  $Imag(n_{eff}) \leq 0$ . These constraints are generally not applicable to active AMM; nevertheless, assuming that the input energy to the cell is very small compared to the incident acoustic energy, these conditions should still be applicable. The second issue is the branching problem, which concerns the correct estimation of the branch number  $m$ . Fokin *et al.* [89] suggested determining the effective parameters of a minimum thickness AMM cell, for which  $m$  is zero, and using this solution to estimate higher frequencies. Zhu *et al.* [93] suggested using an iterative approach to ensure the continuity of the parameters. On the other hand, Szabo *et al.* [98] suggested a more rigorous approach to estimate the branch number. They suggested an algorithm based on Kramers-Kronig relationship between the imaginary and real components of  $n$  which uniquely determines the value of  $m$ . While their algorithm was only developed for electromagnetic metamaterials, it was extended to be applied in acoustics[102]. And since it depends on fundamental physical relations based on the principle of causality [103], it can be used directly for the acoustic domain.

## 2.2 Piezoelectricity

Piezoelectricity is the phenomenon in which a material generates electric charges when a mechanical stress is applied to it. Materials that exhibit this phenomenon are called piezoelectric materials. Piezoelectric materials usually exhibit the reverse-piezoelectric effect as well, *i.e.* the material is strained when an electric voltage is applied to them. This direct two-way coupling between the electric and mechanical domains allows their use in many forms of transducers and electric actuators. Piezoelectricity is caused by the crystal structure of the material and its orientation. The atoms of piezoelectric material are arranged in a polarized crystal form, *i.e.* the crystal has negative and positive

polarities. The crystals are normally arranged randomly inside the material and thus the net charge produced by the material is zero. When the grains of the material are oriented in a single direction, the piezoelectric effect is observed. This can happen due to natural causes as in quartz. It also could be artificially synthesized by applying a temporary large electric field to the heated material. This process is called poling the material (Figure 2.5). In practice, poling usually involves subsequent heating above the Curie point, application of the electric field, cooling below the Curie point, and finally removal of the electric field. The electric field orients all the crystals of the material to a single direction called the poling direction. The IEEE 179-1987[104] standard on piezoelectricity denotes to the poling direction by the subscript (1) and the two normal directions are given by the subscripts (2) and (3). Piezoelectric materials can be classified

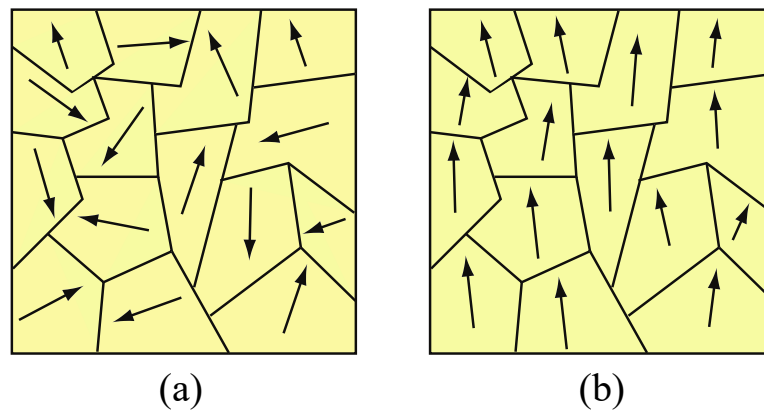


FIGURE 2.5: The crystal structure of a piezoelectric material (a) before the poling process and (b) after the poling process

due to their nature into ceramic and polymer types. Piezoelectric polymers are usually manufactured in the form of ductile films. This makes them more suitable to be used as sensors. Piezoelectric ceramics on the other hand are stiff and brittle, they are more commonly used in composite structures with other materials to enhance their ductility. The most common types of piezoelectric ceramics are Lead Zirconate Titanates (PZT), they are manufactured in different forms including disks, plates, bars and cylinders. The strain caused in ceramic piezoelectric materials due to the applied voltages is usually small compared to their dimensions. When operating as actuators, they are commonly used with other metallic materials in unimorph and bimorph composite configurations. These configurations convert the lateral strain introduced in the material to a bending action in the composite material amplifying the transverse deflections (Figure 2.6).

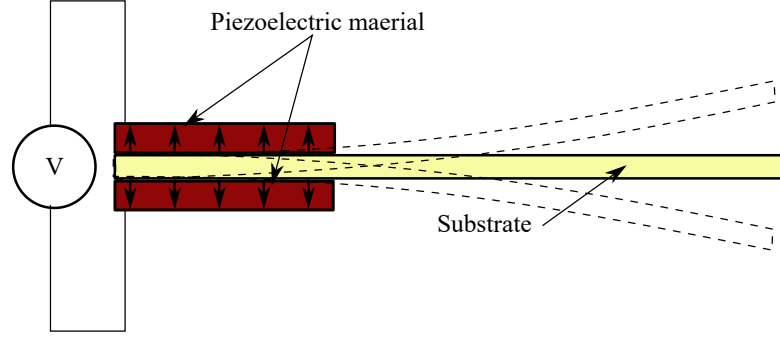


FIGURE 2.6: Piezoelectric bimorph for the amplification of the displacement of piezo-electric material.

The linear theory of piezoelectricity defines the constitutive equations of piezoelectricity in the stress-charge vector form to be given by:

$$\begin{aligned}\sigma_p &= C_{pq}^E S_q - e_{kp} E_k \\ D_i &= e_{iq} S_q + \epsilon_{ik}^S E_k\end{aligned}\quad (2.15)$$

where  $\sigma_p$  are the stress components,  $S_q$  are the strain components,  $D_i$  are the electric displacement components,  $E_k$  are the electric field components,  $C_{pq}$  are the stiffness components,  $e_{kq}$  is the piezoelectric coefficient components and  $\epsilon_{ik}^S$  is the permittivity components. The superscript  $E$  and  $S$  indicates that the coefficient is evaluated at constant electric field and strain respectively. Equations(2.15) can be written in compact matrix form:

$$\begin{bmatrix} \boldsymbol{\sigma} \\ \boldsymbol{D} \end{bmatrix} = \begin{bmatrix} \boldsymbol{C}^E & -\boldsymbol{e}^\sigma \\ \boldsymbol{e} & \boldsymbol{\epsilon}^s \end{bmatrix} \begin{bmatrix} \boldsymbol{S} \\ \boldsymbol{E} \end{bmatrix}\quad (2.16)$$

where  $\boldsymbol{C}^E$  is the elasticity matrix,  $\boldsymbol{\epsilon}$  is the permittivity matrix,  $\boldsymbol{e}$  is the piezoelectric stress/electric field matrix and  $\boldsymbol{\sigma}, \boldsymbol{S}, \boldsymbol{E}, \boldsymbol{D}$  are vectors given by:

$$\boldsymbol{\sigma} = \begin{bmatrix} \sigma_1 \\ \sigma_2 \\ \sigma_3 \\ \sigma_4 \\ \sigma_5 \\ \sigma_6 \end{bmatrix}, \quad \boldsymbol{S} = \begin{bmatrix} S_1 \\ S_2 \\ S_3 \\ S_4 \\ S_5 \\ S_6 \end{bmatrix}, \quad \boldsymbol{E} = \begin{bmatrix} E_1 \\ E_2 \\ E_3 \end{bmatrix}, \quad \boldsymbol{D} = \begin{bmatrix} D_1 \\ D_2 \\ D_3 \end{bmatrix}\quad (2.17)$$

When the material is transversely isotropic, *i.e.* the material properties in the directions (2,3) normal to the polling direction is isotropic, the elasticity matrix is given by:

$$\mathbf{C} = \begin{bmatrix} C_{11} & C_{12} & C_{13} & & & \\ & C_{11} & C_{13} & & & \\ & & C_{33} & & & \\ & & & C_{55} & & \\ & Sym & & & C_{55} & \\ & & & & & C_{66} \end{bmatrix} \quad (2.18)$$

The permittivity matrix is given by:

$$\boldsymbol{\epsilon} = \epsilon_o \begin{bmatrix} \epsilon_{11} & 0 & 0 \\ 0 & \epsilon_{11} & 0 \\ 0 & 0 & \epsilon_{33} \end{bmatrix} \quad (2.19)$$

where  $\epsilon_o$  is the permittivity of free space. The piezoelectric matrix is given by:

$$\mathbf{e} = \begin{bmatrix} 0 & 0 & 0 & 0 & e_{15} & 0 \\ 0 & 0 & 0 & e_{15} & 0 & 0 \\ e_{31} & e_{31} & e_{33} & 0 & 0 & 0 \end{bmatrix} \quad (2.20)$$

The material properties of piezoelectric material may also be given in the strain charge form:

$$\begin{aligned} S_q &= s_{qp}^E \sigma_p + d_{kq}^T E_k \\ D_i &= d_{ip} \sigma_p + \epsilon_{ik}^\sigma E_k \end{aligned} \quad (2.21)$$

$$\begin{bmatrix} \mathbf{S} \\ \mathbf{D} \end{bmatrix} = \begin{bmatrix} \mathbf{s}^E & \mathbf{d}^T \\ \mathbf{d} & \boldsymbol{\epsilon}^\sigma \end{bmatrix} \begin{bmatrix} \boldsymbol{\sigma} \\ \mathbf{E} \end{bmatrix} \quad (2.22)$$

where  $\mathbf{d}$  is the piezoelectric strain/electric field matrix, which is related to the matrix  $\mathbf{e}$  by:

$$\mathbf{e} = \mathbf{dC} \quad (2.23)$$

and  $\mathbf{s} = \mathbf{C}^{-1}$  is the elastic compliance matrix.

## Chapter 3

# Open loop 1D active AMM

Membrane/Plate type Acoustic Metamaterials (MAMs) have a relatively simple cell structure which facilitates their characterization and implementation; nevertheless, they operate in a limited frequency range, moreover because of their resonant nature, they are very sensitive to geometrical variations in the membrane structure and boundary conditions. To overcome these limitations as well as provide a mean to control the effective properties of the material, active elements were recently used in MAMs in order to construct active MAMs. The active elements within the material are used to control its material properties, as well as, to enhance the frequency range of the desired material properties.

In this chapter, we propose a novel design for active MAMs consisting of an active piezoelectric PZT plate with air as a background fluid. The stiffness of the plate is controlled by the application of an electric potential difference across its two surfaces; this enables us to control the effective (homogenized) density of the AMM. This kind of control would open the door for the realization of various devices whose operation depends on the spatial distribution of density between positive and negative values as well as density near zero (DNZ) applications.

This chapter is divided into four sections. In Section 3.1, the construction of the suggested metamaterial cell is introduced, and an analytic model for the deflection of the plate inside the material is discussed. In Section 3.2, a numerical model is constructed using the FEM to verify the analytic model. In Section 3.3, the results obtained from

both models are compared and the overall performance of the new design is evaluated and analyzed. Finally, a summary of the main findings is presented.

### 3.1 Theoretical formulation

A suggested design for a 1D active MAM cell, shown in Figure 3.1, consists of clamped thin circular elastic piezoelectric plates suspended in air. The unit cell is repeated in the wave propagation direction to form the material (Figure 3.2) and its largest feature size is assumed to be much smaller than the wave length of the incident acoustic wave, thus homogenized effective material properties could be used to describe the wave propagation in the material. The material properties of the cell are controlled by applying a static electric voltage across the thickness of the piezoelectric plate. This voltage changes the stiffness of the plate and thus its acoustic impedance and hence the effective material properties of the cell.

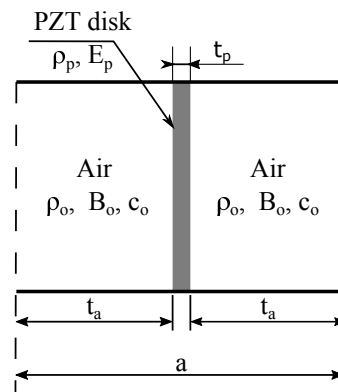


FIGURE 3.1: Construction of the suggested active open loop AMM cell.

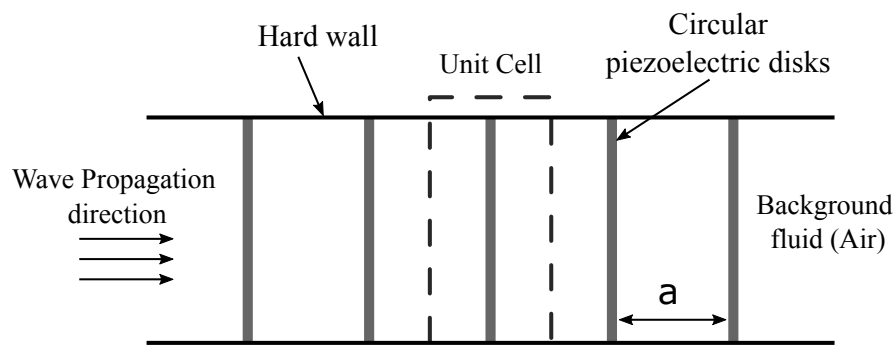


FIGURE 3.2: Material model of the suggested 1D active plate-type AMM.

### 3.1.1 Characterizing the open loop AMM cell

To estimate the effective material properties of a layered AMM cell analytically using Two-port formulation: first, the local transfer matrix of every layer is calculated depending on the nature of the layer. The transfer matrix of the whole metamaterial cell is then estimated using Equation (2.5) and converted to the scattering matrix form. Finally, the complex pressure and reflection coefficients are estimated using (2.9) and inserted into Equations (2.11) to (2.14) in order to estimate the effective material properties.

The suggested cell, shown in Figure 3.1, consists of three layers, two of them are just straight acoustic layers and thus their transfer matrices can be easily determined from Equation (2.6). In order to determine the transfer matrix of the third layer which is the elastic plate, the thickness of the plate ( $t_p$ ) is assumed to be small enough compared to the width of the cell ( $a$ ) and the incident wavelength; Thus, it could be assumed as a lumped element with lumped impedance ( $Z_p$ ). For a lumped element, the transfer matrix is given by ([92]):

$$T = \begin{bmatrix} 1 & Z \\ 0 & 1 \end{bmatrix} \quad (3.1)$$

where the acoustic impedance of a lumped element ( $Z$ ) can be calculated from:

$$Z = \frac{p}{v} \quad (3.2)$$

Since the traverse velocity of the elastic plate is not uniform across its cross-section, the averaged velocity over the area of the plate ( $\tilde{v}$ ) is used to estimate the acoustic impedance of the plate.

The acoustic impedance of passive clamped elastic plates is a classical problem in acoustics ([105]), however we shall consider the active case where the plate is subjected to in-plane stresses caused by the piezoelectric effect.

Considering a circular piezoelectric plate with very thin metallic electrodes plated to its upper and lower surfaces. The plate is subjected to a static voltage  $V$  applied between the two metallic electrodes. The dynamics of the plate will be approached as an elastic plate with constant uniform in-plane stresses caused by the piezoelectric effect due to

the applied static voltage. For a transversely isotropic thin plate, Equation (2.16) can be reduced to ([106]):

$$\begin{bmatrix} \sigma_{11} \\ D_3 \end{bmatrix} = \begin{bmatrix} \bar{Q}_{11} & -\bar{e}_{31} \\ \bar{e}_{31} & \bar{\epsilon}_{33} \end{bmatrix} \begin{bmatrix} s_{11} \\ E_3 \end{bmatrix} \quad (3.3)$$

where  $\sigma_{11}$  is the longitudinal stress,  $E_3, D_3$  is the components of the electric field and the electric displacement in the thickness direction, and

$$\begin{aligned} \bar{Q}_{11} &= C_{11} - \frac{(C_{13})^2}{C_{33}}, & \bar{e}_{31} &= e_{31} - \frac{C_{13}e_{33}}{C_{33}} \\ \bar{\epsilon}_{33} &= \epsilon_{33} + \frac{e_{33}^2}{C_{33}} \end{aligned}$$

The stress  $\sigma$  in the plate due to the applied electric field in the thickness direction can then be given by:

$$\sigma = -\bar{e}_{31}E_3 \quad (3.4)$$

Hence, the in-plane stress due to an applied static voltage  $V$  across the electrode can be given by:

$$\sigma = \frac{-\bar{e}_{31}V}{t_p} \quad (3.5)$$

For a Kirchhoff plate subject to a uniform in-plane stress, the equation of motion for the free transverse vibration of the plate could be written as ([107]):

$$\begin{aligned} \rho_p t_p \frac{d^2 w(r, \theta, t)}{dt^2} + D_a \nabla^4 w(r, \theta, t) - T \nabla^2 w(r, \theta, t) \\ = P(r, \theta, t) \end{aligned} \quad (3.6)$$

where  $\rho_p$  is the mass density of the plate material,  $t_p$  is the thickness of the plate,  $w(r, \theta, t)$  is the transverse deflection of the plate,  $T$  is the in-plane force per unit tangent length which is given by:

$$\begin{aligned} T &= \sigma t_p \\ &= -\bar{e}_{31}V \end{aligned} \quad (3.7)$$

$D_a$  is the anisotropic flexural rigidity of the plate and for a transversely isotropic plate it is given by:

$$D_a = \frac{\bar{Q}_{11} t_p^3}{12} \quad (3.8)$$

For a plate under forced harmonic excitation, Equation (3.6) can be modified to:

$$\begin{aligned} \rho_p t_p \frac{d^2 w(r, \theta, t)}{dt^2} + D_a \nabla^4 w(r, \theta, t) - T \nabla^2 w(r, \theta, t) \\ = P(r, \theta, t) \end{aligned} \quad (3.9)$$

where  $P(r, \theta, t)$  is the pressure difference across the plate due to incident acoustic waves.

If viscous damping is to be considered, Equation (3.9) can be written as:

$$\begin{aligned} \rho_p t_p \frac{d^2 w(r, \theta, t)}{dt^2} + 2\beta \frac{dw(r, \theta, t)}{dt} + D_a \nabla^4 w(r, \theta, t) \\ - T \nabla^2 w(r, \theta, t) = p(r, \theta, t) \end{aligned} \quad (3.10)$$

where  $\beta$  is the viscous damping coefficient. For harmonic excitation, the incident acoustic pressure and the deflection of the plate could be written as:

$$p(r, \theta, t) = P(r, \theta) e^{j\omega t}, \quad (3.11)$$

$$w(r, \theta, t) = W(r, \theta) e^{j\omega t} \quad (3.12)$$

Substituting in Equation (3.10) and canceling the exponential:

$$\begin{aligned} -\rho_p t_p \omega^2 W(r, \theta) + 2j\beta\omega W(r, \theta) + D_a \nabla^4 W(r, \theta) \\ - T \nabla^2 W(r, \theta) = P(r, \theta) \end{aligned} \quad (3.13)$$

Reordering:

$$\left( \nabla^4 - \frac{T}{D_a} \nabla^2 - g^4 \right) W(r, \theta) = \frac{P(r, \theta)}{D_a} \quad (3.14)$$

where  $g$  is the complex wave number of the flexural waves traveling through the plate:

$$g^4 = \frac{\rho_p t_p \omega^2 - 2j\beta\omega}{D_a} \quad (3.15)$$

The solution of Equation (3.13) can be written as the sum of the solution of the homogeneous equation and the solution of the particular equation. The homogeneous equation is written as:

$$\left( \nabla^4 - \frac{T}{D_a} \nabla^2 - g^4 \right) W(r, \theta) = 0 \quad (3.16)$$

Since  $\nabla$  is a linear operator Equation (3.16) can be written in the form:

$$(\nabla^2 - g_1^2)(\nabla^2 + g_2^2)W(r, \theta) = 0 \quad (3.17)$$

where:

$$g_1^2 = \frac{T + \sqrt{4D_a^2g^4 + T}}{2D_a} \quad (3.18)$$

$$g_2^2 = \frac{-T + \sqrt{4D_a^2g^4 + T}}{2D_a} \quad (3.19)$$

For a polar coordinate system whose origin is at the center of the circular plate the solution of Equation (3.16) is given by:

$$W(r, \theta) = W_n(r) \cos(n\theta) \quad (3.20)$$

$$W_n(r) = A_n J_n(g_1 r) + B_n I_n(g_2 r) \quad (3.21)$$

where  $J_n()$ ,  $I_n()$  are the Bessel function and the modified Bessel function of the first kind. Considering acoustic waves incident normal to the plate can only excite axi-symmetric modes ([108]), Equation (3.21) can be further reduced to:

$$W(r) = A J_0(g_1 r) + B I_0(g_2 r) \quad (3.22)$$

Adding the particular solution to the homogeneous solution. The solution of Equation (3.13) is then:

$$W(r) = A J_0(g_1 r) + B I_0(g_2 r) - \frac{P}{D_a g^4} \quad (3.23)$$

The values of  $A$  and  $B$  can be determined from the boundary conditions of the plate. For a clamped boundary:

$$W(b) = 0, \quad \left. \frac{dW}{dr} \right|_{r=b} = 0 \quad (3.24)$$

where  $b$  is the radius of the plate. Substituting in Equation (3.23) with the boundary conditions then we get:

$$0 = A J_0(g_1 b) + B I_0(g_2 b) - \frac{P}{D_a g^4} \quad (3.25)$$

$$0 = -A g_1 J_1(g_1 b) + B g_2 I_1(g_2 b) \quad (3.26)$$

Then

$$A = \frac{Pg_2I_1(g_2b)}{D_ag^4(g_2J_0(g_1b)I_1(g_2b) + g_1J_1(g_1b)I_0(g_2b))}$$

$$B = \frac{Pg_1J_1(g_1b)}{D_ag^4(g_2J_0(g_1b)I_1(g_2b) + g_1J_1(g_1b)I_0(g_2b))}$$

For convenience let  $A = MP$ ,  $B = NP$  then:

$$M = \frac{g_2I_1(g_2b)}{D_ag^4(g_2J_0(g_1b)I_1(g_2b) + g_1J_1(g_1b)I_0(g_2b))}$$

$$N = \frac{g_1J_1(g_1b)}{D_ag^4(g_2J_0(g_1b)I_1(g_2b) + g_1J_1(g_1b)I_0(g_2b))}$$

The solution of the equation of motion of the clamped plate is then:

$$W(r) = P \left( MJ_0(g_1r) + NI_0(g_2r) - \frac{1}{D_ag^4} \right) \quad (3.27)$$

To calculate the acoustic impedance of the plate, it is required to calculate its area averaged displacement  $\widetilde{W}$  which is given by:

$$\begin{aligned} \widetilde{W} &= \frac{1}{Area} \int_0^b W(r) dA \\ &= \frac{P}{\pi b^2} \int_0^b P(MJ_0(g_1r) + NI_0(g_2r) - \frac{1}{D_ag^4}) \cdot 2\pi r dr \\ \widetilde{W} &= P \left( \frac{2MJ_1(g_1b)}{g_1b} + \frac{2NI_1(g_2b)}{g_2b} - \frac{1}{D_ag^4} \right) \end{aligned} \quad (3.28)$$

The averaged velocity of the membrane  $\widetilde{v}$  is then given by:

$$\widetilde{v} = j\omega\widetilde{W} = j\omega P \left( \frac{2MJ_1(g_1b)}{g_1b} + \frac{2NI_1(g_2b)}{g_2b} - \frac{1}{D_ag^4} \right) \quad (3.29)$$

The acoustic impedance of the plate is thus given by:

$$Z_p = \frac{P}{\widetilde{v}} = \frac{1}{j\omega \left( \frac{2MJ_1(g_1b)}{g_1b} + \frac{2NI_1(g_2b)}{g_2b} - \frac{1}{D_ag^4} \right)} \quad (3.30)$$

## 3.2 The finite element model

To validate the analytic approach, a 3D piezo-acoustic finite element model is constructed using ANSYS® commercial software. The model is constructed to mimic the

4-Microphone experimental procedure for the evaluation of the normal incidence sound transmission ([109, 110]). The model consists of one or more structural circular plates placed in a circular impedance tube of the same radius (Figure 3.4). Since the whole model has quarter symmetry only a quarter sector of the tube and the plate is modeled and symmetry boundary conditions are applied to the structural and acoustic domains. The impedance tube is modeled as two acoustic domains (Upstream and Downstream), each domain is discretized using 20-node brick acoustic elements (FLUID220), and the length of each domain is taken to be 500mm long. The piezoelectric plates are discretized using 20-node brick coupled-field structural elements (SOLID226). The element size in the acoustic domain is chosen to follow the rule that there should be at least six elements per wave length at the maximum frequency. The maximum frequency allowed in the analysis is limited by two factors:

1. To maintain plane wave propagation in the impedance tube the upper frequency limit should be defined as follows ([110]):

$$f_u < \frac{0.586c_o}{d} \quad (3.31)$$

where  $c_o$  is the speed of sound in the tube and  $d$  is the diameter of the tube.

2. The homogenization limit of the AMM cell which is chosen so that the wavelength of the incident wave is at least an order of magnitude larger than the largest dimension of the cell in the propagation direction *i.e.*:

$$f < \frac{c_o}{10a} \quad (3.32)$$

where  $a$  is the width of the AMM cell.

The element size of the piezoelectric domain is chosen so that the error between the estimated first three modes of the circular plate using the analytic approach and that evaluated using modal analysis is less than 1%. An infinite surface boundary condition is applied at the ends of the impedance tube to model the anechoic terminations suggested by the ASTM-E2611 procedure while hard wall boundary conditions are applied to its external surface to account for the symmetry of the model. The structural displacements along the circumference of the plate are set to zero to ensure the clamped boundary

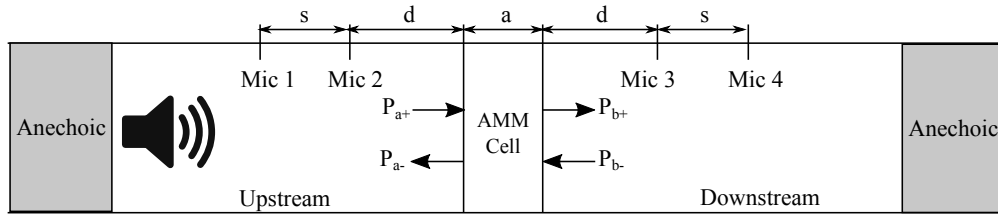


FIGURE 3.3: Four microphone setup for estimating the reflection and transmission coefficients of an acoustic sample.

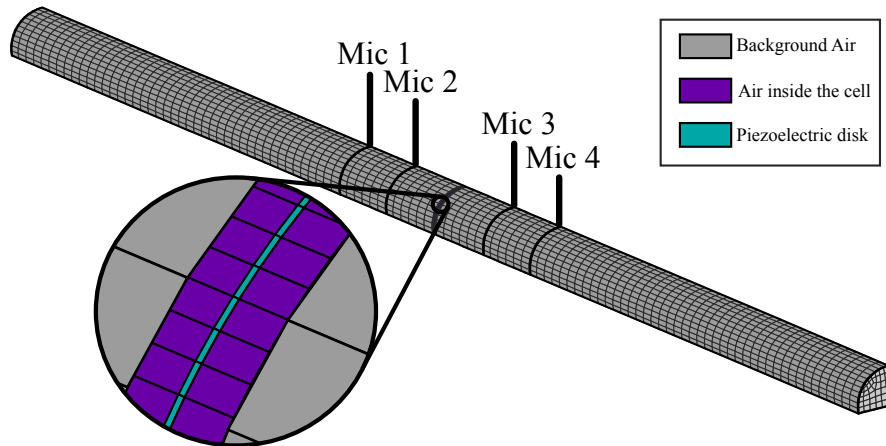


FIGURE 3.4: Finite element mesh including the impedance tube and the open loop AMM cell. The positions of the virtual microphones are indicated and the open loop AMM cell is highlighted.

conditions. Also, for each surface of the plate, the voltage degree of freedom is coupled to simulate the effect of the presence of thin metallic electrodes. The solution is done in two steps; The stresses on the piezoelectric plate due to the applied voltage are determined using a static structural solution, then the voltage is removed and the stresses calculated in the first step are applied as pre-stresses in a linear perturbation harmonic analysis with incident acoustic pressure waves ([111]). The harmonic analysis is carried out at frequencies ranging between 250 Hz and 2000 Hz with a frequency step of 5 Hz. The AMM sample is excited twice using a surface acoustic velocity source located once at the upstream end of the tube and the other at the downstream end. Its response is then captured by four virtual microphones located at the positions shown in Figure 3.3 and 3.4, the distances  $s, d$  are chosen as per the guidelines of the ASTM-E2611[110].

The readings of the four microphones are recorded and converted to the S-matrix using the procedure found in [109].

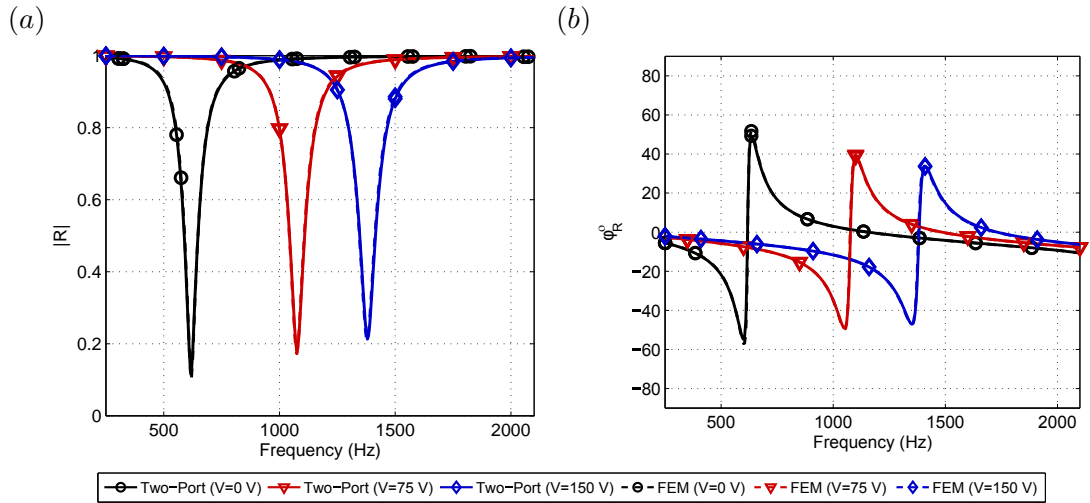


FIGURE 3.5: Amplitude and phase of the complex pressure reflection coefficient with no voltage applied to the piezoelectric disk (Black lines with circular markers) and subjected to a static voltage of 75V (Red lines with triangular markers) and 150V (Blue lines with diamond markers).

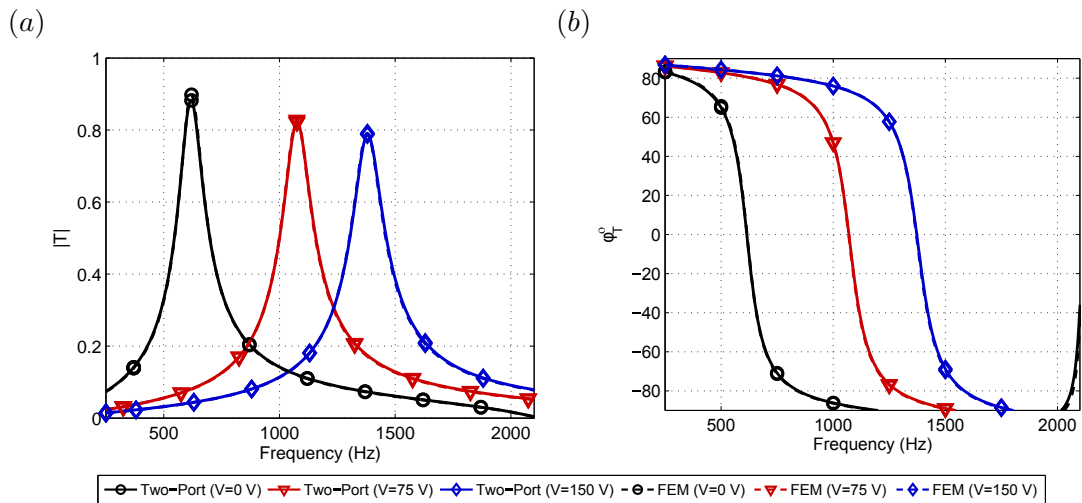


FIGURE 3.6: Amplitude and phase of the complex pressure transmission coefficient with different voltages applied to the piezoelectric disk  $V = 0, 75, 100V$ .

### 3.3 Results and discussion

#### 3.3.1 Characterization of a single cell

A single AMM cell with the construction shown in Figure 3.1 is used as a test case to compare the analytic results obtained from the two port approach and the results are compared to that obtained from the FEM. The dimensions of the cell used in the comparison are  $a = 5mm$ ,  $t_p = 125\mu m$  and radius  $r = 17mm$ . The piezoelectric disk is made of PZT-5A with the material properties given in Table 3.1.

TABLE 3.1: Properties of PZT-5A.

Property	Unit	Value
$\rho$	kg/m <sup>3</sup>	7500
$C_{11}$	GPa	132
$C_{12}, C_{23}$	GPa	73
$C_{33}$	GPa	115
$e_{31}$	C/m <sup>2</sup>	-4.1
$e_{33}$	C/m <sup>2</sup>	14.3
$e_{15}$	C/m <sup>2</sup>	10.5
$\epsilon_{11}$		804.6
$\epsilon_{33}$		659.7
$Q_m = \eta^{-1}$		50

A comparison between the amplitude and phase of the complex reflection coefficient obtained by the use of acoustic 2-Port model and that obtained using the FEM, for three different values of applied voltages, is shown in Figure 3.5. Excellent agreement is observed between the two methods for the range of applied voltages. The same comparison is shown in Figure 3.6 but for the complex transmission coefficient. Figure 3.7 shows the TL of one cell under three different applied voltages. The TL is defined as:

$$TL = 20 \log_{10} \left( \frac{1}{S_{21}} \right) \quad (3.33)$$

It should be noted that the trend of the transmission loss in Figure 3.7 agrees with the general trend reported for the measured TL of circular elastic plates clamped in ducts ([105]). The real and imaginary components of the effective material properties, mainly the effective density, bulk modulus and speed sound calculated from the complex reflection and transmission coefficients are shown in Figure 3.8. The real component of the speed of sound (Figure 3.8e), which represents the phase velocity of the sound waves inside the AMM, vanishes below the natural frequency of the piezoelectric disk. This indicates the presence of stop band in this frequency region, which is similar to what was measured experimentally by Lee *et al.* [25] for a membrane type AMM. The effect of the applied voltage on the effective bulk modulus (Figure 3.8c) for frequencies less than (900 Hz) is very small compared to its effect on the effective density (Figure 3.8a), this gives the ability to control the density of the AMM with minimal effect on the bulk modulus which facilitates using transformation acoustic techniques in the fabrication of acoustic devices, for example, the realization of acoustic cloaks. Figure 3.8a shows that with no applied voltage on the piezoelectric plate, and for a frequency range between

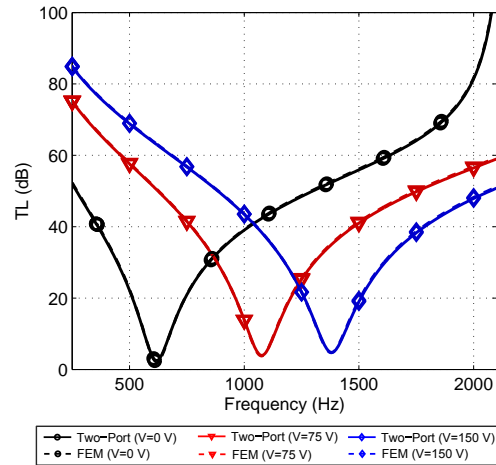


FIGURE 3.7: Transmission loss calculated analytically (Solid) and using the FEM (Dashed) with different voltages applied to the piezoelectric disk  $V = 0, 75, 100V$ .

200-1500 Hz, the effective density of the membrane ranges increases from large negative values (about  $-1500\text{kg/m}^3$ ) passing by zero density at around 616 Hz up to large positive values ( $2000\text{kg/m}^3$ ) with the increase of the frequency. By applying an electric voltage, we can shift the resonance of the piezoelectric plate and thus the dispersion of the density. The magnitude of the shift is dependent on the magnitude of the applied voltage. If we consider controlling the effective density for a single frequency, Figure 3.9a shows the dependency of the effective density, as well as the bulk modulus (Figure 3.9b), within the cell on the applied voltage at different frequencies. For a frequency of 600 Hz (just below the resonance of the piezoelectric plate under zero voltage) the relation between the applied voltage and the density is almost linear, up to a voltage of 300 V, with a sensitivity of  $-3.9\text{kg/m}^3/\text{V}$ . This means that a simple controller can be used to adjust the density of the cell around this frequency. For higher frequencies, just below what is called the anti-resonance frequency of plate, the density of the plate is very sensitive to low applied voltages, while it is less sensitive for higher voltages. However, it should be noted that with a suitable value of applied voltage, the effective density at this frequency range can be controlled to vary between large positive and large negative values. The sensitivity of the effective bulk modulus to the applied voltage is very low compared to its effect on the density; this is suitable for devices whose operation depends on the spatial distribution of the density with a nearly constant bulk modulus.

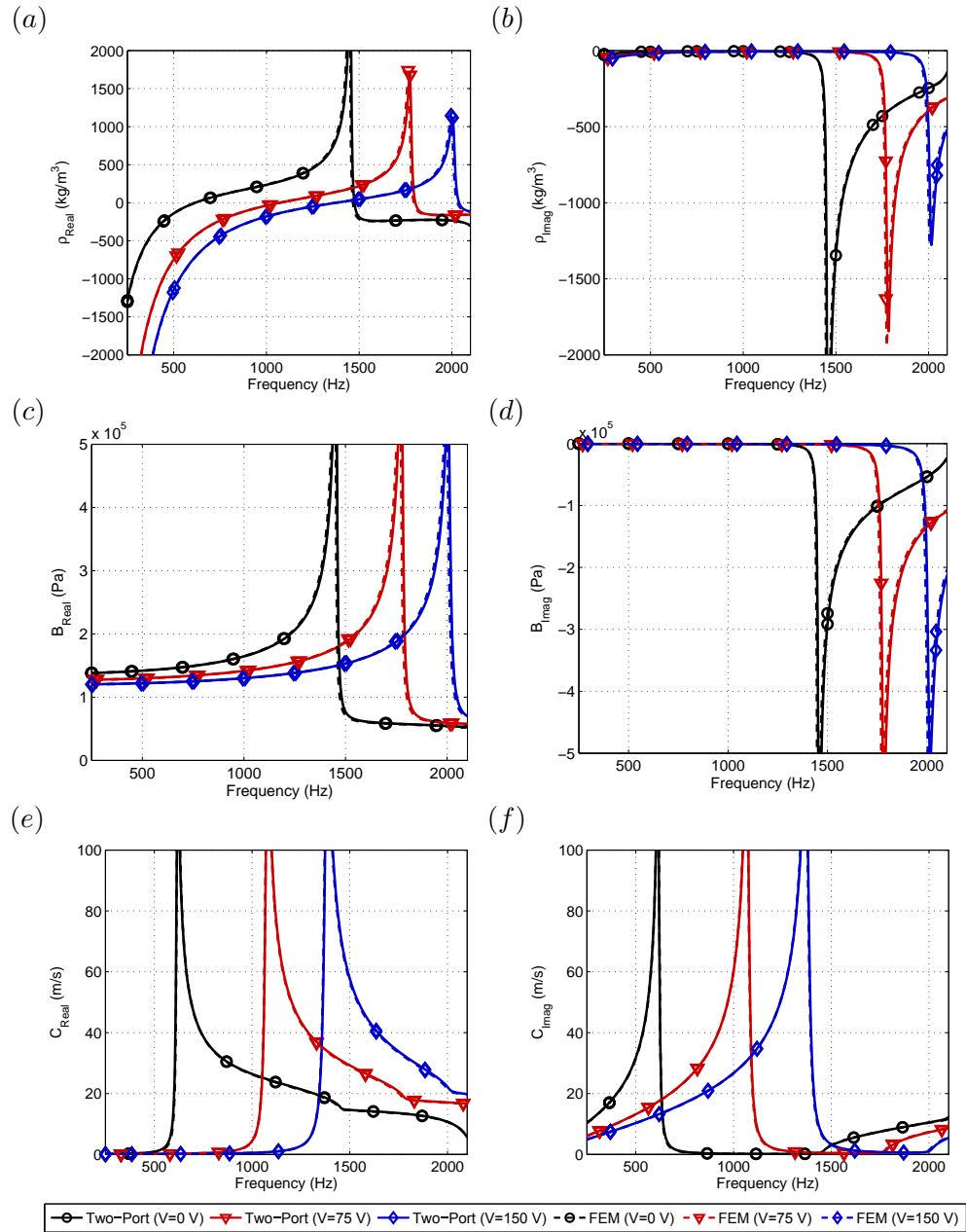


FIGURE 3.8: Real and imaginary components of the (a,b)effective density , (c,d) effective Bulk's modulus and (e,f) effective speed of sound . With no voltage applied to the piezoelectric disk (Black lines with circular markers) and subjected to a static voltage of 75V (Red lines with triangular markers) and 150V (Blue lines with diamond markers).

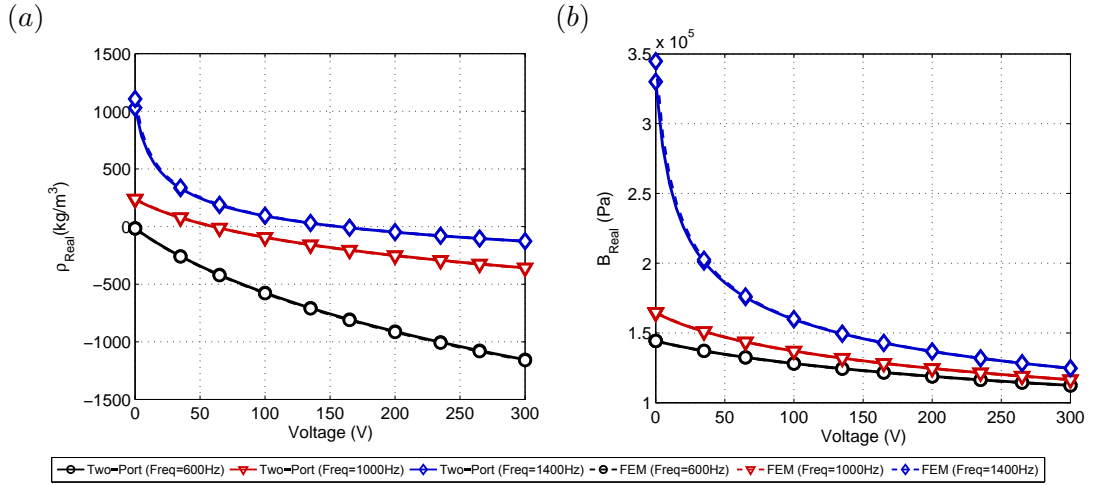


FIGURE 3.9: The effect of the applied voltage on the real component of (a) the effective density and (b) Bulk's modulus calculated analytically (Solid) and using the FEM (Dashed) at a constant frequency of  $600\text{Hz}$  (Black lines with circular markers),  $1000\text{Hz}$  (Red lines with triangular markers) and  $1400\text{Hz}$  (Blue lines with diamond markers).

### 3.3.2 Characterization of multiple cells

A periodic arrangement of cells can only be considered as a material, if its effective material properties are invariant to its length. Thus, in order to fulfill this condition, the effective material properties of different lengths of the suggested material should be compared to determine the frequency regions where the effective properties are invariant. This can be done by characterizing a sample consisting of more than a single cell and using the same homogenization technique. Analytically, this is done using the relation:

$$T_t = T_{\text{cell}}^N \quad (3.34)$$

where  $N$  is the number of cells in the sample and  $T_t$  is the transfer matrix of the whole sample.

It should be noted that when calculating the effective material properties of multiple cells, the branch number  $m$  in Equations (2.10) and (2.11) play an important role in calculating the correct properties. While for a sample consisting of one sample,  $m$  can be safely assumed to be zero (minimum thickness material), for multiple cells this is usually not the case and a proper method for selecting the branch number should be used. This problem is demonstrated in Figure 3.10, where the use of a constant branch number  $m = 0$  yields different material properties for different number of cells used in the sample (Figure 3.10a). While in Figure 3.10b the correct branch number is selected using Kramers-Kronig relationship between the real and imaginary parts of the acoustic

refractive index.

With the proper branch number used, it is clear from Figure 3.10b that the effective density (material properties) of the studied cell is invariant to the length for the entire studied frequency range. This also further supports the claim that only one cell is sufficient to characterize the material using [89] retrieval method, given that the material is symmetric and the long wavelength region is maintained.

The calculated properties for the active case where a voltage is applied to the cell also

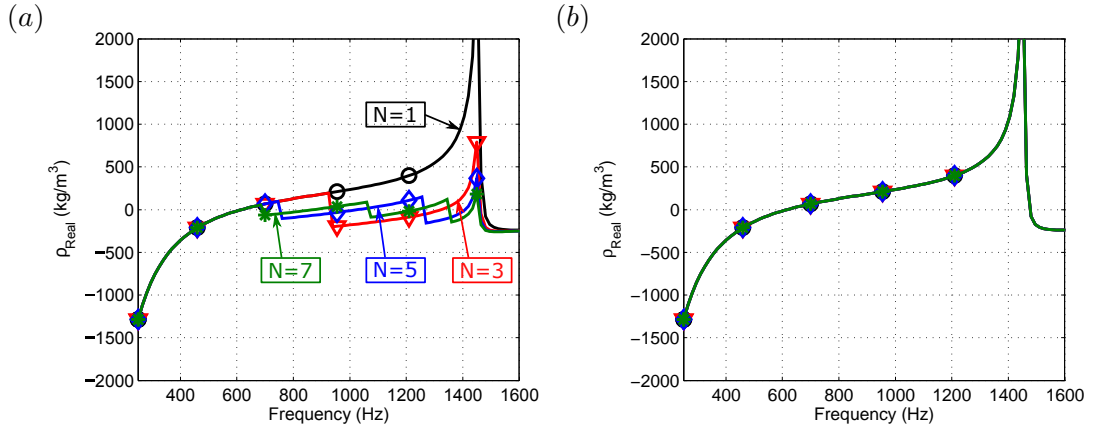


FIGURE 3.10: The effect of the variation of the number of samples on the effective density of the material calculated analytically with no applied voltage to all cells. In (a) a constant branch number  $m = 0$  is used for all frequencies, while in (b) it is chosen correctly using Kramers-Kronig relationship.

shows the same invariance to the number of cells (Figure 3.11). This is also true for the results obtained using the FEM with the observation that using a larger number of cells to estimate the material properties increases the numerical errors. This happens because the transmission loss increases with increasing the number of cells, which causes the readings of the downstream microphones to approach zero; hence, the numerical errors increase.

### 3.4 Conclusion

We have introduced and analyzed a novel structure for active membrane based acoustic metamaterials based on piezoelectric plates in air. The effective material properties of the metamaterial cell are estimated using the S-parameters retrieval method. An analytic model based on the acoustic two-port theory, the theory of piezoelectricity and the pre-stressed plate theory has been developed to analyze the material behavior. A FEM

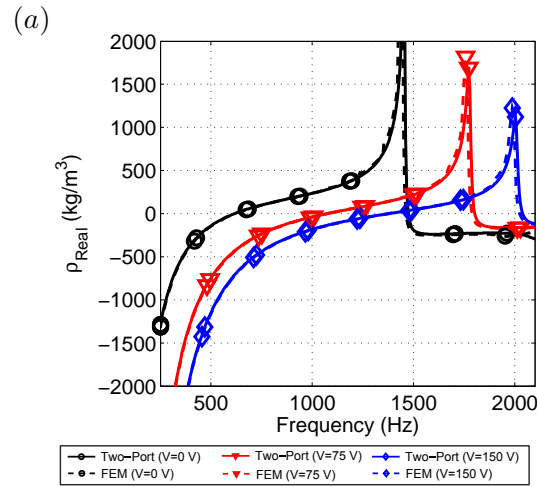


FIGURE 3.11: The effective density calculated from a sample consisting of seven cells ( $N = 7$ ) analytically (Solid) and using the FEM (Dashed) with different voltages applied to the piezoelectric disk  $V = 0, 75, 100V$ .

model was constructed to verify the analytic results using ANSYS®. The analytic results show excellent agreement with the FEM for all the applied control voltages which opens the door to its use in the design of active acoustic metamaterials with similar construction as well as in the implementation of controllers for the effective density of the cell. The novel design has a frequency dependent effective density ranging from  $-2000\text{kg/m}^3$  to  $2000\text{kg/m}^3$  within a frequency range of (200-2000 Hz). We could analytically and numerically demonstrate that the effective density of the material can be controlled by applying a static voltage to the piezoelectric plate within orders of magnitudes of the uncontrolled density while maintaining a minimum effect on the effective Bulk's modulus at frequencies around and less than the resonance of the plate. The linear nature of the control characteristics of the material cell suggests that simple control techniques could be used to program each AMM cell to a desired effective density. This facilitates the construction of devices consisting of large number of AMM cells and hence the fabrication of devices which have full control on the directivity and dispersion characteristics of acoustic waves.

## Chapter 4

# Open loop 2D AMM

In the previous chapter, a new design for 1D active AMM was discussed. Its effective density was tunable by means of a static external voltage signal. The analysis was limited to placing the material in 1D circular ducts and the means to support and clamp the piezoelectric plates were not discussed. In this chapter, the analysis is extended to 2D materials. This requires taking into consideration the supporting structure of the material and the geometrical aspects for constructing the material. We propose a modified design for 2D active MAMs consisting of composite lead-PZT plates supported on an aluminum frame with air as a background fluid. As with the previous design, the stiffness of the plate is controlled by the application of an electric potential difference across the PZT layers; this enables us to control the effective (homogenized) density of the AMM within a wide range of values ranging from negative to positive density values passing by near zero conditions.

This chapter is divided into six sections. In the first section, a brief introduction is presented. In Section 4.1, the construction of the suggested 2D metamaterial cell is introduced, and the analytical model is extended for the new composite plate. In Section 4.2, a numerical model is constructed to verify the analytic model using the FEM. In Section 4.3, the results obtained from both models are compared, and the overall performance of the new design is evaluated and analyzed. In Section 4.4, the developed material is used in the design of a programmable waveguide. Finally, the Chapters main findings are summarized.

## 4.1 Theoretical Formulation

The suggested design for a practical 2D active MAM cell (Figure 4.1) is inspired from the structure of the passive MAM developed by Gu *et al.*[36]. The main building block of the structure (Figure 4.1d) consists of a composite lead-PZT circular plate clamped to a relatively thick (rigid) aluminum structure, and suspended in air. The composite plate has a diameter of 22 mm, and consists of three different layers. The middle layer is made of a lead alloy of thickness  $50 \text{ } \mu\text{m}$ , and extends through the diameter of the plate. Two piezoelectric layers made of PZT-5A material are deposited on the two sides of the middle layer, each of thickness  $125 \text{ } \mu\text{m}$ . The two layers have a shape of an annulus with inner diameter of 14 mm and the same outer diameter as the plate. They are both polled in the thickness direction, and both have the same polling direction. The composite plate is fixed to a square aluminum frame of thickness 1 mm. The dimensions of the active MAM cell and the material properties of the different components are summarized in Table 4.1 and Table 4.2 respectively. The material

TABLE 4.1: Summary of the dimensions of the 2D open loop active MAM cell.

Dimension	Unit	Value
Cell constant ( $a$ )	mm	23
Outer radius of the composite plate ( $R_2$ )	mm	11
Inner radius of the composite plate ( $R_1$ )	mm	7
Thickness of the lead layer ( $t_1$ )	$\mu\text{m}$	20
Thickness of the piezoelectric layer ( $t_2$ )	$\mu\text{m}$	125
Thickness of the aluminum frame ( $t_3$ )	mm	1

TABLE 4.2: Properties of the materials used in the construction of the 2D open loop active MAM cell.

Property	Unit	PZT-5A	Lead	aluminum
$\rho$	$\text{kg/m}^3$	7500	11000	2700
$C_{11}$	GPa	132	75.9	102
$C_{12}, C_{23}$	GPa	73	62	50
$C_{33}$	GPa	115	75.9	102
$e_{31}$	$\text{C/m}^2$	-4.1	-	-
$e_{33}$	$\text{C/m}^2$	14.3	-	-
$\epsilon_{11}$		804.6	-	-
$\epsilon_{33}$		659.7	-	-
$Q_m = \eta^{-1}$		50	50	-

properties of the cell are controlled by applying a static electric voltage across the thickness of two annular piezoelectric layers as shown in Figure 4.1d. The applied electric voltage induces stresses in the piezoelectric layers which changes the tension applied on the middle circular lead membrane. This in turn changes the acoustic impedance, and hence the effective material properties of the cell.

A controllable DC voltage source is connected between the outer surfaces of the piezoelectric layers, which are connected in series. Both are polled in the same direction; thus, any bending of the composite plate due to incident acoustic waves will cause the stretching of one layer and the compression of the other. This will cause equal but opposite voltages to be generated by the two layers, and due to the series connection, almost no time dependent currents will be generated. Thus, for all the subsequent analysis, open circuit boundary conditions will be assumed for any dynamic analysis of the plate. The 2D material is constructed by repeating the 1D unit cell (Figure 4.1d) in two orthogonal directions to form the 2D unit cell shown in Figure 4.1b. The cell constant  $a$  is assumed to be much smaller than the wavelength of the incident acoustic wave, thus homogenized effective material properties could be used to describe the wave propagation in the material.

#### 4.1.1 Characterizing the 2D active MAM cell

One approach to analyze the proposed 2D structure of the AMM cell, shown in Figure 4.1b, is to consider it as four interconnected 1D cells. This is like what Gu *et al.*[36] have done for passive MAM using a lumped parameter model. If the transfer matrix (scattering matrix) for the 1D cell is known, the 2D cell could be modeled using the 2-Port network shown in Figure 4.1c. To analyze this network, or networks formed by multiple cells, the formalism developed by Glav and Abom[112] for analyzing two-port networks will be used. Once the transfer matrix of each element in the cell is known, the formalism could be used to estimate the equivalent transfer matrix between any two nodes in the network. For example, to determine the effective properties of the material represented by Figure 4.1c using only one cell, the formalism could be used to estimate the transfer matrix between nodes 1 and 2, for the properties in x-direction, and between 1 and 3 for the properties in y-direction. This could be easily extended to networks consisting of multiple cells.

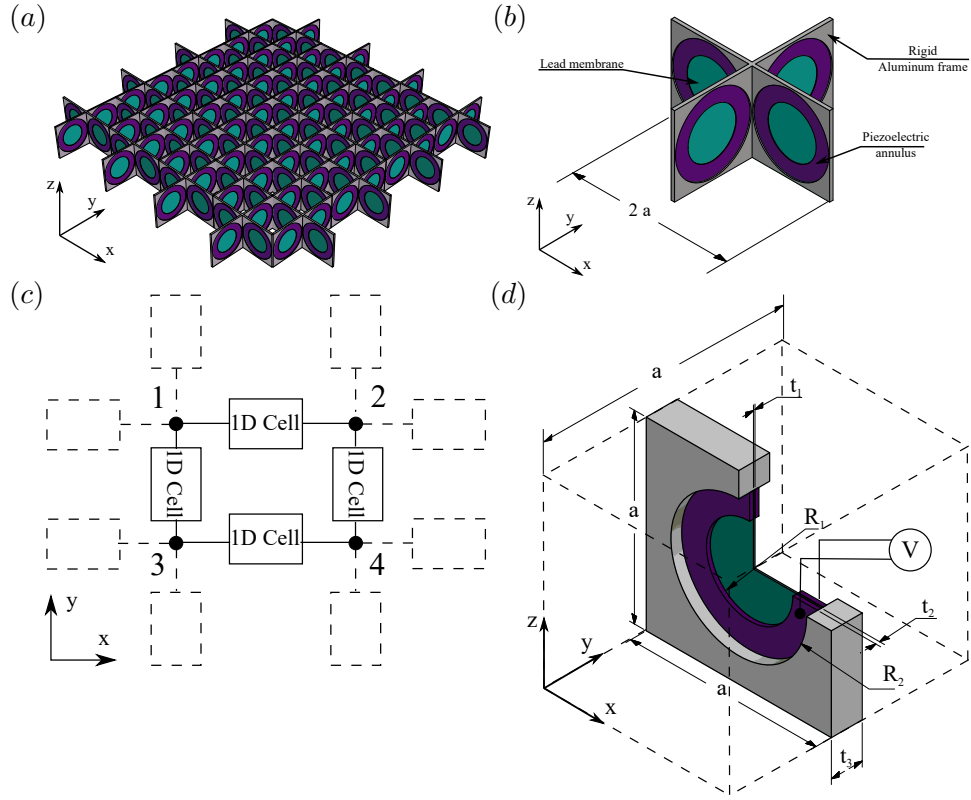


FIGURE 4.1: A new concept for a 2D active membrane-type metamaterial. (a) A visualization for the construction of the suggested 2D AMM. (b) Schematic representation for the 2D building block of the material. (c) Acoustic 2-Port representation for the building block. (d) Schematic representation of the construction of the 1D building block (1D AMM cell).

#### 4.1.2 Characterizing the 1D building block of the 2D active AMM

Since the 2D cell is modeled in terms of a network of 1D cells, the focus is on estimating the transfer matrix of the 1D cell in a similar manner to what was done in Chapter 3. For waves propagating in the  $x$ -direction, the suggested cell, shown in Figure 4.1d, consists of three main layers which are the elastic composite plate and two straight air layers. The local transfer matrix of every layer is calculated depending on the nature of the layer. The transfer matrix of the whole 1D metamaterial cell is then estimated using Equation (2.5) and converted to the scattering matrix form.

The transfer matrices of the straight air layers can be easily determined from Equation (2.6). In order to determine the transfer matrix of the third layer which is the elastic plate, the thickness of the composite plate is assumed to be small enough compared to the width of the cell ( $a$ ) and the incident wavelength; thus, it could be assumed as a lumped element with lumped impedance ( $Z$ ). Again, the averaged volume velocity over the area of the plate ( $\tilde{v}$ ) will be used to estimate its acoustic impedance.  $\tilde{v}$  is given

by:

$$\tilde{v} = \frac{1}{A_{cell}} \left( \frac{1}{A_{cell}} \int_{A_{cell}} \dot{w} dA \right) \quad (4.1)$$

where  $A_{cell}$  is the surface area of the square cell and  $\dot{w}$  is the average point velocity of the plate.

The lead membrane with the piezoelectric annulus is treated as a composite circular plate consisting of two regions. The first region is the circular lead membrane with radius  $R_1$ , and the second is the outer annular region with inner radius  $R_1$  and outer radius  $R_2$ . The annular region consists of multiple layers of different materials. The middle layer is the lead membrane which acts also as a metallic electrode for the lower and upper piezoelectric PZT layers. The other surfaces of the piezoelectric layers are coated with thin metallic electrodes. A static voltage  $V$  is applied between the two metallic electrodes which induces in plane stresses in the composite plate. According to the classical composite thin plate theory, the equations of motion for the transverse deflection of an axisymmetric transversely isotropic composite plate can be written as [113]:

$$\begin{aligned} I_o \frac{\partial^2 w(r, t)}{\partial t^2} + D_{11} \nabla^4 w(r, t) - N \nabla^2 w(r, t) &= p(r, t) \\ I_o &= \int_0^h \rho dz, \\ D_{ij} &= \int_0^h Q_{ij} z^2 dz, \\ Q_{ij} &= C_{ij} - \frac{C_{i3} C_{3j}}{C_{33}} \end{aligned} \quad (4.2)$$

where  $w(r, t)$  is the transverse deflection of the plate,  $r$  is the radial distance from the center of the plate,  $N$  is the in-plane force per unit tangent length,  $p(r, t)$  is the pressure difference between the two sides of the plate,  $\rho$  is the mass density of the different layers,  $h$  is the total thickness of the plate and  $C_{ij}$  are the elements of the stiffness matrix of the different layers of the plate. For the piezoelectric layers, since open circuit electrical boundary conditions are maintained, the stiffness matrix under constant electric displacement  $\mathbf{C}^D$  will be used. Material damping is included in the analysis in the form of a complex stiffness matrix  $\mathbf{C}^{D*}$ .

$$\mathbf{C}^{D*} = \mathbf{C}^D (1 + \eta j) \quad (4.3)$$

where  $\eta$  is loss factor inside the material. For harmonic excitation, the incident acoustic pressure and the deflection of the plate could be written as:

$$\begin{aligned} p(r, t) &= P(r)e^{j\omega t}, \\ w(r, t) &= W(r)e^{j\omega t} \end{aligned} \quad (4.4)$$

Substituting in Equation (4.2), canceling the exponentials and reordering:

$$\left(\nabla^4 - \frac{N}{D_{11}}\nabla^2 - g^4\right)W(r) = \frac{P(r)}{D_{11}} \quad (4.5)$$

where  $g$  is the complex wave number of the flexural waves traveling through the plate:

$$g^4 = \frac{I_o\omega^2}{D_{11}} \quad (4.6)$$

The solution of Equation (4.5) can be written as the sum of the solution of the homogeneous equation and the solution of the particular equation. Since  $\nabla$  is a linear operator, the homogeneous part of Equation (4.5) can be written in the form:

$$(\nabla^2 - g_1^2)(\nabla^2 + g_2^2)W(r) = 0 \quad (4.7)$$

where:

$$g_1^2 = \frac{N + \sqrt{4D_{11}^2g^4 + N}}{2D_{11}} \quad (4.8)$$

$$g_2^2 = \frac{-N + \sqrt{4D_{11}^2g^4 + N}}{2D_{11}} \quad (4.9)$$

For a polar coordinate system whose origin is at the center of the circular plate the complete solution of Equation (4.5) is then:

$$\begin{aligned} W(r) &= E_1J_0(g_1r) + E_2Y_0(g_1r) \\ &+ E_3I_0(g_2r) + E_4K_0(g_2r) - \frac{P}{D_{11}g^4} \end{aligned} \quad (4.10)$$

where  $J_0()$ ,  $I_0()$ ,  $Y_0()$ ,  $K_0()$  are the zeroth order Bessel and modified Bessel functions of the first and second kind.  $E_1$  to  $E_4$  are constants to be determined from the boundary and continuity conditions for each region of the plate in a similar manner to what was done in Chapter 3.

To calculate the acoustic impedance of the plate it is required to calculate its area

averaged displacement  $\widetilde{W}$  which is given by:

$$\widetilde{W} = \frac{1}{A_{cell}} \left( \int_0^{R_2} 2\pi r W(r) dr \right) \quad (4.11)$$

The average volume velocity of the composite plate  $\widetilde{v}$  is then given by:

$$\widetilde{v} = \frac{j\omega \widetilde{W}}{A_{cell}} \quad (4.12)$$

The acoustic impedance of the elastic layer  $Z_e$  can then be calculated from the relation:

$$Z_e = \frac{P}{\widetilde{v}} \quad (4.13)$$

Only one issue remains before Equation (4.13) can be used to determine the acoustic impedance of the composite plate, which is the estimation of the static in-plane forces  $N_a, N_b$ . This can be done by solving the static equation of motion for the in-plane displacements of the composite plate. It is given for axisymmetric displacements of a transversely isotropic plate by [113]

$$\frac{\partial^2 u(r)}{\partial r^2} + \frac{1}{r} \frac{\partial u(r)}{\partial r} - \frac{u(r)}{r^2} = 0 \quad (4.14)$$

The exact solution for Equation (4.14) is given by:

$$u(r) = E_5 r + \frac{E_6}{r} \quad (4.15)$$

where  $E_5$  and  $E_6$  are again constants to be determined from the boundary and continuity conditions for each region of the plate. The in-plane force  $N$  is given as a function of the in-plane displacement by:

$$N(r) = A_{11} u'(r) + \frac{A_{12} u(r)}{r} - N_p \quad (4.16)$$

$$A_{ij} = \int_0^h Q_{ij} dz$$

where  $N_p$  is the in-plane force due to the piezoelectric effect

$$N_p = \int_0^h \bar{e}_{31}^k E_3^k dz \quad (4.17)$$

$\bar{e}_{31}^k$  is the modified piezoelectric stress coefficient for layer  $k$  and it is given by:

$$\bar{e}_{31}^k = e_{31}^k - \frac{C_{13}^k e_{33}^k}{C_{33}^k} \quad (4.18)$$

$E_3^k$  is the electric field across the thickness of layer  $k$  and it is related to the applied voltage  $V^k$  and the thickness of the layer  $t^k$  by:

$$E_3^k = \frac{V^k}{t^k} \quad (4.19)$$

## 4.2 Numerical Model

To validate the analytic approach, a 3D piezo-acoustic finite element model is developed using ANSYS® commercial software. The model is constructed to mimic the 4-Microphone experimental procedure for the evaluation of the normal incidence sound transmission [109, 110]. The sample, whose material properties are to be determined, is placed in a rectangular impedance tube having the same cross-sectional area (Figure 3.3). As in Chapter 3, it is excited twice using a surface acoustic velocity source located once at the upstream end of the tube, and the other at the downstream end. Its response is captured by four virtual microphones located at the positions shown in Figure 3.3. The distances  $s, d$  are chosen as per the guidelines defined by the ASTM E2611[110]. The readings of the four microphones are then recorded and used to determine the S-matrix of the sample using the procedure found in [109].

The impedance tube is modeled as two acoustic domains (Upstream and Downstream), each domain is discretized using 20-node brick acoustic elements (FLUID220), and the length of each domain is 500 mm long. The piezoelectric layers are discretized using 20-node brick coupled-field structural elements (SOLID226). The lead layer is discretized using 20-node brick structural elements (SOLID186). Since the aluminum structure is very rigid compared to the composite plate, it is modeled as rigid wall boundary conditions for the acoustic domain and fixed boundary conditions for the outer diameter of the composite plate. An infinite surface boundary condition is applied at the terminations of the impedance tube to model the anechoic terminations suggested by the 4-Microphone procedure. For each surface of the piezoelectric layers, the voltage degrees of freedom of the nodes forming it are coupled to simulate the effect of the presence of the thin metallic electrodes.

The solution is done in two steps; the stresses on the piezoelectric plates due to the applied voltage are determined using a static structural solution. The stresses calculated in the first step are then applied as pre-stresses on the composite plate in a linear perturbation harmonic analysis with incident acoustic pressure waves [111]. The harmonic analysis is carried out at frequencies ranging between 400 Hz and 1600 Hz with a frequency step of 20 Hz. The element size of the piezoelectric/structural domain is chosen so that the error is less than 1% between the estimated first mode of the circular plate alone using the analytic approach, and that evaluated using numerical modal analysis. The element size in the acoustic domain is chosen to follow the rule that there should be at least six elements per wavelength at the maximum frequency of the incident wave. The maximum frequency allowed in the analysis is limited by the same factors mentioned in Section 3.2. For all the tested samples, the upper frequency limit was mainly limited by the homogenization limit. For the dimensions of the cell in Table 4.1, it is around 1500 Hz.

For the 2D cell shown in Figure 4.1b, the construction of the cell is the same for acoustic waves propagating in either x or y directions. This indicates that the material properties determined from one direction is sufficient to estimate the anisotropic material properties. The cell has also half symmetry about the normal to the propagation direction, which suggests that the results obtained from the 1D cell could be used to characterize the 2D cell. To verify this assumption two different types of samples, shown in Figure 4.2, are used to estimate the material properties. The first is a sample consisting of the full construction of the 2D cell (Figure 4.1b), while the second is a simplified version consisting of only the 1D cell (Figure 4.1d). For the 1D sample (Figure 4.2a), since its cross section has a quarter symmetry, only a quarter sector of the tube and the cell is modeled. Symmetry boundary conditions were applied to the structural and acoustic domains. For the 1D active MAM, the number of cells forming the sample in the propagation direction are varied from 1 to 7 cells. This is done to check effect of varying the length of the material on the estimated material properties.

### 4.3 Results and Discussion

The results obtained from the two types of FEM samples are found to be almost identical for the same number of cells in the direction of the incident excitation (Figure 4.3

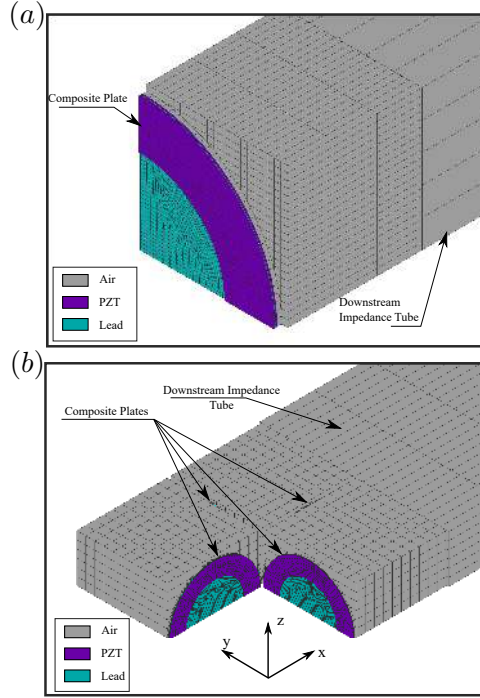


FIGURE 4.2: A cross section in the finite element mesh of the (a) 1D building block sample with quarter symmetry placed in a square impedance tube, and (b) 2D AMM sample with half symmetry placed in a rectangular impedance tube.

and Figure 4.4). The same observation is noted for the results obtained from the analytic model whether using the 1D cell or by solving the acoustic network (Figure 4.1c). Figure 4.3 and Figure 4.5 also show that the calculated properties in the propagation direction (e.g.  $x$ ) are independent from those of the direction normal to the propagation (e.g.  $y$ ). The voltage applied to the cells normal to the  $x$ -direction is kept constant at zero voltage, and the voltage applied to those normal to the  $y$ -direction is varied from 0 to 300 V. No change in the properties estimated in the  $x$ -direction were observed. These two observations also confirm the assumption that the 1D cell shown in Figure 4.1d can be used to design and characterize the 2D material formed by repeating the same cell in two orthogonal directions. Figure 4.3 shows the complex transmission and reflection coefficients obtained using the acoustic 2-Port model and the FEM. The results are evaluated for three different values of applied voltages. Good agreement is observed between the two methods for the range of the studied frequencies. Figure 4.5a shows the Transmission Loss (TL) of a single 1D cell under three different applied voltages. The effective material properties, mainly the effective density, bulk modulus and speed of sound, are calculated from the complex reflection and transmission coefficients. Their real components are shown in Figure 4.4. As with the 1D cell analyzed in Chapter 3, the

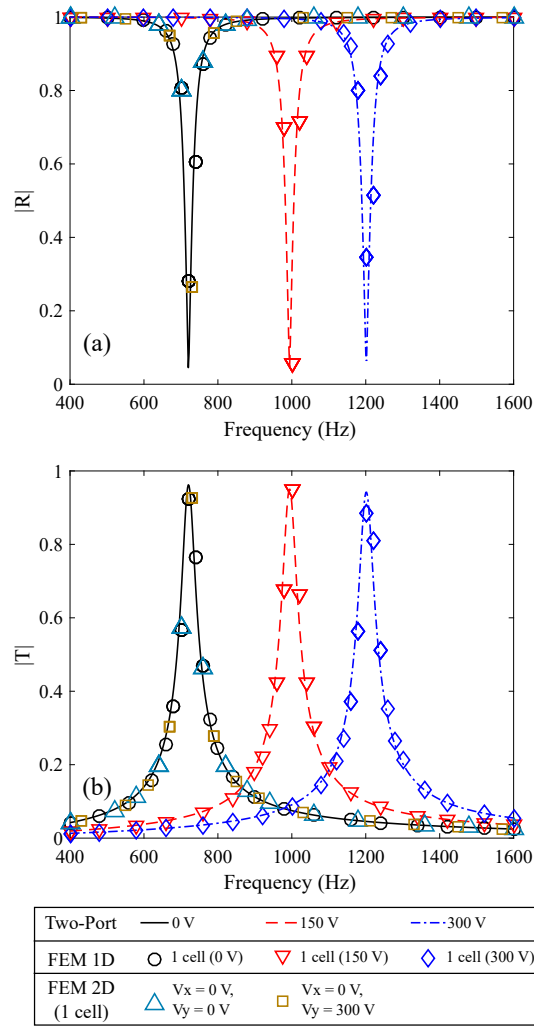


FIGURE 4.3: The effect of applying different voltages on the amplitude of (a)  $R$  and (b)  $T$ . The analytic two-port values are compared to those obtained from the FEM using one 1D cell in the incident wave propagation direction ( $x$ -direction), as well as, one 2D cell with the voltage being varied on the plates normal to the  $y$ -direction.

real component of the speed of sound (Figure 4.4c), which represents the phase velocity of the sound waves inside the AMM, vanishes below the natural frequency of the composite plate. This indicates the presence of a stop band in this frequency region, which is similar to what was measured experimentally by Lee *et al.*[25] for a membrane type AMM. They attributed the presence of the unusual stop band at this frequency region to the fact that the elastic restoring forces of the membrane below resonance cause a step reduction in the acoustic pressure across it. This leads to an exponential decay of the acoustic waves propagating through the material. From a material point of view, the effective density turns negative in this band (Figure 4.4a), while the bulk modulus remains positive (Figure 4.4b); as a result, the speed of sound becomes imaginary, since

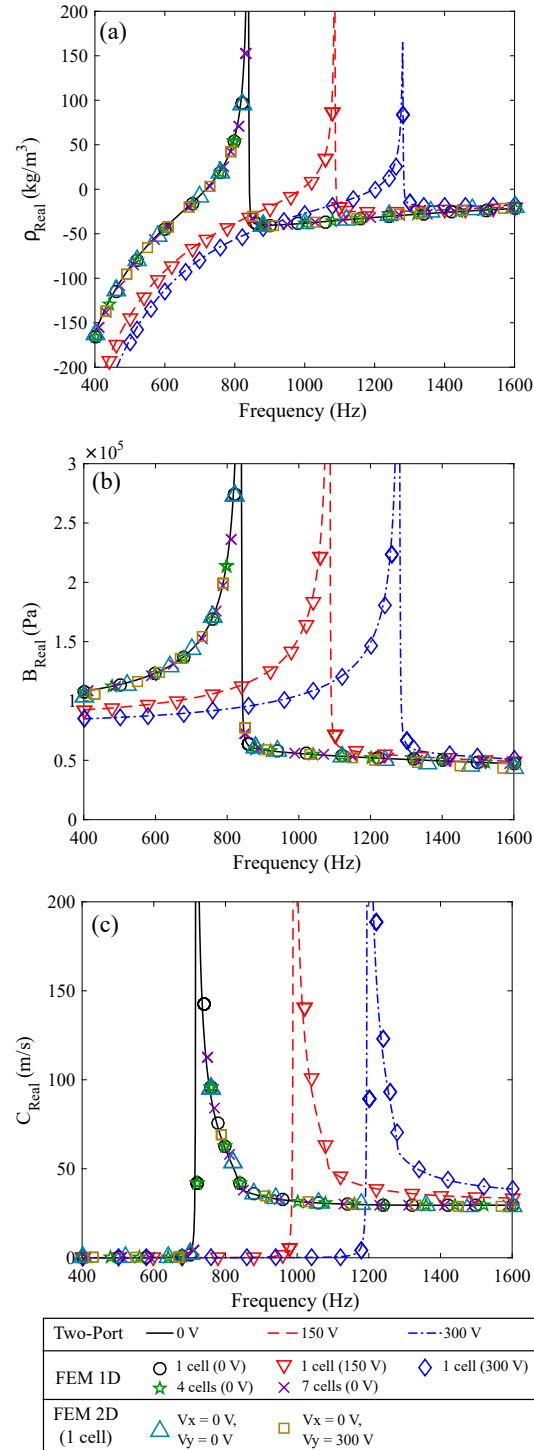


FIGURE 4.4: The analytic and numerical results for the real components of (a) the effective density, (b) effective bulk modulus and (c) the effective speed of sound estimated from (1, 4 and 7) 1D cells placed in the wave propagation direction (x-direction), as well as, one 2D cell while varying the voltage applied to the plates normal to the y-direction.

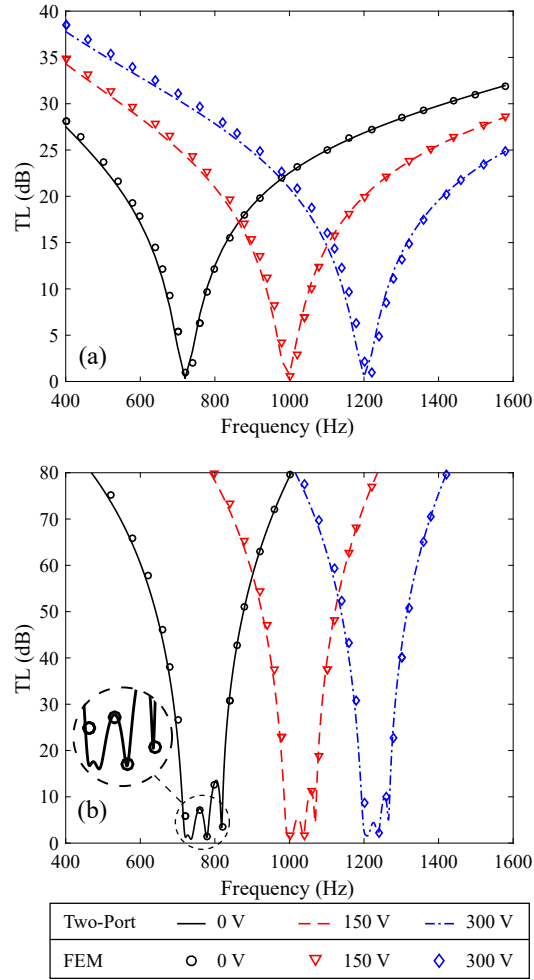


FIGURE 4.5: The TL estimated from a sample consisting of (a) only one 1D cell and (b) four 1D cells in the propagation direction. The TL is calculated analytically (Lines) and using the FEM (Markers) with different voltages applied to the piezoelectric annulus  $V=0,150,300$  V.

$$c = \sqrt{B/\rho}.$$

The effect of the applied voltage on the effective bulk modulus (Figure 4.4b) for frequencies less than 700 Hz is small compared to its effect on the effective density (Figure 4.4a). This enables us to control the density of the AMM with minimal effect on the bulk modulus in this region. This in turn, facilitates using transformation acoustic techniques in the fabrication of acoustic devices, for example, the realization of acoustic cloaks. Figure 4.4a shows that with no applied voltage, and for frequencies between 400-800 Hz, the effective density of the membrane increases from large negative values (about  $-200 \text{ kg/m}^3$ ) passing by zero density at around 725 Hz up to large positive values ( $200 \text{ kg/m}^3$ ) with the increase of the frequency. These values are however less than those obtained for the open loop 1D cell in Chapter 3. This is mainly attributed to the geometrical

restrictions imposed by the 2D analysis in the current case which increase the air volume inside the cell thus decreasing its density. By applying an electric voltage, we can shift the resonance of the composite plate, and thus the curve of the density. The magnitude of the shift is dependent on the magnitude of the applied voltage. If we consider controlling the effective density for a single frequency, Figure 4.6 shows the dependency of the effective density on the applied voltage at different frequencies. For the frequencies (600, 720 Hz), *i.e.* below the resonance of the composite plate under zero voltage, the relation between the applied voltage and the density is almost linear up to a voltage of 300 V. This means that a simple controller can be used to adjust the density of the cell at this frequency range. The effective material properties of different lengths of the

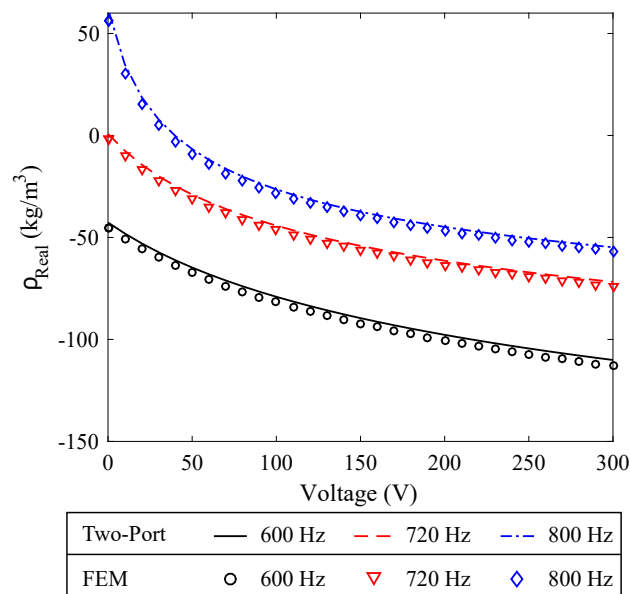


FIGURE 4.6: The effect of the applied voltage on the real component of the effective density, which is calculated analytically (Lines) and using the FEM (Markers) for one 1D cell at three different frequencies namely 600,720 and 800 Hz.

suggested material are compared to determine the frequency regions where the effective properties are invariant to the length. This can be done by the characterization of a sample consisting of more than a single cell in the propagation direction using the same homogenization technique. The results for a sample consisting of four cells in the propagation direction are shown in Figure 4.5b. Three new peaks appear in the plot of the transmission loss versus the frequency, that weren't observed in the single-cell sample (Figure 4.5a). The calculated effective density, on the other hand, didn't show any variation if compared to the single-cell sample (Figure 4.4a). The same observation was made for samples consisting of more than four cells, with a new peak appearing for

each added cell and the same estimated effective properties (Figure 4.4a). This confirms that the effective density (the material properties) of the studied cell is invariant to the length for the entire studied frequency range. This again supports the claim that only one cell is sufficient to characterize the material using the retrieval method given in [89], given that the material is symmetric and the long wavelength region is maintained.

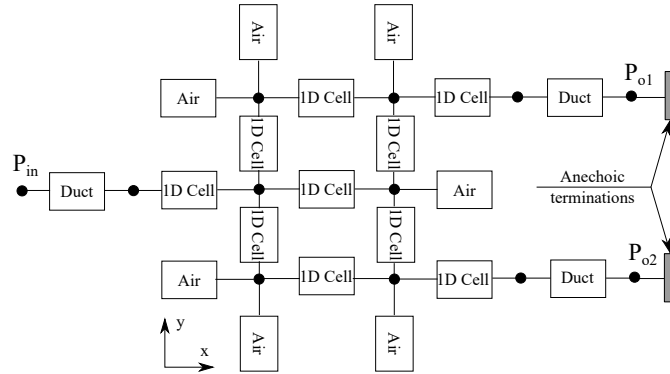


FIGURE 4.7: The developed 2-port network model for the reconfigurable waveguide. The “Air” blocks indicate quarter cell sections terminated by the rigid walls of the guide. Incident pressure is applied to the node donated  $P_{in}$ .

## 4.4 Applications

The structure of the 2D active MAMs enables us to control its effective density in two different directions independently; moreover, the purposed structure can achieve near zero effective density. AMMs with density-near-zero (DNZ) have been shown to possess extraordinary sound transmission characteristics [34, 36]. Combining the two advantages enables the developed material to be used in the fabrication of different acoustic devices which require controlling and manipulating the spatial propagation of acoustic waves. This includes reconfigurable waveguides, reconfigurable acoustic tunnels, tunable acoustic cloaks and efficient noise control.

As a demonstration for the capabilities of the new designed cell, a simple controllable waveguide is constructed. The guide consists of a  $69 \times 46$  mm rectangular chamber filled with the new 2D active MAM and connected to three ducts. The ducts have  $23 \times 23$  mm cross sections and are fitted with anechoic terminations at the other ends.

Acoustic waves are incident to the guide from the left duct, and their direction of propagation is manipulated inside the chamber. By controlling the anisotropic effective density of each cell, the incident acoustic waves can be manipulated to exit the guide

at any chosen location. This is done by setting the density of the required path for the wave inside the guide to near zero density, and at the same time setting the density of the other cells to large negative values which prevents the propagation of acoustic waves through them. The guide was modeled using the FEM by following a procedure similar to that mentioned in the Section 4.2. An analytical model for the waveguide was also constructed using the network model for the 2D cell. The construction of the analytic network is shown in Figure 4.7. Figures 4.8a and 4.8b show the waveguide when all cells are set to density near zero,  $\rho_{eff} = 0.2\text{kg/m}^3$ . This was done by applying 0 V on all the cells for an incident wave of frequency 727 Hz. An efficient wave splitting is observed between the two output ducts. The configuration of the waveguide is changed in Figures 4.8c and 4.8d, so that the wave propagation is limited to a path in which it is guided to exit from the upper duct. This was done by setting the density of the cells that are not on the desired path to  $-70.15\text{ kg/m}^3$  by applying 300 V to them and leaving the cells on the path at near zero density. In the same manner, the wave propagation could be controlled to exit from the lower duct. It is worth mentioning that by increasing the size of the waveguide, more ports and paths could be added to it. This would enable the usage of transformation acoustics techniques to create density fields that would allow for even more complex manipulations of the propagation of acoustic waves.

## 4.5 Conclusion

We have introduced and analyzed a novel structure for 2D active membrane-type acoustic metamaterials based on composite lead-PZT plates in air. The effective material properties of the metamaterial are estimated using the S-parameters retrieval method. An analytic model based on the acoustic two-port theory, the theory of piezoelectricity and the pre-stressed laminated plate theory has been developed to analyze the material behavior. A FEM model was constructed to verify the analytic results using ANSYS®. The analytic results show good agreement with the FEM for all the applied control voltages, which opens the door to its use in the design of active acoustic metamaterials with similar construction. The novel design has a frequency dependent effective density ranging from  $-200\text{ kg/m}^3$  to  $200\text{ kg/m}^3$  within a frequency range of (400-1600 Hz). We can analytically and numerically demonstrate that the effective density of the material can be controlled by applying a static voltage to the composite plate. The range of the

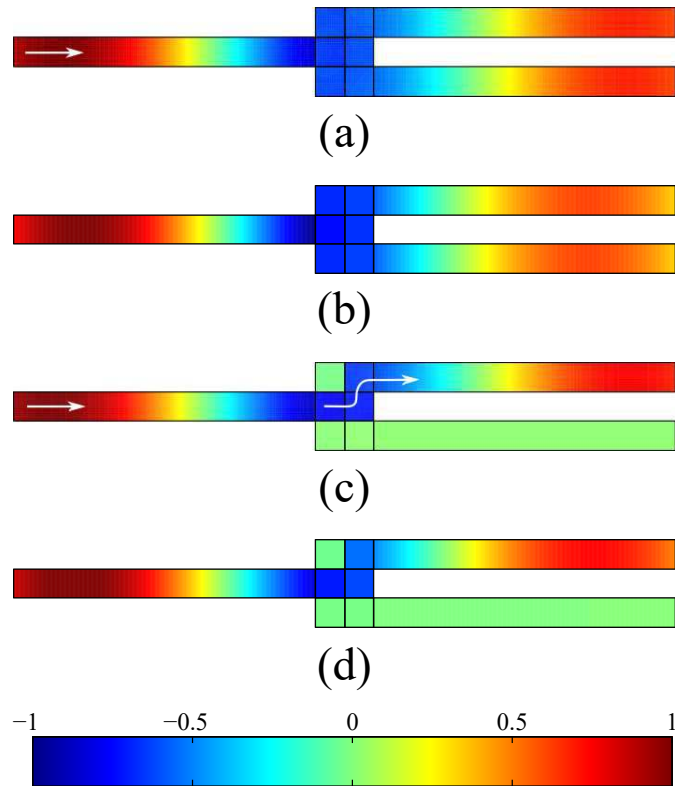


FIGURE 4.8: The normalized pressure inside the suggested waveguide for an incident acoustic wave of frequency 727 Hz. The pressure is estimated using the FEM (a) and (c) and the analytic network model (b) and (d). The incident excitation and the propagation direction are marked with white arrows. The incident wave is controlled to (a),(b) split between the two ducts and (c),(d) exit from the upper duct only

controllable density lies within orders of magnitudes of the uncontrolled density while maintaining a minimum effect on the effective bulk modulus at frequencies below the resonance of the plate. This is achievable for the 2D cell where the anisotropic density could be controlled for two orthogonal directions independently from each other. The capabilities of the new design were demonstrated by the construction of fully reconfigurable waveguide in which the direction of propagation of incident acoustic waves could be arbitrarily programmed and controlled.



## Chapter 5

# Closed loop 1D AMM

In this chapter, we propose an active 1D AMM whose effective density can be controlled and programmed to a desired set value. The material unit cell consists of a circular composite piezoelectric plate clamped in air. The diaphragm consists of two piezoelectric layers with a brass layer in the middle. The dynamic properties of the material are manipulated by constructing a feedback loop by measuring the voltage generated by one of the layers and applying a control signal to the other layer. A vibro-acoustic analytic model is developed to analyze the behavior of the proposed AMM with the feedback loop. A single cell of the proposed AMM is fabricated and an experimental setup is constructed to verify the material properties of the AMM. Several designs for the control system of the cell are proposed and their performance is evaluated. The effective density of the cell is then controlled using an outer control loop with an adaptive control algorithm that estimates the density of the material and adjusts the dynamics of the cell to achieve the desired density value.

This chapter is divided into eight sections. In Section 5.1, the structure of the building block of the AMM is introduced. In Section 5.2, an analytic model for the prediction of the material properties of the introduced AMM is discussed. In Section 5.3, the stability of the AMM cell under closed loop operation is discussed. In Section 5.4, a test setup for the experimental evaluation of the material properties of the suggested AMM is introduced and the experimental and analytic results are compared. In Section 5.5, several types of controllers for the AMM cell are discussed and their performance is

TABLE 5.1: Properties of the materials used in the construction of the AMM cell.

Property	Unit	PZT-4	Brass	Silver
$\rho$	kg/m <sup>3</sup>	7500	8750	10490
$C_{11}$	GPa	139	169	125
$C_{12}, C_{23}$	GPa	78	87	74
$C_{33}$	GPa	115	169	125
$e_{31}$	C/m <sup>2</sup>	-5.2	-	-
$e_{33}$	C/m <sup>2</sup>	15	-	-
$\epsilon_{11}$		1475	-	-
$\epsilon_{33}$		1300	-	-

evaluated. In Section 5.6 a closed feedback loop for controlling the density of the AMM cell through an adaptive control algorithm is introduced.

## 5.1 Material Construction

The suggested one dimensional active metamaterial consists of an array of clamped piezoelectric diaphragms (piezoelectric buzzers) with air as the background material. The material is formed by repeating the unit cell shown in Figure 5.1 along the shown propagation ( $x$ ) direction. The unit cell consists of circular piezoelectric diaphragm clamped along the circumference at a diameter of 38 mm and the unit cell has a total length of 10 mm along the propagation direction. The diaphragm consists of three layers; a brass disk of thickness 140  $\mu$ m in the middle with two piezoelectric layers, each of thickness 140  $\mu$ m, deposited on each side. The piezoelectric layers are made from PZT-4 material and they have a diameter of 30 mm. They are covered with silver electrodes of thickness 10  $\mu$ m from the external sides. The electrodes cover a circle of diameter 28 mm. The material properties of the different components of the cell are summarized in Table 5.1.

## 5.2 Theoretical Formulation

### 5.2.1 Acoustic impedance of the piezoelectric diaphragm

Considering the piezoelectric diaphragm as a laminated plate. According to the classical laminated plate theory, the constitutive equations for each orthotropic lamina  $k$  can be

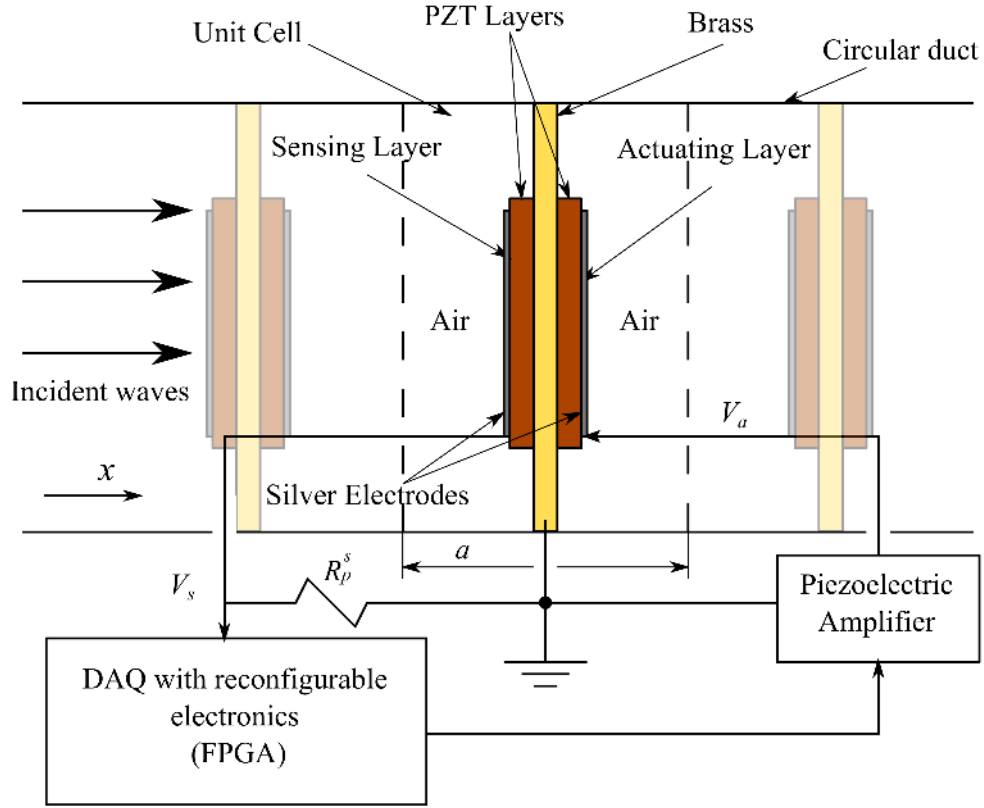


FIGURE 5.1: Schematic for the construction of the suggested 1D AMM unit cell.

written as [113]:

$$\begin{bmatrix} \sigma_1 \\ \sigma_2 \\ \sigma_6 \end{bmatrix} = \begin{bmatrix} Q_{11} & Q_{12} & 0 \\ Q_{21} & Q_{22} & 0 \\ 0 & 0 & Q_{66} \end{bmatrix} \begin{bmatrix} \varepsilon_1 \\ \varepsilon_2 \\ \varepsilon_6 \end{bmatrix} - \begin{bmatrix} 0 & 0 & \bar{e}_{31} \\ 0 & 0 & \bar{e}_{32} \\ 0 & 0 & 0 \end{bmatrix} \begin{bmatrix} \mathcal{E}_1 \\ \mathcal{E}_2 \\ \mathcal{E}_3 \end{bmatrix} \quad (5.1)$$

where  $\sigma_1, \sigma_2, \varepsilon_1, \varepsilon_2$  are the in-plane normal stresses and strains respectively,  $\sigma_6, \varepsilon_6$  are the in-plane shear stress and strain respectively,  $\mathcal{E}_1, \mathcal{E}_2, \mathcal{E}_3$  are the components of the electric field applied to the lamina,  $Q_{ij}$  are the plane stress reduced stiffness and  $\bar{e}_{31}, \bar{e}_{32}$  are the plane stress reduced voltage coefficients.  $Q_{ij}$  and  $\bar{e}_{ij}$  can be calculated from the components of the complex elastic compliance matrix  $\mathbf{C}^*$  and the piezoelectric matrix  $\mathbf{e}$  using the following relations:

$$Q_{ij} = C_{ij}^* - \frac{C_{i3}^* C_{3j}^*}{C_{33}^*} \quad (5.2)$$

$$\bar{e}_{ij} = e_{ij} - \frac{C_{i3}^*}{C_{33}^*} e_{33} \quad (5.3)$$

The complex compliance matrix  $\mathbf{C}^*$  includes material damping effects, and it is calculated by:

$$\mathbf{C}^* = \mathbf{C}(1 + \eta j) \quad (5.4)$$

where  $\mathbf{C}$  is the compliance matrix and  $\eta$  is the material loss factor.

Given that the layers of the diaphragm are transversely isotropic, have the same orientation and that their distribution about the mid-plane is symmetric, the deflection of the diaphragm in the transverse direction is decoupled from the in-plane directions. Hence, the transverse and the in-plane deflection of the diaphragm are then given by:

$$(D_{11}\nabla^4 - N^F\nabla^2 + I_o\frac{\partial^2}{\partial t^2})w(r, t) = p_i(t) + f_3^P(t) \quad (5.5)$$

$$(A_{11}\nabla^2 + I_o\frac{\partial^2}{\partial t^2})u(r, t) = f_1^P(t) \quad (5.6)$$

where  $\nabla^4$  is the bi-harmonic operator,  $\nabla^2$  is the Laplacian operator,  $w$  is the transverse deflection of the plate,  $u$  is the in-plane deflection in the radial direction,  $N^F$  are the in-plane forces,  $p_i(t)$  is the acoustic pressure incident on the diaphragm,  $A_{ij}$  are the extensional stiffnesses and  $D_{ij}$  are the bending stiffnesses.

The terms  $f_i^P$  are determined from the resultant forces  $N^P$  and moments  $M^P$  induced by the piezoelectric effect:

$$f_1^P = \nabla^2 N^P, \quad f_3^P = -\nabla^2 M^P \quad (5.7)$$

The in-plane forces due to the piezoelectric effect are only present at the lateral edges of the area covered by the electrodes. When the electric potential applied to the piezoelectric layers is uniform across the area, the terms  $f_1^P$  and  $f_3^P$  are reduced to zero except at the lateral boundaries of the electrode. Assuming rest initial conditions Equations (5.5) and (5.6) can be converted to the frequency domain by the aide of Laplace transform. The transformed equation is given by:

$$\begin{aligned} (D_{11}\nabla^4 - N^P\nabla^2 + I_0s^2)W(s) &= P_i(s) \\ (A_{11}\nabla^2 + I_0s^2)U(s) &= 0 \end{aligned} \quad (5.8)$$

For an axisymmetric diaphragm, the solutions of Equation (5.8) have the form:

$$\begin{aligned}
 W(r, s) &= E_1(s)J_0(g_1(s)r) + E_2(s)Y_0(g_1(s)r) \\
 &\quad + E_3(s)I_0(g_2(s)r) + E_4(s)K_0(g_2(s)r) \\
 &\quad - \frac{P_i(s)}{D_{11}g^4(s)} \\
 U(r, s) &= E_5(s)J_1(g_p(s)r) + E_6(s)Y_1(g_p(s)r)
 \end{aligned} \tag{5.9}$$

where  $g$  is wave number of the flexural waves traveling through the diaphragm and is given by:

$$g^4 = \frac{-I_o s^2}{D_{11}} \tag{5.10}$$

$g_1, g_2$  are given by:

$$g_1^2 = \frac{-N^F + \sqrt{4D_{11}^2 g^4 + N^F}}{2D_{11}} \tag{5.11}$$

$$g_2^2 = \frac{-N^F - \sqrt{4D_{11}^2 g^4 + N^F}}{2D_{11}} \tag{5.12}$$

$g_p$  is defined as:

$$g_p^2 = \frac{-I_o s^2}{A_{11}} \tag{5.13}$$

$E_1 \dots E_6$  are constants to be determined from the boundary conditions of the plate. From this point forward, the dependency of the variables on  $s$  will be omitted for brevity. Assuming the diaphragm consisting of  $N_c$  uniform annular sections. Equation (5.8) can be solved for each section  $l$  and the transverse and in-plane deflections at section  $l$  are then given by:

$$\begin{aligned}
 W_l(r) &= E_{1l}J_0(g_{1l}r) + E_{2l}Y_0(g_{1l}r) \\
 &\quad + E_{3l}I_0(g_{2l}r) + E_{4l}K_0(g_{2l}r) - \frac{P_i}{D_{11l}g_{kl}^4} \\
 U_l(r) &= E_{5l}J_1(g_{pl}r) + E_{6l}Y_1(g_{pl}r)
 \end{aligned} \tag{5.14}$$

The constants  $E_{1l} \dots E_{6l}$  are determined by the boundary conditions of the diaphragm, in addition to the continuity conditions between each two neighboring sections. The

boundary and continuity conditions are hence given by:

$$\begin{aligned}
W_1(0) &= \text{finite}, & U_1(0) &= \text{finite} \\
M_l(R_l) &= M_{l+1}(R_l), & Q_l(R_l) &= Q_{l+1}(R_l) \\
W_l(R_l) &= W_{l+1}(R_l), & \left. \frac{\partial W_l}{\partial r} \right|_{R_l} &= \left. \frac{\partial W_{l+1}}{\partial r} \right|_{R_l} \\
U_l(R_l) &= U_{l+1}(R_l), & N_l(R_l) &= N_{l+1}(R_l) \\
W_{N_c}(R_{N_c}) &= 0, & \left. \frac{\partial W_{N_c}}{\partial r} \right|_{R_{N_c}} &= 0, & U_{N_c}(R_{N_c}) &= 0
\end{aligned} \tag{5.15}$$

where  $M_l(r)$  is the moment at section  $l$  and it is given by:

$$M_l(r) = -D_{11l} \frac{\partial^2 W_l}{\partial r^2} - D_{12l} \frac{1}{r} \frac{\partial W_l}{\partial r} - M_l^P \tag{5.16}$$

$Q_l(r)$  is the shear force at section  $l$  and it is given by:

$$Q_l(r) = -D_{11l} \frac{\partial}{\partial r} \left( \frac{\partial^2 W_l}{\partial r^2} + \frac{1}{r} \frac{\partial W_l}{\partial r} \right) \tag{5.17}$$

$N_l(r)$  is the harmonic in-plane force:

$$N_l(r) = A_{11l} \frac{\partial U_l}{\partial r} + A_{12l} \frac{U_l(r)}{r} + N_l^P \tag{5.18}$$

and  $N_l^P, M_l^P$  are the resultant forces and moments due to the piezoelectric effect and they are calculated from the relation:

$$N_l^P = \sum_{k=1}^N \int_{z_k}^{z_{k+1}} \bar{e}_{31}^{(k)} \mathcal{E}_3^{(k)} dz \tag{5.19}$$

$$M_l^P = \sum_{k=1}^N \int_{z_k}^{z_{k+1}} \bar{e}_{31}^{(k)} \mathcal{E}_3^{(k)} z dz \tag{5.20}$$

where  $\mathcal{E}_3^{(k)}$  is the traverse electric field applied to layer  $k$ . Equations (5.15) can be reorganized in matrix form:

$$\boldsymbol{\eta} \bar{E} = \bar{L}^{Pi} + \bar{L}^{Pr} \tag{5.21}$$

where  $\boldsymbol{\eta}$  is a  $6N_c \times 6N_c$  matrix which is only dependent on the diaphragm properties regardless of the excitation,  $\bar{E}$  is a  $6N_c \times 1$  vector of all the unknown constants,  $\bar{L}^{Pi}$  and  $\bar{L}^{Pr}$  are  $6N_c \times 1$  load vectors caused by the piezoelectric and the pressure excitations on

the diaphragm. The piezoelectric loads depend on the electric circuits connected to the piezoelectric layers. The electric charge generated on the piezoelectric layer  $k$  in section  $l$  is given in polar form by [114]:

$$\begin{aligned} Q_{e_l}^{(k)} = & 2\pi e_{31}^{(k)} \int_{R_{l-1}}^{R_l} \left[ r \frac{\partial U_l}{\partial r} + U_l(r) \right] dr \\ & + 2\pi \epsilon_{33}^{(k)} \int_{R_{l-1}}^{R_l} \mathcal{E}_3^{(k)} r dr \\ & - 2\pi e_{31}^{(k)} z^{0(k)} \int_{R_{l-1}}^{R_l} \left[ r \frac{\partial^2 W_l}{\partial r^2} + \frac{\partial W_l}{\partial r} \right] dr \end{aligned} \quad (5.22)$$

where  $\epsilon_{33}^{(k)}$  is the electric permittivity under constant stress of piezoelectric layer  $k$  and  $z^{0(k)}$  is defined by:

$$z^{0(k)} = \frac{z_{k+1} + z_k}{2} \quad (5.23)$$

For the part of the piezoelectric layers that is fully covered with electrodes,  $\mathcal{E}_3^{(k)}$  could be written in terms of the potential difference applied to the layer  $V_p^{(k)}$ :

$$\mathcal{E}_3^{(k)} = \frac{-V_p^{(k)}}{h^{(k)}} \quad (5.24)$$

where  $h^{(k)}$  is the thickness of layer  $k$ . Rewriting Equation (5.22) in terms of  $V_p^{(k)}$  and generated electric current  $I_e^{(k)}(s)$ :

$$\begin{aligned} I_e^{(k)}(s) = & sQ_e^{(k)}(s) \\ = & 2\pi e_{31} s \int_{R_{l-1}}^{R_l} \left[ r \frac{\partial U_l}{\partial r} + U_l(r) \right] dr - C_p^{(k)} s V_p^{(k)} - 2\pi e_{31} z_k^0 s \int_{R_{l-1}}^{R_l} \left[ r \frac{\partial^2 W_l}{\partial r^2} + \frac{\partial W_l}{\partial r} \right] dr \end{aligned} \quad (5.25)$$

where  $C_p^{(k)}$  is the electric capacitance of layer  $k$ :

$$C_p^{(k)} = \frac{\pi(R_l^2 - R_{l-1}^2)\epsilon_{33}}{h^{(k)}} \quad (5.26)$$

Equation (5.25) can be used to construct the equivalent electric circuit model for piezoelectric layer  $k$ , which is shown in Figure 5.2 where:

$$I_g^{(k)}(s) = 2\pi e_{31} s \int_{R_{l-1}}^{R_l} \left[ r \frac{\partial U_l}{\partial r} + U_l(r, s) \right] dr - 2\pi e_{31} z_k^0 s \int_{R_{l-1}}^{R_l} \left[ r \frac{\partial^2 W_l}{\partial r^2} + \frac{\partial W_l}{\partial r} \right] dr \quad (5.27)$$

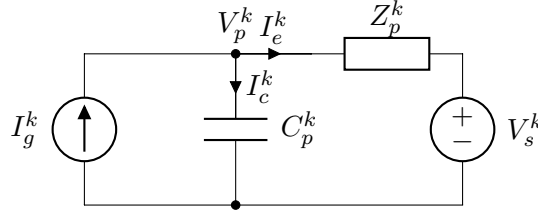


FIGURE 5.2: An electrical circuit model for piezoelectric layer  $k$  connected to an arbitrary circuit represented by its Thevenin's equivalent

$I_g^{(k)}$  only depends on the deflections of the diaphragm and not the external circuit, it can be written in matrix form as:

$$I_g^{(k)} = \bar{\alpha}^{(k)} \bar{E} \quad (5.28)$$

where  $\bar{\alpha}$  is a  $1 \times 6N_c$  vector whose elements are evaluated from Equation (5.27). The value of  $V_p^{(k)}$  is determined by the nature of the circuit connect to each layer. Considering Thevenin's equivalent circuit shown in Figure 5.2:

$$\begin{aligned} I_e^{(k)} &= I_g^{(k)} - C_p^{(k)} s V_p^{(k)} \\ &= \frac{V_p^{(k)} - V_s^{(k)}}{Z_p^{(k)}} \end{aligned} \quad (5.29)$$

Rearranging to determine the value of  $V_p^{(k)}$ :

$$V_p^{(k)} = G_e^{(k)} Z_p^{(k)} I_g^{(k)} + G_e^{(k)} V_s^{(k)} \quad (5.30)$$

where:

$$G_e^{(k)} = \frac{1}{1 + Z_p^{(k)} C_p^{(k)} s} \quad (5.31)$$

For the diaphragm shown in Figure 5.1, the voltage generated by one of the piezoelectric layers (sensing layer) is measured and fed to a network of reconfigurable electronics ( $G_e$ ) which is connected to a voltage amplifier ( $G_a$ ). The amplifier applies excitation voltage on the other layer (actuating layer). The presence of the reconfigurable electronics (reconfigurable controller) in the loop allows for programming the dynamics of the cell in an arbitrary manner, as long as the stability of the loop is maintained and the maximum allowable excitation voltage is not reached. Applying Equation (5.30) on the sensing layer results in:

$$V_p^s = G_e^s R_p^s I_g^s \quad (5.32)$$

where the superscript (*s*) indicates the sensing piezoelectric layer. Similarly, for the actuating layer:

$$V_p^a = G_e^a R_p^a I_g^a + G_e^a V_s^a \quad (5.33)$$

where  $R_p^a$  is the output impedance of the piezoelectric amplifier. The applied voltage on the actuating layer  $V_s^a$  can be calculated from:

$$V_s^a = G_c G_a V_p^s = G_a G_c G_e^s R_p^s I_g^s \quad (5.34)$$

Thus:

$$V_p^a = G_e^a R_p^a I_g^a + G_e^a G_a G_c G_e^s R_p^s I_g^s \quad (5.35)$$

Substituting for  $I_g^a$  and  $I_g^s$  using Equation (5.28):

$$V_p^a = G_e^a R_p^a \bar{\alpha}^a \bar{E} + G_e^a G_a G_c G_e^s R_p^s \bar{\alpha}^s \bar{E} \quad (5.36)$$

$$V_p^s = G_e^s R_p^s \bar{\alpha}^s \bar{E} \quad (5.37)$$

Combining Equations (5.19,5.20,5.24,5.36,5.37), the piezoelectric load vector is then:

$$\bar{L}^{Pi} = \bar{\phi}^s G_e^s R_p^s \bar{\alpha}^s \bar{E} + \bar{\phi}^a G_e^a R_p^a \bar{\alpha}^a \bar{E} + \bar{\phi}^a G_c G_a G_e^a G_e^s R_p^s \bar{\alpha}^s \bar{E} \quad (5.38)$$

where  $\bar{\phi}^s$  and  $\bar{\phi}^a$  are  $6N_e \times 1$  vectors constructed by substituting by Equations (5.19, 5.20, 5.24) into Equations (5.15). They represent the effect of the applied voltage on the two piezoelectric layers on the deflection of the diaphragm. Substituting by Equation (5.38) in Equation (5.21):

$$\boldsymbol{\eta} \bar{E} = \bar{\phi}^s G_e^s R_p^s \bar{\alpha}^s \bar{E} + \bar{\phi}^a G_e^a R_p^a \bar{\alpha}^a \bar{E} + \bar{\phi}^a G_c G_a G_e^a G_e^s R_p^s \bar{\alpha}^s \bar{E} + \bar{L}^{Pr} \quad (5.39)$$

Equation (5.39) can be reorganized in the form:

$$\boldsymbol{\eta}_o \bar{E} = \bar{\phi}^a G_e^a G_a G_c G_e^s R_p^s \bar{\alpha}^s \bar{E} + \bar{L}^{Pr} \quad (5.40)$$

and

$$\boldsymbol{\eta}_o = \boldsymbol{\eta} - \bar{\phi}^s G_e^s R_p^s \bar{\alpha}^s \bar{E} + G_e^a R_p^a \bar{\alpha}^a \bar{E} \quad (5.41)$$

where  $\boldsymbol{\eta}_o$  represents the dynamics of the cell with no control action applied on the actuation layer. The dynamics of the closed loop cell are summarized in the block

diagram shown in Figure 5.3. The unknown coefficients are then given by:

$$\bar{E} = \left( \eta_o - \bar{\phi}^a G_e^a G_a G_c G_e^s R_p^s \bar{\alpha}^s \right)^{-1} \bar{L}^P r \quad (5.42)$$

Now that the unknown coefficients are determined, the average displacement of the diaphragm  $\widetilde{W}$  is given by:

$$\widetilde{W} = \frac{1}{A_t} \int_{A_t} W(r) dA \quad (5.43)$$

where  $A_t$  is the total area of the diaphragm. The previous equation could be rewritten in matrix form

$$\widetilde{W} = \bar{\alpha}_p \bar{E} + \gamma \quad (5.44)$$

where  $\bar{\alpha}_p$  is a  $1 \times 6N_c$  vector of the coefficients resulting from Equation (5.43) and  $\gamma$  represents the feed through terms that don't depend on the boundary conditions. The impedance of the diaphragm is then given by:

$$Z_{dia} = \frac{\widetilde{W}}{P_i} \quad (5.45)$$

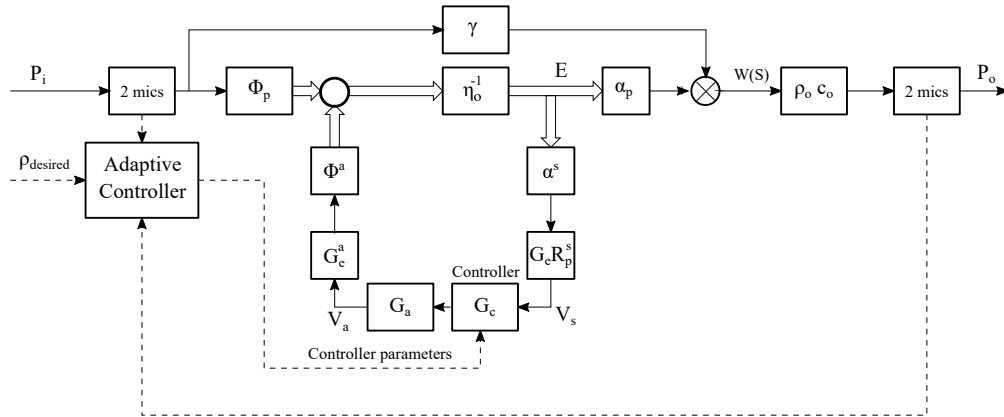


FIGURE 5.3: A block diagram representing the dynamics of the closed loop cell with adaptive control

### 5.3 Stability of the Cell

The controller transfer function  $G_c$  can be chosen to set the effective material properties of the AAM to arbitrary values. However, this must be done while keeping the cell stable and avoiding any self-sustained oscillations. This is done by examining the open loop

transfer function of the system  $G_{OL}$ . From Figure 5.3, the open loop transfer function of the cell can be calculated from:

$$G_{OL} = G_c G_a G_e^a G_e^s R_p^s \bar{\alpha}^s \eta_o \bar{\phi}^a \quad (5.46)$$

Since the diaphragm is a continuous structure, the estimation of the stability of the system is not straight forward. The estimated open loop transfer function ( $G_{OL}$ ) is not rational; hence, it is difficult to estimate the stability of the cell analytically. It is possible however to determine the stability margin of the system graphically by examining the bode plot of  $G_{OL}$  around the frequency region targeted by the controller ( $G_c$ ). Thus, to ensure the stability of the system,  $G_c$  should be chosen to have a decaying response outside the targeted frequency region.

## 5.4 Characterization of the AMM cell

The test setup shown in Figure 5.4 is used to characterize the effective material properties of the cell using the two-source method[110]. The setup has an inner tube diameter of 25 mm. Three PCB model 378C10 1/4" IEPE microphones are flush mounted to each tube. Two SEAS W18EX001 100W speakers powered by a Yamaha P3500S audio amplifier are used to provide upstream and downstream acoustic excitation. The signals of the microphones are connected to the channels of a NI PXI-4472 eight channel input module mounted on a NI PXI-1042Q data acquisition system. The sensitivity of each microphone is calibrated using a B&K 4231 sound calibrator. The relative phase between them is calibrated using a phase calibrator. The control circuit of the cell is constructed by connecting the signal of the sensing PZT layer to an input channel of an NI PXI-7854R multifunction reconfigurable I/O. The output channel of the NI PXI-7854R is connected to a Piezodrive MX200 200V 1A Piezo Driver, which supplies the voltage signal to the actuating PZT layer.

A single AMM cell is constructed by clamping a AB4113B commercial bender (piezo-electric diaphragm) using the mechanical clamp shown in Figure 5.4. The diameter of the designed cell (38 mm) is different from that of the impedance tubes (25 mm) so the clamp was designed with a cone adaptor to connect the cell to the upstream and

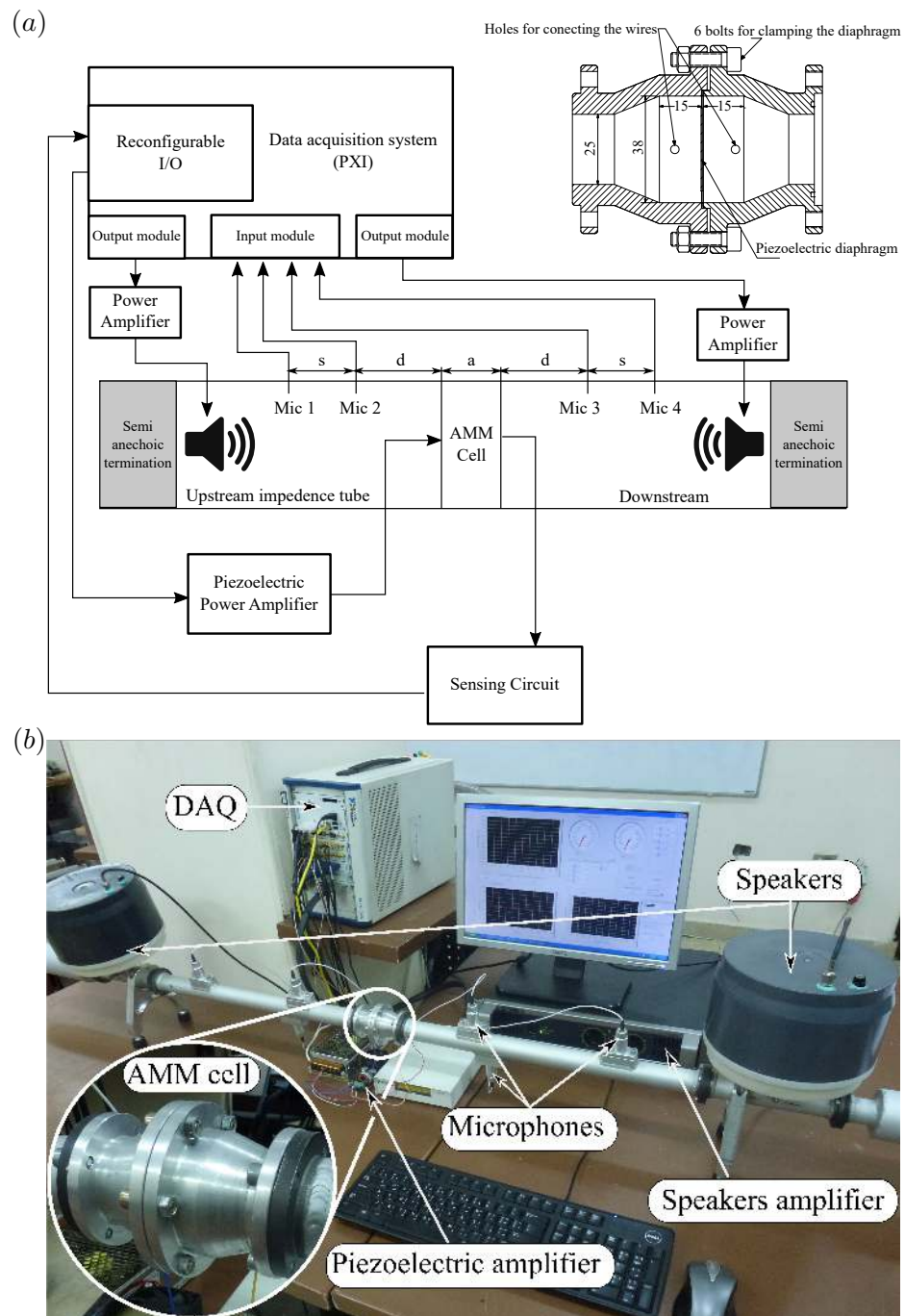


FIGURE 5.4: (a) Schematic for the test setup connections and the construction of the AMM cell (b) Photo of the actual test setup.

downstream impedance tubes. The effective material properties of the cell are determined by exciting the cell with band limited white-noise excitations up to 2000 Hz. For each measurement 100 readings are recorded and averaged to reduce the measurement noise. With the controller gain set to zero, open loop cell, the dispersion of the effective density is estimated experimentally and compared to the analytic results obtained from the developed model (Figure 5.5). An excellent agreement is observed between the predicted and measured values over the studied frequency range, even though a commercial diaphragm is used and no special manufacturing techniques were used to ensure its properties. Figure 5.5 shows that the value of the density approaches zero near the first resonance frequency, around 1100 Hz. It changes from large negative values for frequencies below the resonance to large positive values for a certain frequency range above the first resonance.

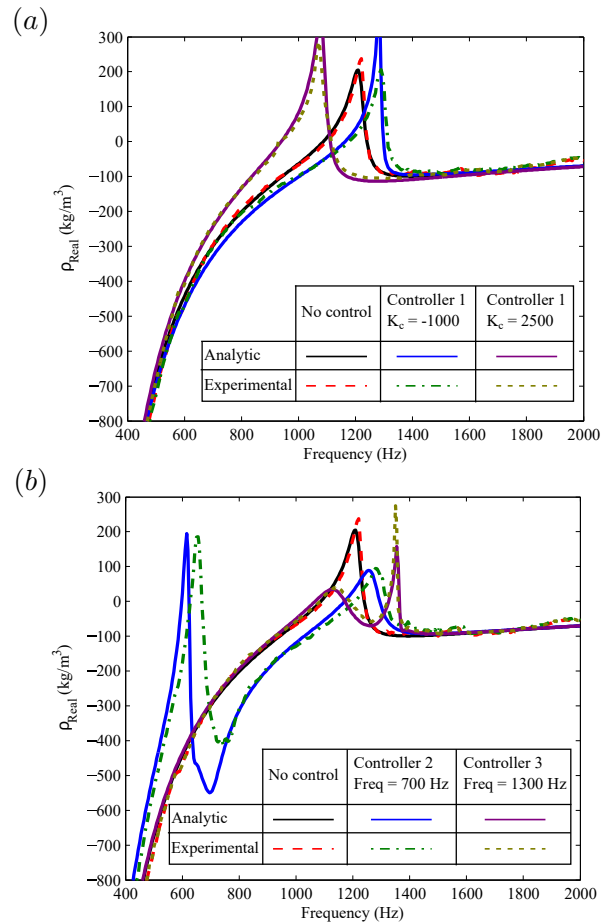


FIGURE 5.5: The dispersion effective density of the developed AMM characterized analytically and experimentally. The results obtained without any control applied to the cell are compared to those obtained (a) using controller 1 (Equation (5.47)) with  $K_c=-1000$  and  $K_c=2500$  and (b) using controller 2 (Equation (5.48)) with  $f_c=700$  Hz and  $K_c = 4 \times 10^6$  and controller 3 (Equation (5.49)) with  $f_c=1300$  Hz and  $K_c=-120$ .

## 5.5 Controller transfer function

The dispersion of the density suggests that shifting the first resonance to lower or higher frequencies would allow for controlling the effective density within a limited frequency range near the resonance of the cell. This shift could be done using a lead-lag controller with the following transfer function:

$$G_c = \frac{K_c(s + z_1)}{(s + p_1)(s + p_2)} \quad (5.47)$$

The value of the gain  $K_c$  controls the amount of the shift and its sign controls its direction, where the locations of the poles ( $p_1, p_2$ ) and the zero ( $z_1$ ) are chosen to maximize the allowable frequency shift before the system becomes unstable. This controller approach however limits the controllable frequency range to a small region around the open loop resonance of the diaphragm. The effect of applying this controller to the cell is shown in Figure 5.5(a). The parameters of the controller were set to  $z_1=1000$ ,  $p_1=p_2=-4500$  and  $K$  set to 2500 for negative shift and -1000 for positive shift of the resonance. The values of the poles and zeros were chosen to achieve maximum shift in the resonance of the cell without causing instability. This was done by shaping the open loop transfer function of the cell  $G_{OL}$ . Good agreement between the predicted and measured dispersion of the density was observed for both negative and positive frequency shift controller configurations.

An alternative approach would be to set the transfer function of the controller so that it adds an additional resonance frequency to the closed loop transfer function. This induces a similar behavior to what happens near the open loop resonance at the selected additional frequency. For frequencies below the open loop resonance, this could be done by setting the transfer function of the controller  $G_c$  to:

$$G_c = \frac{K_c}{s^2 + 2\zeta_c\omega_c s + \omega_c^2} \quad (5.48)$$

where  $\omega_c = 2\pi f_c$  and  $f_c$  is calculated from the target resonant frequency of the controller in Hz,  $\zeta_c$  is damping ratio of the controller and  $K_c$  is the controller gain. To control the density of the cell around a certain target frequency,  $\omega_c$  of the controller could be initially set to match this frequency. By shifting  $\omega_c$  to higher or lower values, the effective density could be fully controlled within the reachable limits of the controller. These limits are

bounded by the values of  $K_c$  and  $\zeta_c$  which maintain the system's stability. If the target frequency is above the open loop resonance, the transfer function could be set to:

$$G_c = \frac{K_c(s + z_1)}{s^2 + 2\zeta_c\omega_c s + \omega_c^2} \quad (5.49)$$

where ( $z_1$ ) is an additional zero, used to tune the phase of the open loop transfer function of the system to ensure its stability. Figure 5.5(b) shows the effect of setting the controller transfer function to the resonant controllers (Equation (5.48) with  $\zeta_c=0.04$ ,  $K_c = 4 \times 10^6$  and  $f_c=700$  Hz and Equation (5.49)  $\zeta_c=0.04$ ,  $K_c=-120$  and  $f_c=1300$  Hz) on the dispersion of the density of the cell. The analytic model succeeds in the estimation of the general behavior of the dispersion plots of the cell under the effect of the two controllers. The resonant controllers achieve their target objective by adding an additional zero-crossing frequency (additional resonance) near the frequency which they are targeting.

## 5.6 Adaptive control of the cell density

The ability to measure the density of the cell in real-time allows for adapting the parameters of the controller transfer function to achieve a desired density at a specific frequency. This first requires the density of the cell to be estimated in real-time. A density estimator is developed based on the same two-source method[110] used in the measurements. Two microphones at each side of the cell are used to decompose the acoustic waves passing through the cell and estimate its real-time reflection and transmission coefficients. The two-source method however requires the cell to be excited at least once from each side in order to evaluate the 4 elements of the scattering matrix. To overcome this limitation, the fact that the cell is symmetrical in the propagation direction will be used to reduce the number of excitations to one. This means that the elements of the scattering matrix could be evaluated in the presence of incident acoustic waves from any direction. The signals acquired from the microphones are sampled with a constant sampling time ( $T_s$ ) until a predetermined number of samples, time window ( $T_w$ ), are acquired. The window is then converted to the frequency domain, and the transfer functions between the microphones are determined and converted to the reflection and transmission coefficients of the cell[109]. These coefficients are then fed to an

inverse program which is based on the retrieval method developed by Fokin *et al.*[89] to estimate the real-time effective density of the cell. An adaptive control algorithm is designed to use the frequency content of the incident waves to determine the dominant frequency of the acoustic waves passing through the cell. It then uses the density estimator to determine the effective density of the cell. Knowing the error between the desired effective density and the required density, it uses a traditional PID controller to adjust the parameters of the feedback controller ( $G_c$ ). A discrete PID controller is used to tune the parameters of the feedback controller. The resonant controller frequency  $\omega_c$  is determined from the following relation:

$$\omega_c = \omega_{c_o} + \Delta\omega_c \quad (5.50)$$

where  $\omega_{c_o}$  is the detected frequency of the incident excitation and  $\Delta\omega_c$  is the output of the PID controller.

$$\Delta\omega_c = K_p + \frac{K_i T_w z}{z - 1} + \frac{K_d N (z - 1)}{(1 + N T_w) z - 1} \quad (5.51)$$

where  $K_p$ ,  $K_i$  and  $K_d$  are the proportional, integral and differential gains of the controller,  $z$  is the z-transform variable and  $N$  is the cutoff frequency of the low pass filter of the derivative term. The gains of the PID controller as well as the gain of the resonant controller ( $K_c$ ) are determined based on the incident frequency ( $\omega_{c_o}$ ) from a set of tuned values which are determined offline for each frequency range separately. The damping of the controller ( $\zeta_c$ ) is kept constant for all controllers.

To realize the adaptive controller, the signals of the microphones used in the measurement process are branched and connected to a second NI PXI-4472 eight channel input module mounted on the data acquisition system. The readings from the first input module are used in the measurement process, while those of the second input module are used in the control process. This was done on the hardware level to ensure the complete separation between the two processes.

The adaptive control algorithm is implemented as a standalone C program using the NI Labwindows/CVI libraries to interface with the microphones' signal from the input module and to set the parameters of the controller. The flow of the adaptive control algorithm is summarized in Figure 5.6. To test the performance of the adaptive controller, the cell is excited using upstream and downstream stepped sine excitations between 500 Hz and 1500 Hz. Each single frequency excitation is applied on the cell for 10 seconds so that

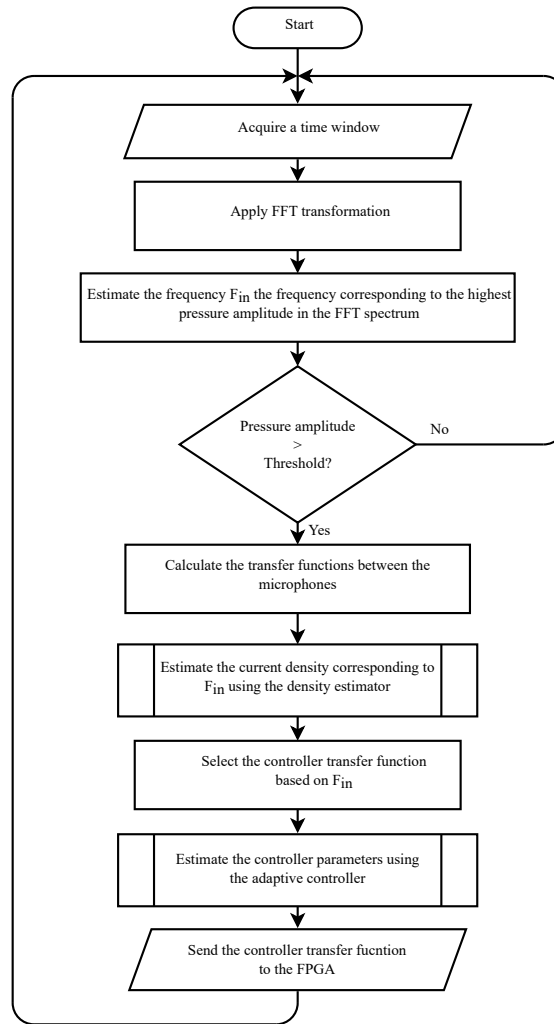


FIGURE 5.6: Flowchart for the procedure of the adaption of the cell density based on the incident excitation.

the response of the controller completely settles before recording the measurement data. The effect of applying the adaptive control algorithm on the effective density of the AMM cell is shown in Figure 5.7(a). It shows that the controller can achieve any desired density value between  $-100 \text{ kg/m}^3$  and  $100 \text{ kg/m}^3$  including near zero density conditions. This is achievable for any single frequency between 500 Hz and 1500 Hz. For most of the studied frequency range, the controller can change the dynamics of the AMM cell to a value within 10% of the desired density set-point regardless of the open loop density value at the targeted frequency. An exception to this are frequencies near 1500 Hz, for a set value of  $100 \text{ kg/m}^3$ , the error reaches about 30%. This defines the limits of the controllable region of the adaptive controller. The effect of the controller on the bulk modulus of the AMM is shown in Figure 5.7(b). While the controller varies the density between large negative and positive values, the bulk modulus of the material

remained almost constant around that of air  $B_o \approx 10^5 \text{N/m}^2$ . This is expected, since membrane type metamaterials are mainly known for unusual effective density[23]. This is also desirable, the control effort only affects the effective density of the AMM and has minimal side effects on the effective bulk modulus. An AMM material with fully controllable material properties could be constructed by implementing a hybrid design, which incorporates another active element to control the bulk modulus. The time response of the controller was also evaluated. Figure 5.8 shows the step response of the cell when the control point is initially set to zero density and then suddenly changed to  $100 \text{ kg/m}^3$ . It shows that the cell density settles after around 3 seconds for all the studied frequencies, with different frequencies having different settling times. This is expected due to the non-linear nature of the adaptive control algorithm and the use of a different type of controller for each frequency range. An abnormal behavior is observed for the step response at 900 and 1300 Hz where the density diverges from the target set-point, before converging. These frequencies lie between the application regions of the lead/lag controller and the resonant controller since they are close to the resonance of the open loop, but not close enough for the lead/lag controller to cover the required density range of cell. The observed divergence happens because the adaptive control algorithm is set switch between the two types of controllers at this particular frequency range if the density set-point is not within the range of one of the controllers.

The achieved performance of the AMM cell opens the door to a set of possible applications for the developed material. Asymmetric transmission of acoustic waves could be easily achieved for single tone excitations. Given that the excitation is of a single sided nature, the material could be programmed to detect the propagation direction of the incident waves and adjust its density accordingly. The material could be programmed to work as an active acoustic filter with arbitrary stop (negative density) and pass (near zero density) bands within the material's controllable frequency range. The material could be also programmed to achieve any desired density gradient, given that a sufficient number of cells is used.

## 5.7 Conclusion

A design for a one-dimensional active acoustic membrane type metamaterial is introduced. The material consists of clamped composite piezoelectric diaphragms suspended

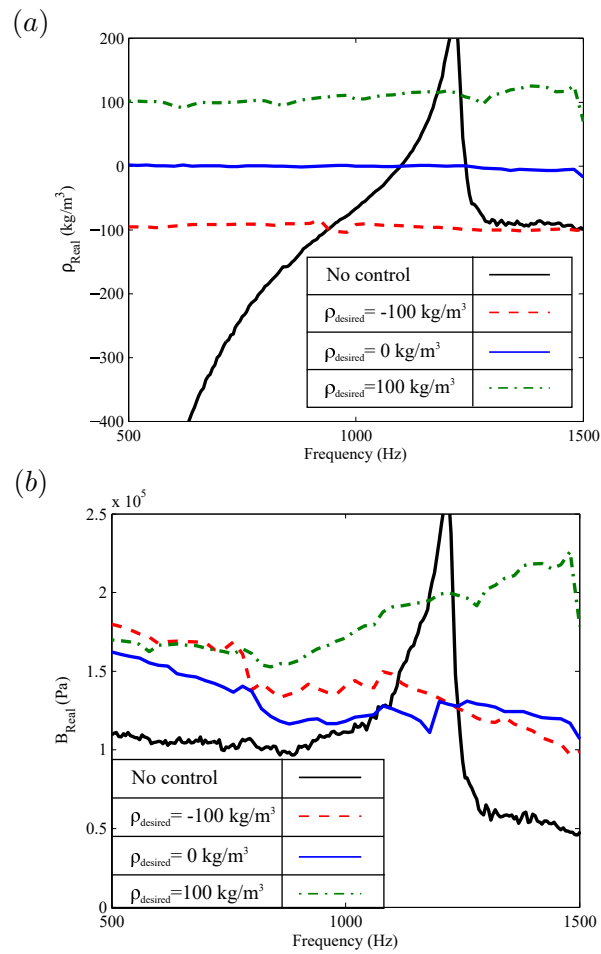


FIGURE 5.7: Dispersion plot of the (a) effective density and (b) Bulk modulus of the closed loop AMM cell with the adaptive control algorithm. Three different set points for the controller are compared  $\rho_{desired}=-100 \text{ kg/m}^3$ ,  $\rho_{desired}=0 \text{ kg/m}^3$  and  $\rho_{desired}=100 \text{ kg/m}^3$ . The measured open loop effective density is also plotted as a reference.

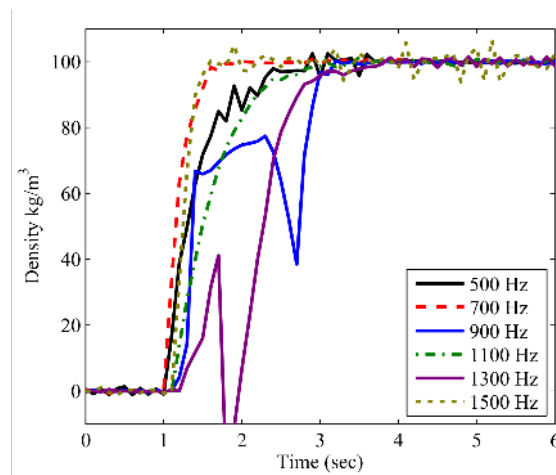


FIGURE 5.8: Step response of the closed loop AMM cell with the adaptive control algorithm. The density set-point is initially set for zero density and later stepped to  $100 \text{ kg/m}^3$ . This is done for different excitation frequencies.

in air. The effective density of the material is manipulated by adjusting the dynamic properties of the diaphragms through a closed loop feedback controller. An analytic model based on the acoustic two-port theory and the composite laminated plate theory is developed to predict the behavior of the AMM. Three different types of controllers for manipulating the material properties of the cell are introduced. An experimental test setup for the evaluation of the material properties of the AMM is constructed to verify the analytic results. Good agreement is observed between the measured and predicted values for the open loop cell. The proposed resonant feedback controllers are verified to add an additional predetermined resonance frequency to the cell and thus add a new zero-crossing point for the effective density of the material. An adaptive control algorithm is developed to achieve a closed loop control over the density of the AMM. The algorithm estimates the density of the AMM in real-time and adjusts the feedback control transfer function to reach a predetermined value for density of the material at the frequency corresponding to maximum incident acoustic pressure amplitude. The adaptive controller was proven experimentally to set the density of the cell to values ranging from  $-100 \text{ kg/m}^3$  up to  $100 \text{ kg/m}^3$  for acoustic waves with frequency between 500 and 1500 Hz. Potential applications for the developed material include controllable asymmetric sound transmission, programmable active filters and in the manufacturing of a programmable acoustic superlens.

## Chapter 6

# Conclusion and Future Work

### 6.1 Conclusion

Three different designs for active plate-type AMM have been introduced and analyzed. The three designs involved the use of piezoelectric PZT material to modify the dynamic behavior of the structure of the AMM. This was done by shifting the resonance frequency of resonators within the structure of the material in the first two designs and by implementing a closed feedback loop through a reconfigurable digital controller through the third design. An analytical model was constructed for each design. The three models involved the use of the acoustic two-port theory, the theory of piezoelectricity and the thin plate theory. While the suggested design for the first membrane consisted of a single layered plate. The second and third designs involved the use of composite plates with lead being used as a substrate in the second design and brass in the third design. The first two designs were studied analytically and numerically while the third design was implemented in practice and studied analytically and experimentally.

The first design was an open loop 1D AMM. It has the advantages of having the simplest construction and the largest achievable effective density compared to the other two; however, it has practical issues regarding the structure being very brittle.

In an attempt to mitigate the problems that appeared with the first design as well as study the implications of extending the approach to two dimensions, a more practical open loop 2D design was proposed. A composite plate was used to enhance the strength of the structure and the frame used to support the structure was also included in the

analysis. All the numerical results showed excellent agreement with the ones predicted analytically.

The open loop 1D AMM had a frequency dependent effective density ranging from  $-2000 \frac{kg}{m^3}$  to  $2000 \frac{kg}{m^3}$  within a frequency range up to  $(2000Hz)$ . The range of reachable density values was reduced in the second design to  $\pm 200 \frac{kg}{m^3}$  within a frequency range up to  $(1600Hz)$ . The 2D construction of the 2D design reduced its operating frequency range and reachable effective densities compared to the first 1D design. This happened because of the space limitations imposed by the material being two dimensional; in addition to the consideration of the supporting structure. For the three designs, the control action had a minimal effect on the bulk modulus. The results of the 2D active AMM showed that the effective density of the structure could be controlled for two orthogonal directions independently from each other. This means that the structure had an anisotropic tunable density. The capabilities of the developed 2D material were demonstrated by the construction of fully reconfigurable wave guide in which the direction of propagation of incident acoustic waves could be arbitrarily programmed and controlled. The behavior of the new structure was demonstrated both analytically and numerically.

The third design was for a 1D closed loop AMM. It consists of clamped composite piezoelectric diaphragms suspended in air. The effective density of the material is manipulated by adjusting the dynamic properties of the diaphragms through a closed loop feedback controller. Three controller designs were discussed and analyzed analytically before being verified experimentally. The experimental test setup was made by manufacturing a single cell and placing it between two impedance tubes with two microphones at each size. The microphones were used to analyze the acoustic waves traveling through the pipes and estimate the material properties of the cell. Good agreement is observed between the measured and predicted values of the open loop cell. The same microphones were used as density sensors and were used to estimate the real-time density of the cell. This density value was fed to an adaptive control algorithm in a closed loop control behavior. The experimental results showed that the density of the 1D closed loop cell could be adapted to any value between  $\pm 100 \frac{kg}{m^3}$  for single tone acoustic waves with frequency between 500 and 1500 Hz.

## 6.2 Future Work

Acoustic metamaterials have been the research focus in the past ten years. Many interesting and unforeseen discoveries and applications are still revealed on a monthly basis. This rapidly changing field has a lot of still undiscovered phenomena in the theoretical side, as well as, a lot of opportunities for better practical realizations and more practical problems to be tackled. The current work considered numerically open loop control for 2D active AMMs and experimentally closed loop control for a single 1D active AMM cell. A natural extension for this work would be to study the closed loop control of a multi-cell 1D structure, before extending this analysis to 2D and even 3D structures. Another path to follow would be to consider the possible applications for the developed material using the developed tunable density in the realization of different reconfigurable acoustic devices such as cloaks, lenses, filters, absorbers and sensing applications. Another path would be to consider a structure for an AMM whose bulk modulus could be directly controlled in a similar way to that obtained in the current study. The two approaches could be later merged to construct a material with fully controllable acoustic properties. This material properties could be adjusted between negative and positive values enabling all sorts of control on the propagation of waves inside the material. Another trending topic in the field of AMMs is to consider the non-linear behavior that arises from the geometry of the material or from the embedded elastic structures. The non-linear behavior have already yielded a set of interesting phenomena causing the AMM to shift from being perfect conductors to being perfect insulators depending on the amplitude of the applied excitations[115]. It was also being recently used to increase the bandwidth of AMM[116].

# Bibliography

- [1] Viktor G. Veselago. The electrodynamics of substances with simultaneously negative values of  $\epsilon$  and  $\mu$ . *Sov. Phys. Usp.*, 10(4):509, 1968. ISSN 0038-5670. doi:10.1070/PU1968v010n04ABEH003699.
- [2] J. B. Pendry, A. J. Holden, D. J. Robbins, and W. J. Stewart. Low frequency plasmons in thin-wire structures. *J. Phys.: Condens. Matter*, 10(22):4785, 1998. ISSN 0953-8984. doi:10.1088/0953-8984/10/22/007.
- [3] J. B. Pendry, A. J. Holden, D. J. Robbins, and W. J. Stewart. Magnetism from conductors and enhanced nonlinear phenomena. *IEEE Transactions on Microwave Theory and Techniques*, 47(11):2075–2084, November 1999. ISSN 0018-9480. doi:10.1109/22.798002.
- [4] D. R. Smith, Willie J. Padilla, D. C. Vier, S. C. Nemat-Nasser, and S. Schultz. Composite Medium with Simultaneously Negative Permeability and Permittivity. *Phys. Rev. Lett.*, 84(18):4184–4187, May 2000. doi:10.1103/PhysRevLett.84.4184.
- [5] Zhengyou Liu, Xixiang Zhang, Yiwei Mao, Y. Y. Zhu, Zhiyu Yang, C. T. Chan, and Ping Sheng. Locally Resonant Sonic Materials. *Science*, 289(5485):1734–1736, September 2000. ISSN 0036-8075, 1095-9203. doi:10.1126/science.289.5485.1734.
- [6] Malcolm J. Crocker. *Handbook of Acoustics*. John Wiley & Sons, March 1998. ISBN 978-0-471-25293-1.
- [7] Christophe Caloz. *Electromagnetic metamaterials: transmission line theory and microwave applications: the engineering approach*. John Wiley & Sons, Hoboken, N.J, 2006. ISBN 0-471-66985-7.

- 
- [8] Zhengyou Liu, C. T. Chan, and Ping Sheng. Analytic model of phononic crystals with local resonances. *Phys. Rev. B*, 71(1):014103, January 2005. doi:10.1103/PhysRevB.71.014103.
- [9] Ping Sheng, Jun Mei, Zhengyou Liu, and Weijia Wen. Dynamic mass density and acoustic metamaterials. *Physica B: Condensed Matter*, 394(2):256–261, May 2007. ISSN 0921-4526. doi:10.1016/j.physb.2006.12.046.
- [10] Yiqun Ding, Zhengyou Liu, Chunyin Qiu, and Jing Shi. Metamaterial with Simultaneously Negative Bulk Modulus and Mass Density. *Phys. Rev. Lett.*, 99(9):093904, August 2007. doi:10.1103/PhysRevLett.99.093904.
- [11] Graeme W. Milton and John R. Willis. On modifications of Newton’s second law and linear continuum elastodynamics. *P. Roy. Soc. Lond. A Mat*, 463(2079):855–880, March 2007. ISSN 1364-5021, 1471-2946. doi:10.1098/rspa.2006.1795.
- [12] Graeme W. Milton. New metamaterials with macroscopic behavior outside that of continuum elastodynamics. *New J. Phys.*, 9(10):359, October 2007. ISSN 1367-2630. doi:10.1088/1367-2630/9/10/359.
- [13] H. H. Huang and C. T. Sun. Wave attenuation mechanism in an acoustic metamaterial with negative effective mass density. *New J. Phys.*, 11(1):013003, January 2009. ISSN 1367-2630. doi:10.1088/1367-2630/11/1/013003.
- [14] Shanshan Yao, Xiaoming Zhou, and Gengkai Hu. Experimental study on negative effective mass in a 1d mass–spring system. *New J. Phys.*, 10(4):043020, April 2008. ISSN 1367-2630. doi:10.1088/1367-2630/10/4/043020.
- [15] Nicholas Fang, Dongjuan Xi, Jianyi Xu, Muralidhar Ambati, Werayut Srituravanich, Cheng Sun, and Xiang Zhang. Ultrasonic metamaterials with negative modulus. *Nat Mater*, 5(6):452–456, June 2006. ISSN 1476-1122. doi:10.1038/nmat1644.
- [16] Y. Cheng, J. Y. Xu, and X. J. Liu. Broad forbidden bands in parallel-coupled locally resonant ultrasonic metamaterials. *Applied Physics Letters*, 92(5):051913, February 2008. ISSN 0003-6951, 1077-3118. doi:10.1063/1.2839401.

- [17] Xinhua Hu, Kai-Ming Ho, C. T. Chan, and Jian Zi. Homogenization of acoustic metamaterials of Helmholtz resonators in fluid. *Phys. Rev. B*, 77(17):172301, May 2008. doi:10.1103/PhysRevB.77.172301.
- [18] Sam Hyeon Lee, Choon Mahn Park, Yong Mun Seo, Zhi Guo Wang, and Chul Koo Kim. Acoustic metamaterial with negative modulus. *J. Phys.: Condens. Matter*, 21(17):175704, April 2009. ISSN 0953-8984. doi:10.1088/0953-8984/21/17/175704.
- [19] Shu Zhang, Leilei Yin, and Nicholas Fang. Focusing Ultrasound with an Acoustic Metamaterial Network. *Phys. Rev. Lett.*, 102(19):194301, May 2009. doi:10.1103/PhysRevLett.102.194301.
- [20] Jordan Fey and William M. Robertson. Compact acoustic bandgap material based on a subwavelength collection of detuned Helmholtz resonators. *Journal of Applied Physics*, 109(11):114903, June 2011. ISSN 0021-8979, 1089-7550. doi:10.1063/1.3595677.
- [21] Fabrice Lemoult, Mathias Fink, and Geoffroy Lerosey. Acoustic Resonators for Far-Field Control of Sound on a Subwavelength Scale. *Phys. Rev. Lett.*, 107(6):064301, August 2011. doi:10.1103/PhysRevLett.107.064301.
- [22] Fabrice Lemoult, Nadège Kaina, Mathias Fink, and Geoffroy Lerosey. Wave propagation control at the deep subwavelength scale in metamaterials. *Nat Phys*, 9(1):55–60, January 2013. ISSN 1745-2473. doi:10.1038/nphys2480.
- [23] Tai-Yun Huang, Chen Shen, and Yun Jing. Membrane- and plate-type acoustic metamaterials. *The Journal of the Acoustical Society of America*, 139(6):3240–3250, June 2016. ISSN 0001-4966. doi:10.1121/1.4950751.
- [24] Z. Yang, Jun Mei, Min Yang, N. Chan, and Ping Sheng. Membrane-Type Acoustic Metamaterial with Negative Dynamic Mass. *Phys. Rev. Lett.*, 101(20):204301, November 2008. doi:10.1103/PhysRevLett.101.204301.
- [25] Sam Hyeon Lee, Choon Mahn Park, Yong Mun Seo, Zhi Guo Wang, and Chul Koo Kim. Acoustic metamaterial with negative density. *Phys. Lett. A*, 373(48):4464–4469, December 2009. ISSN 0375-9601. doi:10.1016/j.physleta.2009.10.013.
- [26] Christina J. Naify, Chia-Ming Chang, Geoffrey McKnight, and Steven Nutt. Transmission loss and dynamic response of membrane-type locally resonant acoustic

- metamaterials. *J. Appl. Phys.*, 108(11):114905, December 2010. ISSN 0021-8979, 1089-7550. doi:10.1063/1.3514082.
- [27] Christina J. Naify, Chia-Ming Chang, Geoffrey McKnight, and Steven Nutt. Transmission loss of membrane-type acoustic metamaterials with coaxial ring masses. *Journal of Applied Physics*, 110(12):124903, December 2011. ISSN 0021-8979, 1089-7550. doi:10.1063/1.3665213.
- [28] Christina J. Naify, Chia-Ming Chang, Geoffrey McKnight, Florian Scheulen, and Steven Nutt. Membrane-type metamaterials: Transmission loss of multi-celled arrays. *J. Appl. Phys.*, 109(10):104902, May 2011. ISSN 0021-8979, 1089-7550. doi:10.1063/1.3583656.
- [29] Christina J. Naify, Chia-Ming Chang, Geoffrey McKnight, and Steven R. Nutt. Scaling of membrane-type locally resonant acoustic metamaterial arrays. *The Journal of the Acoustical Society of America*, 132(4):2784–2792, October 2012. ISSN 0001-4966. doi:10.1121/1.4744941.
- [30] Z. Yang, H. M. Dai, N. H. Chan, G. C. Ma, and Ping Sheng. Acoustic metamaterial panels for sound attenuation in the 50–1000 Hz regime. *Applied Physics Letters*, 96(4):041906, January 2010. ISSN 0003-6951, 1077-3118. doi:10.1063/1.3299007.
- [31] Jun Mei, Guancong Ma, Min Yang, Zhiyu Yang, Weijia Wen, and Ping Sheng. Dark acoustic metamaterials as super absorbers for low-frequency sound. *Nature Communications*, 3:756, March 2012. ISSN 2041-1723. doi:10.1038/ncomms1758.
- [32] Guancong Ma, Min Yang, Songwen Xiao, Zhiyu Yang, and Ping Sheng. Acoustic metasurface with hybrid resonances. *Nat Mater*, 13(9):873–878, September 2014. ISSN 1476-1122. doi:10.1038/nmat3994.
- [33] Mathias Fink. Acoustic metamaterials: Nearly perfect sound absorbers. *Nat Mater*, 13(9):848–849, August 2014. ISSN 1476-1122, 1476-4660. doi:10.1038/nmat4067.
- [34] Romain Fleury and Andrea Alù. Extraordinary Sound Transmission through Density-Near-Zero Ultranarrow Channels. *Phys. Rev. Lett.*, 111(5):055501, July 2013. doi:10.1103/PhysRevLett.111.055501.

- [35] Jong Jin Park, K. J. B. Lee, Oliver B. Wright, Myoung Ki Jung, and Sam H. Lee. Giant Acoustic Concentration by Extraordinary Transmission in Zero-Mass Metamaterials. *Phys. Rev. Lett.*, 110(24):244302, June 2013. doi:10.1103/PhysRevLett.110.244302.
- [36] Yuan Gu, Ying Cheng, Jingshi Wang, and Xiaojun Liu. Controlling sound transmission with density-near-zero acoustic membrane network. *J. Appl. Phys.*, 118(2):024505, July 2015. ISSN 0021-8979, 1089-7550. doi:10.1063/1.4922669.
- [37] Sam Hyeon Lee, Choon Mahn Park, Yong Mun Seo, Zhi Guo Wang, and Chul Koo Kim. Composite Acoustic Medium with Simultaneously Negative Density and Modulus. *Phys. Rev. Lett.*, 104(5):054301, February 2010. doi:10.1103/PhysRevLett.104.054301.
- [38] Frédéric Bongard, Hervé Lissek, and Juan Mosig. Acoustic transmission line metamaterial with negative/zero/positive refractive index. *Phys. Rev. B*, 82(9):094306, September 2010. doi:10.1103/PhysRevB.82.094306.
- [39] L. Fok and X. Zhang. Negative acoustic index metamaterial. *Phys. Rev. B*, 83(21):214304, June 2011. doi:10.1103/PhysRevB.83.214304.
- [40] Yong Mun Seo, Jong Jin Park, Seung Hwan Lee, Choon Mahn Park, Chul Koo Kim, and Sam Hyeon Lee. Acoustic metamaterial exhibiting four different sign combinations of density and modulus. *J. Appl. Phys.*, 111(2):023504–023504–5, January 2012. ISSN 0021-8979. doi:10.1063/1.3676262.
- [41] Min Yang, Guancong Ma, Zhiyu Yang, and Ping Sheng. Coupled Membranes with Doubly Negative Mass Density and Bulk Modulus. *Phys. Rev. Lett.*, 110(13):134301, March 2013. doi:10.1103/PhysRevLett.110.134301.
- [42] Guancong MA, Min Yang, Ping Sheng, and Zhiyu Yang. Acoustic metamaterial with simultaneously negative effective mass density and bulk modulus, October 2014. URL <http://www.google.com/patents/US8857564>. U.S. Classification 181/286, 181/284; International Classification E04B1/82; Cooperative Classification G10K11/18.
- [43] J. O. Vasseur, P. A. Deymier, B. Chenni, B. Djafari-Rouhani, L. Dobrzynski, and D. Prevost. Experimental and Theoretical Evidence for the Existence of Absolute

- Acoustic Band Gaps in Two-Dimensional Solid Phononic Crystals. *Phys. Rev. Lett.*, 86(14):3012–3015, April 2001. doi:10.1103/PhysRevLett.86.3012.
- [44] Suxia Yang, J. H. Page, Zhengyou Liu, M. L. Cowan, C. T. Chan, and Ping Sheng. Ultrasound Tunneling through 3d Phononic Crystals. *Phys. Rev. Lett.*, 88(10):104301, February 2002. doi:10.1103/PhysRevLett.88.104301.
- [45] Suxia Yang, J. H. Page, Zhengyou Liu, M. L. Cowan, C. T. Chan, and Ping Sheng. Focusing of Sound in a 3d Phononic Crystal. *Phys. Rev. Lett.*, 93(2):024301, July 2004. doi:10.1103/PhysRevLett.93.024301.
- [46] Liang Feng, Xiao-Ping Liu, Yan-Bin Chen, Zhi-Peng Huang, Yi-Wei Mao, Yan-Feng Chen, Jian Zi, and Yong-Yuan Zhu. Negative refraction of acoustic waves in two-dimensional sonic crystals. *Phys. Rev. B*, 72(3):033108, July 2005. doi:10.1103/PhysRevB.72.033108.
- [47] T. Gorishnyy, C. K. Ullal, M. Maldovan, G. Fytas, and E. L. Thomas. Hypersonic Phononic Crystals. *Phys. Rev. Lett.*, 94(11):115501, March 2005. doi:10.1103/PhysRevLett.94.115501.
- [48] Xinhua Hu, C. T. Chan, and Jian Zi. Two-dimensional sonic crystals with Helmholtz resonators. *Phys. Rev. E*, 71(5):055601, May 2005. doi:10.1103/PhysRevE.71.055601.
- [49] Rosa Martínez-Sala, Constanza Rubio, Luis M. García-Raffi, Juan V. Sánchez-Pérez, Enrique A. Sánchez-Pérez, and J. Linares. Control of noise by trees arranged like sonic crystals. *Journal of Sound and Vibration*, 291(1–2):100–106, March 2006. ISSN 0022-460X. doi:10.1016/j.jsv.2005.05.030.
- [50] Xiangdong Zhang and Zhengyou Liu. Extremal Transmission and Beating Effect of Acoustic Waves in Two-Dimensional Sonic Crystals. *Phys. Rev. Lett.*, 101(26):264303, December 2008. doi:10.1103/PhysRevLett.101.264303.
- [51] F. Cervera, L. Sanchis, J. V. Sánchez-Pérez, R. Martínez-Sala, C. Rubio, F. Meseguer, C. López, D. Caballero, and J. Sánchez-Dehesa. Refractive Acoustic Devices for Airborne Sound. *Phys. Rev. Lett.*, 88(2):023902, December 2001. doi:10.1103/PhysRevLett.88.023902.

- [52] Daniel Torrent, Andreas Håkansson, Francisco Cervera, and José Sánchez-Dehesa. Homogenization of Two-Dimensional Clusters of Rigid Rods in Air. *Phys. Rev. Lett.*, 96(20), May 2006. ISSN 0031-9007, 1079-7114. doi:10.1103/PhysRevLett.96.204302.
- [53] Daniel Torrent and José Sánchez-Dehesa. Effective parameters of clusters of cylinders embedded in a nonviscous fluid or gas. *Phys. Rev. B*, 74(22), December 2006. ISSN 1098-0121, 1550-235X. doi:10.1103/PhysRevB.74.224305.
- [54] Daniel Torrent and José Sánchez-Dehesa. Anisotropic mass density by two-dimensional acoustic metamaterials. *New J. Phys.*, 10(2):023004, February 2008. ISSN 1367-2630. doi:10.1088/1367-2630/10/2/023004.
- [55] Daniel Torrent and José Sánchez-Dehesa. Anisotropic Mass Density by Radially Periodic Fluid Structures. *Phys. Rev. Lett.*, 105(17):174301, October 2010. doi:10.1103/PhysRevLett.105.174301.
- [56] Rogelio Graciá-Salgado, Victor M. García-Chocano, Daniel Torrent, and José Sánchez-Dehesa. Negative mass density and  $\rho$ -near-zero quasi-two-dimensional metamaterials: Design and applications. *Phys. Rev. B*, 88(22):224305, December 2013. doi:10.1103/PhysRevB.88.224305.
- [57] Zixian Liang and Jensen Li. Extreme Acoustic Metamaterial by Coiling Up Space. *Phys. Rev. Lett.*, 108(11):114301, March 2012. doi:10.1103/PhysRevLett.108.114301.
- [58] Yong Li, Bin Liang, Xu Tao, Xue-feng Zhu, Xin-ye Zou, and Jian-chun Cheng. Acoustic focusing by coiling up space. *Applied Physics Letters*, 101(23):233508, December 2012. ISSN 0003-6951, 1077-3118. doi:10.1063/1.4769984.
- [59] Yangbo Xie, Bogdan-Ioan Popa, Lucian Zigoneanu, and Steven A. Cummer. Measurement of a Broadband Negative Index with Space-Coiling Acoustic Metamaterials. *Phys. Rev. Lett.*, 110(17):175501, April 2013. doi:10.1103/PhysRevLett.110.175501.
- [60] Tobias Frenzel, Jan David Brehm, Tiemo Bückmann, Robert Schittny, Muamer Kadic, and Martin Wegener. Three-dimensional labyrinthine acoustic metamaterials. *Applied Physics Letters*, 103(6):061907, August 2013. ISSN 0003-6951, 1077-3118. doi:10.1063/1.4817934.

- [61] Yangbo Xie, Adam Konneker, Bogdan-Ioan Popa, and Steven A. Cummer. Tapered labyrinthine acoustic metamaterials for broadband impedance matching. *Applied Physics Letters*, 103(20):201906, November 2013. ISSN 0003-6951, 1077-3118. doi:10.1063/1.4831770.
- [62] Steven A. Cummer and David Schurig. One path to acoustic cloaking. *New J. Phys.*, 9(3):45, March 2007. ISSN 1367-2630. doi:10.1088/1367-2630/9/3/045.
- [63] Huanyang Chen and C. T. Chan. Acoustic cloaking in three dimensions using acoustic metamaterials. *Applied Physics Letters*, 91(18):183518, October 2007. ISSN 0003-6951, 1077-3118. doi:10.1063/1.2803315.
- [64] Steven Cummer, Bogdan-Ioan Popa, David Schurig, David Smith, John Pendry, Marco Rahm, and Anthony Starr. Scattering Theory Derivation of a 3d Acoustic Cloaking Shell. *Phys. Rev. Lett.*, 100(2):024301, January 2008. ISSN 0031-9007, 1079-7114. doi:10.1103/PhysRevLett.100.024301.
- [65] Daniel Torrent and José Sánchez-Dehesa. Acoustic cloaking in two dimensions: a feasible approach. *New J. Phys.*, 10(6):063015, June 2008. ISSN 1367-2630. doi:10.1088/1367-2630/10/6/063015.
- [66] Wael Akl and Amr Baz. A technique for physical realization of anisotropic density matrices with application to acoustic beam shifters. *J. Appl. Phys.*, 111(2):024907, January 2012. ISSN 0021-8979, 1089-7550. doi:10.1063/1.3678634.
- [67] Huanyang Chen and C. T. Chan. Acoustic cloaking and transformation acoustics. *J. Phys. D: Appl. Phys.*, 43(11):113001, 2010. ISSN 0022-3727. doi:10.1088/0022-3727/43/11/113001.
- [68] Jensen Li, Lee Fok, Xiaobo Yin, Guy Bartal, and Xiang Zhang. Experimental demonstration of an acoustic magnifying hyperlens. *Nat Mater*, 8(12):931–934, December 2009. ISSN 1476-1122. doi:10.1038/nmat2561.
- [69] Choon Mahn Park, Jong Jin Park, Seung Hwan Lee, Yong Mun Seo, Chul Koo Kim, and Sam H. Lee. Amplification of Acoustic Evanescent Waves Using Metamaterial Slabs. *Phys. Rev. Lett.*, 107(19):194301, November 2011. doi:10.1103/PhysRevLett.107.194301.

- [70] Jong Jin Park, Choon Mahn Park, K. J. B. Lee, and Sam H. Lee. Acoustic superlens using membrane-based metamaterials. *Appl. Phys. Lett.*, 106(5):051901, February 2015. ISSN 0003-6951, 1077-3118. doi:10.1063/1.4907634.
- [71] Nadège Kaina, Fabrice Lemoult, Mathias Fink, and Geoffroy Lerosey. Negative refractive index and acoustic superlens from multiple scattering in single negative metamaterials. *Nature*, 525(7567):77–81, September 2015. ISSN 0028-0836. doi:10.1038/nature14678.
- [72] J.-P. Groby, W. Huang, A. Lardeau, and Y. Aurégan. The use of slow waves to design simple sound absorbing materials. *Journal of Applied Physics*, 117(12):124903, March 2015. ISSN 0021-8979, 1089-7550. doi:10.1063/1.4915115.
- [73] Cong Liu, Xiaodong Xu, and Xiaojun Liu. Manipulating acoustic flow by using inhomogeneous anisotropic density-near-zero metamaterials. *Appl. Phys. Lett.*, 106(8):081912, February 2015. ISSN 0003-6951, 1077-3118. doi:10.1063/1.4914005.
- [74] Jiajun Zhao, Zhi Ning Chen, Baowen Li, and Cheng-Wei Qiu. Acoustic cloaking by extraordinary sound transmission. *Journal of Applied Physics*, 117(21):214507, June 2015. ISSN 0021-8979, 1089-7550. doi:10.1063/1.4922120.
- [75] A. Baz. The structure of an active acoustic metamaterial with tunable effective density. *New J. Phys.*, 11(12):123010, December 2009. ISSN 1367-2630. doi:10.1088/1367-2630/11/12/123010.
- [76] Amr M. Baz. An Active Acoustic Metamaterial With Tunable Effective Density. *J. Vib. Acoust.*, 132(4):041011–041011, June 2010. ISSN 1048-9002. doi:10.1115/1.4000983.
- [77] Wael Akl and Amr Baz. Multi-cell Active Acoustic Metamaterial with Programmable Bulk Modulus. *J. Intel. Mat. Sys. Str.*, 21(5):541–556, March 2010. ISSN 1045-389X, 1530-8138. doi:10.1177/1045389X09359434.
- [78] Wael Akl and Amr Baz. Analysis and experimental demonstration of an active acoustic metamaterial cell. *Journal of Applied Physics*, 111(4):044505, February 2012. ISSN 0021-8979, 1089-7550. doi:10.1063/1.3686210.

- [79] Wael Akl and Amr Baz. Experimental characterization of active acoustic metamaterial cell with controllable dynamic density. *J. Appl. Phys.*, 112(8):084912, October 2012. ISSN 0021-8979, 1089-7550. doi:10.1063/1.4759327.
- [80] Xing Chen, Xianchen Xu, Shigang Ai, HaoSen Chen, Yongmao Pei, and Xiaoming Zhou. Active acoustic metamaterials with tunable effective mass density by gradient magnetic fields. *Appl. Phys. Lett.*, 105(7):071913, August 2014. ISSN 0003-6951, 1077-3118. doi:10.1063/1.4893921.
- [81] Songwen Xiao, Guancong Ma, Yong Li, Zhiyu Yang, and Ping Sheng. Active control of membrane-type acoustic metamaterial by electric field. *Appl. Phys. Lett.*, 106(9):091904, March 2015. ISSN 0003-6951, 1077-3118. doi:10.1063/1.4913999.
- [82] Yabin Jin, Bernard Bonello, and Yongdong Pan. Acoustic metamaterials with piezoelectric resonant structures. *J. Phys. D: Appl. Phys.*, 47(24):245301, June 2014. ISSN 0022-3727. doi:10.1088/0022-3727/47/24/245301.
- [83] A. A. Kutsenko, A. L. Shuvalov, O. Poncelet, and A. N. Darinskii. Tunable effective constants of the one-dimensional piezoelectric phononic crystal with internal connected electrodes. *J. Acoust. Soc. Am.*, 137(2):606–616, February 2015. ISSN 0001-4966. doi:10.1121/1.4906162.
- [84] Zhilin Hou and Badreddine M. Assouar. Tunable solid acoustic metamaterial with negative elastic modulus. *Appl. Phys. Lett.*, 106(25):251901, June 2015. ISSN 0003-6951, 1077-3118. doi:10.1063/1.4922873.
- [85] Zhe Chen, Cheng Xue, Li Fan, Shu-yi Zhang, Xiao-juan Li, Hui Zhang, and Jin Ding. A tunable acoustic metamaterial with double-negativity driven by electromagnets. *Scientific Reports*, 6:30254, July 2016. ISSN 2045-2322. doi:10.1038/srep30254.
- [86] Filippo Casadei, Tommaso Delperio, Andrea Bergamini, Paolo Ermanni, and Massimo Ruzzene. Piezoelectric resonator arrays for tunable acoustic waveguides and metamaterials. *J. Appl. Phys.*, 112(6):064902, September 2012. ISSN 0021-8979, 1089-7550. doi:10.1063/1.4752468.
- [87] Bogdan-Ioan Popa and Steven A. Cummer. Non-reciprocal and highly nonlinear active acoustic metamaterials. *Nature Communications*, 5:3398, February 2014. ISSN 2041-1723. doi:10.1038/ncomms4398.

- [88] Bogdan-Ioan Popa, Durvesh Shinde, Adam Konneker, and Steven A. Cummer. Active acoustic metamaterials reconfigurable in real-time. *arXiv preprint arXiv:1505.00453*, 2015.
- [89] Vladimir Fokin, Muralidhar Ambati, Cheng Sun, and Xiang Zhang. Method for retrieving effective properties of locally resonant acoustic metamaterials. *Phys. Rev. B*, 76(14):144302, October 2007. doi:10.1103/PhysRevB.76.144302.
- [90] Min Yang, Guancong Ma, Ying Wu, Zhiyu Yang, and Ping Sheng. Homogenization scheme for acoustic metamaterials. *Phys. Rev. B*, 89(6):064309, February 2014. doi:10.1103/PhysRevB.89.064309.
- [91] Daniel Torrent and José Sánchez-Dehesa. Acoustic metamaterials for new two-dimensional sonic devices. *New J. Phys.*, 9(9):323, September 2007. ISSN 1367-2630. doi:10.1088/1367-2630/9/9/323.
- [92] M. L. Munjal. *Acoustics of Ducts and Mufflers With Application to Exhaust and Ventilation System Design*. Wiley-Interscience, New York, May 1987. ISBN 978-0-471-84738-0.
- [93] R. Zhu, G. L. Huang, and G. K. Hu. Effective Dynamic Properties and Multi-Resonant Design of Acoustic Metamaterials. *J. Vib. Acoust.*, 134(3):031006–031006, April 2012. ISSN 0739-3717. doi:10.1115/1.4005825.
- [94] Pei Li, Shanshan Yao, Xiaoming Zhou, Guoliang Huang, and Gengkai Hu. Effective medium theory of thin-plate acoustic metamaterials. *J. Acoust. Soc. Am.*, 135(4):1844–1852, April 2014. ISSN 0001-4966. doi:10.1121/1.4868400.
- [95] Stefan Nygård. *Low frequency modelling of complex duct networks*. Tech, Licent. Thesis, KTH, Marcus Wallenb. Lab. Sound Vib., 1999.
- [96] Xudong Chen, Tomasz Grzegorzczuk, Bae-Ian Wu, Joe Pacheco, and Jin Kong. Robust method to retrieve the constitutive effective parameters of metamaterials. *Phys. Rev. E*, 70(1):016608, July 2004. ISSN 1539-3755, 1550-2376. doi:10.1103/PhysRevE.70.016608.
- [97] D. R. Smith, D. C. Vier, Th. Koschny, and C. M. Soukoulis. Electromagnetic parameter retrieval from inhomogeneous metamaterials. *Phys. Rev. E*, 71(3):036617, March 2005. ISSN 1539-3755, 1550-2376. doi:10.1103/PhysRevE.71.036617.

- [98] Zsolt Szabo, Gi-Ho Park, Ravi Hedge, and Er-Ping Li. A Unique Extraction of Metamaterial Parameters Based on Kramers-Kronig Relationship. *IEEE T. Microw. Theory*, 58(10):2646–2653, October 2010. ISSN 0018-9480, 1557-9670. doi:10.1109/TMTT.2010.2065310.
- [99] Bogdan-Ioan Popa and Steven Cummer. Design and characterization of broadband acoustic composite metamaterials. *Phys. Rev. B*, 80(17):174303, November 2009. doi:10.1103/PhysRevB.80.174303.
- [100] Lucian Zigoneanu, Bogdan-Ioan Popa, Anthony F. Starr, and Steven A. Cummer. Design and measurements of a broadband two-dimensional acoustic metamaterial with anisotropic effective mass density. *J. Appl. Phys.*, 109(5):054906, March 2011. ISSN 0021-8979, 1089-7550. doi:10.1063/1.3552990.
- [101] Bogdan-Ioan Popa, Lucian Zigoneanu, and Steven Cummer. Tunable active acoustic metamaterials. *Phys. Rev. B*, 88(2):024303, July 2013. doi:10.1103/PhysRevB.88.024303.
- [102] Norbert Cselyuska, Milan Sečujski, and Vesna Crnojević-Bengin. Analysis of Acoustic Metamaterials - Acoustic Scattering Matrix and Extraction of Effective Parameters. In *Metamaterials*, pages 17–22. Metamorphose VI, 2012.
- [103] V. Lucarini, J.J. Saarinen, K.E. Peiponen, and E.M. Vartianen. *Kramers-Kronig Relations in Optical Materials Research*. Number v. 110 in Springer series in optical sciences. Springer, Berlin ; New York, 2005. ISBN 978-3-540-23673-3. URL <http://www.springer.com/materials/book/978-3-540-23673-3>.
- [104] IEEE Standard on Piezoelectricity. *ANSI/IEEE Std 176-1987*, pages 0.1–, 1988. doi:10.1109/IEEESTD.1988.79638.
- [105] James E. Young. Transmission of Sound through Thin Elastic Plates. *J. Acoust. Soc. Am.*, 26(4):485–492, July 1954. ISSN 0001-4966. doi:10.1121/1.1907361.
- [106] A. Benjeddou, M. A. Trindade, and R. Ohayon. A Unified Beam Finite Element Model for Extension and Shear Piezoelectric Actuation Mechanisms. *J. Intel. Mat. Sys. Str.*, 8(12):1012–1025, December 1997. ISSN 1045-389X, 1530-8138. doi:10.1177/1045389X9700801202.

- [107] Arthur W. Leissa and Mohamad S. Qatu. *Vibrations of continuous systems*. McGraw Hill, New York, 2011. ISBN 978-0-07-142682-4 0-07-142682-5 978-0-07-145728-6 0-07-145728-3 978-0-07-171479-2 0-07-171479-0. URL <http://site.ebrary.com/lib/academiccompletetitles/home.action>.
- [108] Lawrence E. Kinsler, editor. *Fundamentals of acoustics*. Wiley, New York, 4th edition, 2000. ISBN 0-471-84789-5.
- [109] Mats Abom. Measurement of the scattering-matrix of acoustical two-ports. *Mech. Syst. Signal Pr.*, 5(2):89–104, March 1991. ISSN 0888-3270. doi:10.1016/0888-3270(91)90017-Y.
- [110] ASTM E2611 - 09. Standard Test Method for Measurement of Normal Incidence Sound Transmission of Acoustical Materials Based on the Transfer Matrix Method. Technical report, ASTM International, 2009. URL <http://www.astm.org/Standards/E2611.htm>.
- [111] ANSYS, Inc. *ANSYS Mechanical APDL Acoustic Analysis Guide*. ANSYS, Inc., November 2013.
- [112] R. Glav and M. Abom. A general formalism for analyzing acoustic 2-port networks. *J Sound Vib.*, 202(5):739–747, 1997.
- [113] J. N. Reddy. *Mechanics of Laminated Composite Plates and Shells: Theory and Analysis, Second Edition*. CRC Press, Boca Raton, June 2004. ISBN 978-0-203-50280-8.
- [114] C. K. Lee. Theory of laminated piezoelectric plates for the design of distributed sensors/actuators. Part I: Governing equations and reciprocal relationships. *J. Acoust. Soc. Am.*, 87(3):1144–1158, March 1990. ISSN 0001-4966. doi:10.1121/1.398788.
- [115] Yifeng Li, Jun Lan, Baoshun Li, Xiaozhou Liu, and Jiashu Zhang. Nonlinear effects in an acoustic metamaterial with simultaneous negative modulus and density. *Journal of Applied Physics*, 120(14):145105, October 2016. ISSN 0021-8979, 1089-7550. doi:10.1063/1.4964734.

- 
- [116] Xin Fang, Jihong Wen, Jianfei Yin, Dianlong Yu, and Yong Xiao. Broadband and tunable one-dimensional strongly nonlinear acoustic metamaterials: Theoretical study. *Phys. Rev. E*, 94(5):052206, November 2016. doi:10.1103/PhysRevE.94.052206.

# شكر

أود أن أتوجه بالشكر لأساتذتي الذين قاموا بالإشراف على الرسالة أ.د. وائل عقل ود. عادل الصباغ، فقد قدموا لي عونا كبيرا في كل مراحل هذا العمل وهينوا لي الأدوات وبيئة العمل المناسبة لإتمامه. وأود أن أشكر خصيصا أ.د. وائل عقل لطرحه موضوع هذا العمل على ومشاركته لي معرفته العميقة به، كما أود أن أشكر د. عادل الصباغ على تدخله في الأوقات المناسبة كلما شعر أنني قد فقدت البوصلة.

كما أود أن أشكر أ.د. تامر النادى لمساعدته لي في تفاصيل التجارب المعملية للعمل خاصة فيما يتعلق بتحليل الإشارات وعلم الصوتيات التطبيقية.

كما أود أن أشكر كل زملائي في فريق البحث المتقدم في مجال الأنظمة الديناميكية وزملائي في قسم الميكاترونيات، وأخص بالذكر م. وئام السحار وم. محمد طلعت حرب لإسهاماتهم القيمة في المحتوى النظرى والتجارب العملية لهذا العمل. كما أود أن أشكر م. محمد إبراهيم على تزويدي بالخلفية اللازمة عن المواد الكهرومغناطيسية استثنائية الخصائص وم. أحمد بركات على نقاشاتنا المثمرة فيما يخص أنظمة التحكم وم. أحمد أبوسريع لمساعدتي في تصنيع الأجزاء العملية و د. معاذ فاروقى على نقاشاتنا المطولة فيما يخص المواد الصوتية استثنائية الخصائص. كما أود أن أتقدم بالشكر لأصدقائي وزملائي م. يحيى ذكريا وم. على زين وم. أحمد الركابى وم. أحمد هشام، حيث قد قدمت لي عونا كبيرا في مواقف عديدة يصعب عليا حصرها.

لا يمكننى أيضا أن أنسى دور م. فاطمة، فقد كانت نعم العون في كل ما يتعلق بالإجراءات الإدارية والتنظيمية.

ما كان لي لأصل لهذه المرحلة دون الدعم اللامتناهى لعائلتي، فأود أن أشكر أبى وأمى على تشجيعهم المستمر لي لإنهاء هذا العمل بالشكل وفى الوقت المطلوب. كما أود أن أشكر أخى محمد وأختى سماء لمساعدتهم المستمرة في تحضير البيانات والرسومات الخاصة بالرسالة.



تغذية رجعية بعين الطبقات الكهروضغطية للغشاء، ويتم التحكم في الكثافة الفعلية للمادة عن طريق دائرة تغذية رجعية تلاؤمية تم إقامتها بتقدير قيمة الكثافة الفعلية باستخدام طريقة الميكروفونات الأربعة. تضمن التطبيقات المقترحة للمادة الجديدة إنشاء فلاتر صوتية فعالة ويمكن برمجتها وإنشاء عدسات صوتية خارقة وإنشاء أجهزة تسمح بمرور الصوت في اتجاه واحد.

**كلمات المفتاح:** المواد الصوتية، المواد الكهروضغطية، التحكم بالتغذية الرجعية، التحكم التلاؤمي



# الملخص

المواد الصوتية استثنائية الخصائص هي مواد اصطناعية يتم تصنيعها من منشآت ذات حجم دون الطول الموجي، بحيث تمتلك خصائص صوتية غير موجودة في الطبيعة. يمكن التحكم في الخصائص الصوتية للمواد الصوتية الخارقة عن طريق دمج عناصر فعالة في المنشآت المكون منها المادة، ويتم التحكم في خصائص المادة عن طريق إشارة كهربائية خارجية. هذا التحكم يكاد يعدم وجوده في أي نوع من المواد الطبيعية.

في هذه الرسالة تم استعراض وتلخيص التصميمات الموجودة لتصنيع المواد الصوتية استثنائية الخصائص السالبة والإيجابية، بالإضافة إلى استكشاف الطرق المختلفة لتجنيس خصائص المواد الصوتية السالبة وتطويرها لتلائم المواد النشطة. تم طرح ثلاثة تصميمات جديدة للمواد الصوتية اللوحية النشطة استثنائية الخصائص، كما تم التحقق من خصائصهم بطرق تحليلية ورقمية وعن طريق إجراء تجارب معملية.

التصميم المقترح الأول هو تصميم أحادي البعد يتكون من أقراص مصنوعة من مادة كهروضغطية ومثبتة في الهواء. يتم التحكم في الكثافة الفعلية للمادة عن طريق إشارة كهربائية خارجية يتم تطبيقها على الأقراص. تم تطوير نموذج تحليلي مبني على نظرية ثنائيات المنفذ الصوتية بالإضافة للنظرية الكهروضغطية ونظرية الألواح الرفيعة سابقة التحميل للتنبؤ بسلوك المادة، كما تم التحقق من النتائج التحليلية عن طريقة نموذج رقمي بطريقة العناصر المحدودة. تلاحظ وجود توافق ممتاز بين نتائج النموذجين في نطاق الترددات والجهود الكهربائية التي تم دراستها. تظهر النتائج أن الكثافة الفعلية للمادة المطورة يمكن تغييرها لعشرات أضعاف الكثافة الفعلية في الحالة السالبة دون التأثير على معامل الانضغاط الخاص بالمادة. كما تظهر أيضا أنه يمكن استخدام نظم تحكم بسيطة لبرمجة الكثافة الفعلية للمادة.

تم تعديل وتطوير التصميم الأول لتصنيع مواد صوتية ثنائية الأبعاد ذات كثافة متباينة يمكن التحكم فيها. التصميم المقترح يتكون من ألواح مركبة تتكون من شرائح من الرصاص وتيتانيت زيركونيت الرصاص مثبتة بهيكل من الألومينيوم في الهواء. الأمر الذي يتيح التحكم في الكثافة التباينية الفعلية للمادة المطورة في كل اتجاهين مختلفين كل على حدى باستخدام إشارة كهربائية استاتيكية. للتحقق من خصائص المادة التصميم الثاني تم إنشاء نموذج تحليلي مبني على نظرية ثنائيات المنفذ الصوتية والنظرية الكهروضغطية ونظرية الألواح المركبة للتنبؤ بسلوك المادة. وتم أيضا التحقق من النتائج التحليلية بطريقة العناصر المحدودة. تظهر نتائج النموذج الثاني أنه دون تردد الـ ١٦٠٠ هرتز يمكن التحكم في كثافة المادة في اتجاهين مختلفين والوصول لعشرات أضعاف الكثافة السالبة. تم استخدام المادة المطورة في تصميم مرشد للموجات يمكن إعادة ضبطه وتم التحقق من أدائه لوظيفته بطرق رقمية وتحليلية. وأظهرت النتائج أن مرشد الموجات المطور يمكنه التحكم في اتجاه الموجات الصوتية التي تمر من خلاله.

استخدمت النتائج التي تم الحصول عليها من التصميمين الأول والثاني لإقامة تصميم ثالث يمكن من خلاله التحكم في الكثافة الفعلية للمادة لحظيا وبشكل كامل بحيث يمكن التحكم في الكثافة الفعلية للمادة المطورة وضبطها لأى قيمة بين -١٠٠ كجم/م<sup>٣</sup> و ١٠٠ كجم/م<sup>٣</sup> مرورا بالكثافة الصفرية. ويتم هذا الأمر عن طريق واجهة رسومية تفاعلية وفي نطاق الترددات من ٥٠٠ إلى ١٥٠٠ هرتز. التصميم الثالث يتكون من أغشية كهروضغطية مركبة ومعلقة في الهواء. يتم التحكم في الطبيعة الديناميكية للغشاء عن طريق توصيل دائرة



## تعريف بمقدم الرسالة

- الاسم : أحمد عبد الشكور عبد الفتاح الحسينى علام
- تاريخ الميلاد : ٠٢ - ٠٨ - ١٩٩٠
- محل الميلاد : الجيزة، مصر
- آخر درجه جامعية : بكالوريوس العلوم الهندسية في الهندسة الميكانيكية
- الجهة المانحة : جامعة عين شمس
- تاريخ المنح : ٢٠١٢
- الوظيفه الحالية : معيد بقسم الميكاترونيات بكلية الهندسة جامعة عين شمس





كلية الهندسة  
قسم هندسة الميكاترونيات

رسالة الماجستير:

اسم الطالب : أحمد عبد الشكور عبد الفتاح الحسينى علام  
عنوان الرسالة : التحكم في الموجات باستخدام مواد صوتية إيجابية استثنائية الخصائص  
اسم الدرجة : ماجستير العلوم في الهندسة

لجنة الإشراف:

أ.د/ وائل نبيل عقل  
د/ عادل منيب الصباغ

تاريخ البحث : ...../...../.....

الدراسات العليا:

ختم الإجازة: أجزت الرسالة بتاريخ : ...../...../.....

موافقة مجلس الكلية : ...../...../.....

موافقة مجلس الجامعة : ...../...../.....



## الموافقة على المنح

كلية الهندسة  
قسم هندسة الميكاترونيات

### التحكم في الموجات باستخدام مواد صوتية إيجابية استثنائية الخصائص

إعداد  
أحمد عبد الشكور عبد الفتاح الحسينى علام

#### لجنة الحكم

التوقيع	الاسم
.....	أ.د./ عمرو محمد باز قسم الهندسة الميكانيكية، جامعة مير لاند بالولايات المتحدة الأمريكية
.....	أ.د./ عمرو محمد عزت صفوت قسم هندسة الالكترونيات والاتصالات الكهربائية، جامعة عين شمس
.....	أ.د./ وائل نبيل عقل قسم التصميم وهندسة الإنتاج، جامعة عين شمس

٢٠١٧/٤/٥





كلية الهندسة

قسم هندسة الميكاترونيات

# التحكم في الموجات باستخدام مواد صوتية إيجابية استثنائية الخصائص

رسالة مقدمة للحصول على درجة ماجستير العلوم

في الهندسة الميكانيكية

(هندسة الميكاترونيات)

إعداد

أحمد عبد الشكور عبد الفتاح الحسينى علام

حاصل على بكالوريوس العلوم

في الهندسة الميكانيكية

(هندسة الميكاترونيات)

كلية الهندسة، جامعة عين شمس، سنة ٢٠١٢

**المشرفون**

أ.د/ وائل نبيل عقل

أ.م.د/ عادل منيب الصباغ